

DISSERTATION

Electrochemistry of Titanium in Ionic Liquids

Ausgeführt zum Zwecke der Erlangung des akademischen Grades eines Doktors
der technischen Wissenschaften

vorgelegt von

Mag. Yuriy Andriyko

Matrikelnummer: 0527697
Viktor-Kaplan-Strasse 11/307
2700 Wiener Neustadt

164/EC

Institut für Chemische Technologien und Analytik

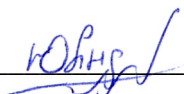
Eingereicht an der Technischen Universität Wien

Fakultät für Technische Chemie

unter der Leitung von

Ao. Univ. Prof. DI Dr. Hermann Kronberger

Wien, am 23.10.2007

 /Y. Andriyko/

Acknowledgement

The work has been performed under the guidance of Prof. Hermann Kronberger. First of all I would like to express my gratitude to him for his advices and giving me the opportunity to complete the thesis at the Technical University of Vienna.

Most of the work has been done on the technical equipment of ECHEM Centre of Competence in Applied Electrochemistry. I would like to thank the head of ECHEM Prof. Nauer for his support and help in fulfilling and improving this work.

The financial support was given via the industrially oriented project at ECHEM.

Thanks to my former project manager Dr. Krendelsberger, for his advices and fruitful discussions.

I'm grateful to Dr. Babushkina for introducing me to the infrared spectroscopy and cooperation in course of the project.

Finally thanks to all the team of ECHEM for their nice support and willing to help.

Last but not least, I would like to thank my father, Prof. Andriiko, for the knowledge and experience that I could gain in discussions with him.

Abstract

The possibility of Ti electrodeposition was always attractive to the scientific community, therefore the electrochemistry of Ti was widely investigated in high temperature molten salt electrolytes like chlorides and fluorides.

The introduction of ionic liquids (ILs) as low temperature electrolytes opened new possibilities to the electrodeposition of refractory metals. Water free, low melting and completely ionic medium seems to be a good candidate for studying the possibilities of getting Ti and Ti-alloy coatings with desirable characteristics.

The aim of this work was to investigate the electrochemistry of titanium in various ILs. As the physico-chemical properties of ILs are still poorly studied, the temperature dependence of the density, viscosity and conductivity of 1-butyl-2,3-dimethyl imidazolium (BMMIm) cation-based ILs with different anions (tetrafluoroborate and azide) and their mixtures were measured. Activation energies of flow and Walden products were calculated. The values range in between, (40 to 45) kJ mol⁻¹ and (70 to 80) cm² mPa s Ω⁻¹ mol⁻¹.

The electrochemical properties of the pure ILs were investigated as well.

Titanium electrochemistry was studied by means of cyclic voltammetry and chronopotentiometry at different concentrations of the electroactive species in BMMImN₃ and BMMImBF₄ ILs. For determining the nature of the complexes in the electrolyte, infrared spectroscopy was used.

On the basis of the electrochemical data obtained, Ti(IV) reduction mechanism was proposed and diffusion coefficients of the electroactive species were calculated: in BMMImN₃ (1.3±0.6)·10⁻⁶ cm² s⁻¹ and in BMMImBF₄ - between 1.1·10⁻⁷ cm² s⁻¹ and 7·10⁻⁸ cm² s⁻¹ depending on the concentration. The electroreduction of Ti(IV) was found to proceed via the sequence of one-electron steps with formation of Ti(0) in BMMImBF₄ IL and Ti(III) in BMMImN₃, as a final product.

The deposition experiments were performed from the ILs containing trisubstituted imidazolium ILs. Ti was deposited in small quantities.

The work presented in this thesis was done at ECHEM Centre of competence in Applied Electrochemistry (Wr. Neustadt) as a part of a joint project with industrial partners.

Kurzfassung

Die Möglichkeit der elektrochemischen Abscheidung von Titan war für die Wissenschaft schon immer interessant, deshalb wurde die Elektrochemie des Titans in Hochtemperatur-Salzschmelzen aus Chloriden bzw. Fluoriden bereits früher intensiv studiert.

Die Einführung von ionischen Flüssigkeiten (Ionic Liquids, ILs) eröffnete die Möglichkeit, Refraktärmetalle bei niedrigerer Temperatur abzuscheiden. Wasserfreie, niedrigschmelzende und vollständig ionische Medien sind vielversprechende Kandidaten, um die Möglichkeiten zur Abscheidung neuartiger Schichten mit attraktiven Eigenschaften zu studieren.

Das Ziel dieser Arbeit war es, die Elektrochemie von Titankomplexen in verschiedenen ILs zu untersuchen. Da die physikalisch-chemischen Eigenschaften der ILs bisher wenig untersucht wurden, wurde die Temperaturabhängigkeit der Dichte, Viskosität und Leitfähigkeit von 1-Butyl-2,3-dimethylimidazolium (BMMIm)-basierten ILs (Tetrafluoroborat und Azid) sowie Mischungen daraus gemessen. Weiters wurden die Aktivierungsenergie des Fließens und die Walden-Produkte bestimmt; die Werte liegen im Bereich zwischen (40 to 45) kJ mol⁻¹ und (70 to 80) cm² mPa s Ω⁻¹ mol⁻¹.

Die elektrochemischen Eigenschaften der ILs wurden ebenfalls untersucht.

Die elektrochemischen Eigenschaften von Titankomplexen in ILs wurden mittels Zyklovoltammetrie und Chronopotentiometrie bestimmt; die Messungen wurden bei verschiedenen Konzentrationen in BMMImN₃ und BMMImBF₄ durchgeführt. Die während der Reaktion entstehenden Komplexe wurden mittels Infrarotspektroskopie identifiziert.

Auf der Basis der erhobenen Daten wurde ein Mechanismus für die elektrochemische Reduktion von Ti(IV) Komplexen vorgeschlagen und die Diffusionskonstanten der beteiligten Spezies berechnet: in BMMImN₃ liegen sie bei $(1.3 \pm 0.6) \cdot 10^{-6}$ cm² s⁻¹ und in BMMImBF₄ zwischen $1.1 \cdot 10^{-7}$ cm² s⁻¹ und $7 \cdot 10^{-8}$ cm² s⁻¹, abhängig von der Konzentration. Die elektrochemische Reduktion von Ti(IV) Komplexen erfolgt in einer Folge von Eielektronenschritten; in BMMImBF₄ bis zum Ti(0) und in BMMImN₃ bis zum Ti(III) als Endprodukt.

Die Experimente zur Abscheidung von Titan wurden in trisubstituierten Imidazolium-ILs durchgeführt. Metallisches Ti konnte in kleinen Mengen abgeschieden werden.

Die vorliegende Arbeit wurde im ECHEM Kompetenzzentrum für angewandte Elektrochemie, Wiener Neustadt, als Teil eines gemeinsamen Projekts mit Firmenpartnern durchgeführt.

List of symbols and abbreviations

AllMeImCl	1-allyl-3-methyl imidazolium chloride
BMIm[BTA]	1-butyl-3-methyl imidazolium bis((trifluoromethyl)sulfonyl)amide
BMPy[NTf ₂]	N-butyl-N-methyl pyrrolidinium bis(trifluoromethylsulfonyl)imide
BM ₃ Am[NTf ₂]	1 N-butyl-N-trimethyl ammonium bis(trifluoromethylsulfonyl)imide
BMMImBF ₄	1-butyl-2,3-dimethyl imidazolium tetrafluoroborate
BMMImN ₃	1-butyl-2,3-dimethyl imidazolium azide
BMImCl	1-butyl-3-methyl-imidazolium chloride
BP	N-butylpyridinium
BMImBF ₄	1-butyl-3-methyl-imidazolium tetrafluoroborate
DMABP	(p-dimethylamino-N-butylpyridinium)
EMImI	1-ethyl-3-methyl imidazolium iodide
EMImCl	1-ethyl-3-methyl imidazolium chloride
EMImBF ₄	1-ethyl-3-methyl-imidazolium tetrafluoroborate
PC	propylene carbonate
AUX	auxiliary electrode
BSE	back scattered electrons
CV	cyclic voltammetry
CP	chronopotentiometry
ESEM	environmental scanning electron microscope
EDX	energy-dispersive X-ray spectrometer
GC	glassy carbon
IL	ionic liquid
SE	secondary electrons
VTF	Vogel-Tamman-Fulcher equation
WE	working electrode
α	transfer coefficient
η	viscosity, mPa s (cP)
Λ	molar conductivity, cm ² Ω ⁻¹ mol ⁻¹
σ	ionic conductivity, S cm ⁻¹
τ	transition time (in chronopotentiometry experiments), s

A	area of the electrode, cm^2
C_o^*	bulk concentration of the depolarizer, mol l^{-1}
C	capacitance, F
D	diffusion coefficient $\text{cm}^2 \text{s}^{-1}$
d	density, g cm^{-3}
E_a	the activation energy, J mol^{-1}
F	Faraday constant (charge of one mole electrons), A s mol^{-1}
i	current density, mA cm^{-2}
i_p	peak current density, mA cm^{-2}
I	current, mA
k	constant in the Vogel-Tamman-Fulcher equation
k_r	reaction rate constant, $\text{cm}^3 \text{mol}^{-1} \text{s}^{-1}$
M	molar mass, g mol^{-1}
m	weight of the sample, g
n	number of electrons
Q	charge passed in electrolysis, $\text{A s} = \text{C}$
R	universal gas constant, $\text{J mol}^{-1} \text{K}^{-1}$
R_Ω	electric resistance, Ω
T	temperature, K
T_0	ideal glass transition temperature, K
t	temperature, $^\circ\text{C}$
V_{molar}	molar volume, $\text{cm}^3 \text{mol}^{-1}$
v	potential sweep rate, mV s^{-1}
Z	impedance, Ω

Table of contents

List of symbols and abbreviations.....	v
Table of contents.....	vii
Introduction.....	1
1. Literature overview.....	3
1.1 Ionic liquids (ILs): structure, origin, undesired impurities	3
1.1.1 Low temperature ILs: synthesis and purity issues	5
1.1.2 Imidazolium based IL: synthesis and purity issues.....	6
1.1.3 Cation, anion and impurities influence on the properties of the ILs.....	8
1.2 Physical-chemical properties	11
1.2.1 Phase transition behavior (glass transition, melting)	11
1.2.2 Viscosity	13
1.2.3 Conductivity	14
1.2.4 Temperature stability	17
1.3 Electrochemical behavior of ILs.....	19
1.4 Electrochemical behavior of Ti in different media.....	24
1.4.1 Aqueous solutions.....	24
1.4.2 Organic solvents.....	24
1.4.3 Electrochemical behavior of Ti in high temperature molten salts.....	26
1.4.3.1 Electrochemical behavior of titanium in chloride electrolytes	26
1.4.3.2 Electrochemical behavior of titanium in all-fluoride electrolytes	28
1.4.3.3 Electrochemical behavior of titanium in mixed chloride-fluoride electrolytes	30
1.4.3.4 Diffusion coefficients for titanium species in molten salt systems.....	31
1.4.4 Electrochemical behavior of Ti in ILs	32
1.5 Short description of some industrial processes of Ti production.....	36
2. Experimental part.....	40
2.1 Chemicals.....	40
2.2 Conductivity.	41
2.3 Cyclic voltammetry and chronopotentiometry.....	41

2.4 Viscosity and density.....	42
2.5 IR spectroscopy.....	42
2.6 Surface analysis.....	42
2.7 Deposition experiments.....	42
3. Results and discussion.....	43
3.1 Physical-chemical properties of trialkyl substituted imidazolium based ILs.....	43
3.1.1 Density and molar volume.....	43
3.1.2 Viscosity.....	44
3.1.3 Conductivity.....	48
3.1.4 Electrochemical stability of the ILs.....	52
3.2 Physical-chemical properties of some alternative ILs.....	56
3.2.1 N-butyl-N-trimethyl-ammonium bis(trifluoromethylsulfonyl)imide.....	56
3.2.2 N-butyl-N-methyl-pyrrolidinium bis(trifluoromethylsulfonyl)imide.....	58
3.2.3 1-allyl-3-methyl imidazolium chloride (AllMeImCl).....	60
3.3 Electrochemistry of titanium (IV) in 1-butyl-2,3-dimethyl imidazolium tetrafluoroborate (BMMImBF ₄).....	64
3.4 Anodic dissolution of Ti in BMMImBF ₄	77
3.5 Electrochemistry of Ti(IV) in 1-butyl-2,3-dimethyl imidazolium azide (BMMImN ₃).....	83
3.5.1 Electrochemical behaviour of TiCl ₄ ·2THF in BMMImN ₃	83
3.5.2 Electrochemistry of TiCl ₄ ·in BMMImN ₃	86
3.6 Electrodeposition experiments.....	101
3.6.1 TiCl ₄ in BMMImN ₃	101
3.6.2 TiCl ₄ in BMMImBF ₄ at elevated temperatures.	105
3.6.2.1 Medium concentration of TiCl ₄ in BMMImBF ₄ (0.05 mol l ⁻¹).....	105
3.6.2.2 Saturated solution of TiCl ₄ in BMMImBF ₄	116
3.6.2.3 Pulsed potential electrodeposition at 180°C.....	120
3.6.3 TiF ₄ in BMMImBF ₄ at elevated temperatures.....	123
4. Conclusions.....	126
Literature index.....	129
Appendixes.....	135

Introduction

Imidazolium based Ionic Liquids (ILs) have gained considerable interest due to their property variability. The imidazolium can be substituted easily and therefore a variety of properties is achievable. The probably most well known group of imidazolium based ILs is 1,3-alkyl substituted, due to their low melting points, viscosity and high conductivities. Their physico-chemical properties were studied intensively [1996Bon, 1999McEwen, 2004Was]. The relatively low cathodic stability of the disubstituted imidazolium cation limits their application for electrochemical purposes [2003Nis, 2005Mat] because the cations undergo cathodic dimerisation and dialkylation reactions involving acidic H in 2-position.

Due to the absence of an acidic proton in the 2-position, 1,2,3-trialkylated imidazolium cation-based ILs show superior electrochemical stability compared to the 1,3-substituted ones [1987Gif]. Therefore, their use in electrochemical applications, namely as electrolytes for the deposition of electropositive metals, is preferable to the use of disubstituted imidazolium based ILs. However, prior to their use as electrolytes, basic knowledge about the physico-chemical properties has to be obtained in order to find optimal application conditions. Another important factor appears when using a mixture - the effect of two different anions on the properties of the resulting ionic liquid.

Beside viscosity, density and conductivity measurements, basic electrochemical properties of the ILs were investigated as well.

The possibility of Ti electrodeposition was always attractive for researchers, therefore electrochemistry of Ti was widely investigated in high temperature molten chlorides and fluorides [1992Tar, 1984Mak, 1999Shap, 1998Okab, 2001Tan, 2000Chen, 2002Ono, 2002Suz].

Deposition of Ti from highly concentrated alkaline solutions, claimed by E. Pokorney in 1930 [1930Pok], could not be reproduced. In strongly acidic low temperature salts, it proved to be impossible to reduce Ti(IV) species to Ti(0) [1990Car]. Nevertheless, Al-Ti alloy was deposited from oversaturated Ti(II) solution in 1-ethyl-3-methylimidazolium chloride melt by Tsuda et al. [2003Tsu], as well from Ti(II) in AlCl₃:NaCl melt [1994Staf]. Lisowska and Biallozor [1982Lis] investigated the electroreduction of TiCl₄ in DMSO and reported the mechanism as an irreversible reduction of Ti(IV) to Ti(III) followed by a secondary chemical reaction. The reduction to Ti metal was not achieved.

Electrochemistry of Ti organometallic complexes have been studied in aromatic solvents by Abbot et al. [1993Abb]. The authors claimed to receive dendritic Ti deposits.

The introduction of low temperature ionic liquids (ILs) as electrolytes opened new possibilities to the electrochemistry of refractory metals. The electrochemistry of refractory metals in these electrolytes was investigated by a number of authors [1990Car, 2003Tsu, 2003Muk, 2005Muk, 2005Kat, 2006Abed]. A water free, low-melting and completely ionic medium seems to be a good candidate for studying the possibilities of getting new coatings with desirable characteristics.

Mukhopadhyay et al. investigated Ti in disubstituted imidazolium based IL and managed to deposit micro quantities of Ti on highly oriented graphite [2003Muk] and gold (111) [2005Muk]. In both cases, the deposit was quite hard to trace and in situ electrochemical scanning tunnelling microscopy was applied.

There is yet no clear understanding of the processes and intermediate products of Ti compounds during reduction reactions in imidazolium based ILs. The 1,2,3-trialkylated imidazolium cation-based ILs exhibit higher electrochemical stability [2003Tru], therefore they were chosen for studying electrochemical reduction behaviour of TiCl_4 .

Cyclic voltammetry (CV) and chronopotentiometry (CP) techniques have proven to be useful for determining the multistep reaction mechanism of Ge(IV) [1981Del], Si(IV) [1987And], U(IV), Nb(V) and Hf(IV) [1999Boi] electroreduction in high temperature molten salts.

In the present work, we applied these techniques for studying Ti (IV) electrochemistry in trialkylated imidazolium based ILs.

1.Literature overview

1.1 Ionic liquids (ILs): structure, origin, undesired impurities.

Historic overview.

Lately, a lot of interest has been concentrated around the promising class of solvents which are addressed as low temperature molten salts, ionic solvents, ionic liquids (IL).

So what is an Ionic liquid?

For convenience, there has been an unwritten convention to follow John S. Wilkes who defines ILs as “salts with a melting point below the boiling point of water” [2004Was].

The earliest evidence of substance that meets the current definition was observed in Friedel-Crafts reaction in the middle of 19th century as a separate liquid phase called the “red oil”. It has been proven afterwards using NMR techniques, that it has been a liquid salt.

Some alkylammonium salts were found to be liquid in the early years of the 20th century [1914Wal]. Later, in 1960-s John Yoke at Oregon State University reported that the mixtures of copper (I) chloride and alkylammonium chlorides are often liquids [1963Yok]. Also in 1970-s, Jerry Atwood at the University of Alabama discovered an unusual class of liquid salts he termed “liquid clathrates” [1976Atw]. The formula for the IL is $M[Al_2(CH_3)_6X]$, where M is an inorganic or organic cation and X is a halide.

None of the described materials were direct predecessors of the present generation of ILs.

The driving force for research in the field of low temperature molten salts was getting the advantages (highest concentration of the charge carriers possible, high currents, conductivities and so on) of molten salts without the disadvantages (high energy consuming, problems with the stable electrode and electrolyzer materials etc.).

Originally, the idea of this generation of ILs comes from the aluminium industry. An ionically conductive electrolyte (mixture of $AlCl_3$ and 1-ethylpyridinium halides) has been patented [1948Hur] in 1948.

Significant amount of work has been done in this direction in the U.S. Air Force Academy. They adapted the idea for replacing salts that were used as electrolytes in primary batteries [1982Wil, 1986Hus] and as solvents for electrodeposition of metals [1996Mit, 1986McM, 1992Hus]. It resulted in finding and characterizing another pseudo-binary melt – 1-butylpyridinium chloride/ $AlCl_3$. The properties has been measured and published [1978Gal].

This paper initiated the increase of activities in ILs.

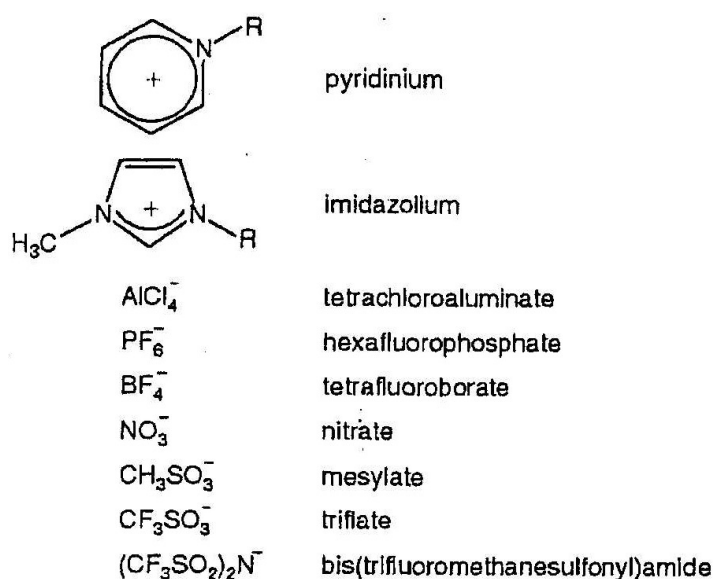


Fig. 1.1 Mostly common cations and anions used to form ILs [2004For].

Alkylpyridinium cations are relatively easy to reduce, but more stable turned out to be imidazolium based ILs.

1-ethyl-3-methyl imidazolium [EMIm]Cl mixtures with AlCl_3 were discovered to be liquid at room temperature over a wide range of compositions [1982Wil].

Pyridinium and imidazolium (Im) based chloroaluminate ILs have the disadvantage of being reactive with water.

In the early 1990s, the first air and water stable ILs were developed and characterized [1992Wil]. The authors discuss as examples ILs with hexafluorophosphate, tetrafluoroborate, nitrate, methanesulfonate ('mesylate'), trifluoromethan sulfonate ('triflate'), and bis(trifluoromethansulfonyl)amide ('TFSA') anions (see Fig.1.1).

Due to these discoveries in the field of ILs the subject has been developing rapidly in the recent years.

1.1.1 Low temperature IL: synthesis and purity issues

The story of low temperature ILs as we consider them now is generally related to the first report of preparation of ethylammonium nitrate in 1914 [1914Wal]. It has been formed by the addition of the concentrated nitric acid to ethylamine, after which the water was removed by distillation. The application of this type of salts is severely limited by a decomposition reaction through deprotonation [2004Was]. The most widely used salt of this type is pyridinium hydrochlorid.

At present, most of the ILs are formed from cations that have at most weakly acidic protons (Fig. 1.2).

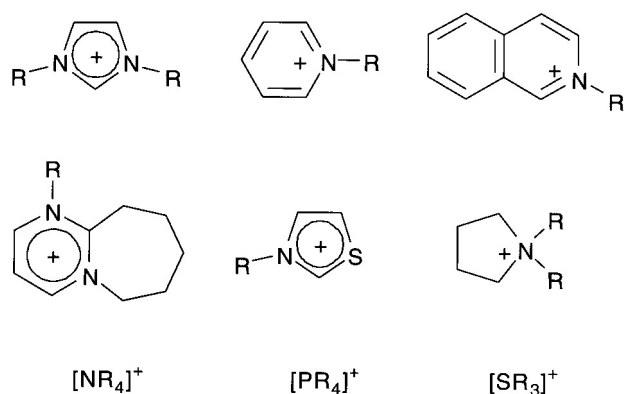


Fig.1.2 Cations used for formation of the ILs [2003Gor].

The preparation of the ILs can be split into two steps: the formation of the desired cation, and ion exchange reaction to form the final product.

The formation of the cations may be carried out either by protonation with a free acid as noted above, or by quaternization of an amine or phosphine, most commonly with the alkyl halide. A similar method has been reported for the formation of the long alkyl chain substituted 1-alkylimidazolium chloride, nitrate and tetrafluoroborate salts [2000Lee].

The most common starting material so far is 1-ethylimidazolium. Also, the synthesis of 1-alkylimidazoles can be achieved without any great difficulty as noted in Fig.1.3.

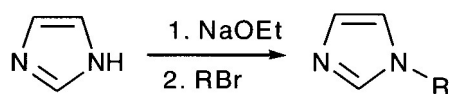


Fig.1.3 Synthesis of 1-alkylimidazoles [2003Gor].

Relatively little information has been reported regarding the determination of the purity of the halide salts other than by standard spectroscopic measurements and microanalysis (NMR, mass-spectrometry). This is mainly because the halide salts are rarely used as solvents themselves, but often used as a source of the desired cation. Also, the impurities likely to be present in any significant quantity are unreacted starting materials and residual reaction solvents [2004Was].

The removal of the haloalkanes and reaction medium is generally not a problem, especially for the relatively volatile haloalkanes with a shorter chain. On the other hand, the presence of small quantities of unreacted 1-methylimidazol could cause problems for many applications. Its high boiling point (198⁰C) makes it hard to separate from ILs.

1.1.2 Imidazolium based ILs: synthesis and purity issues

The subject of the current paragraph is to discuss synthesis of the class of the ILs that are used in the present work.

It is extremely important to estimate all the risks of contamination on each stage of the synthesis process and to account for it in the electrochemical experiments.

The synthesis of water and air stable imidazolium substituted ILs were reported in 1992 [1992Wil]. A metathesis reaction between [EMIm]I and various silver salts in methanol or water – methanol solutions has been performed. Low solubility of AgI in these solutions gave the possibility to separate it from ILs.

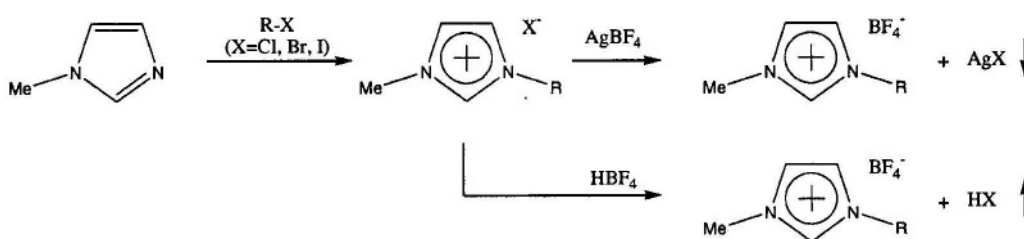


Fig.1.4 Different schemes of 1-alkyl-2-methylimidazolium tetrafluoroborate synthesis [2003Nis].

Ag – halides have limited solubility in ILs and the cost of the initial component for ion exchange reaction (AgBF₄) is also high.

Therefore, a different synthesis method has been found to reduce the quantity of undesired impurities [2001Lan]. The IL was formed by metathesis of BMImCl and HBF₄ in aqueous

solution. The product is then extracted with CH_2Cl_2 , and the organic phase is afterwards washed with successive small portions of deionized water until the washing solutions are pH neutral. The CH_2Cl_2 is then removed by a rotary evaporator, and the IL is further purified by mixing with activated charcoal for 12 hours. Finally the liquid is filtered through a short column of acidic or neutral alumina and dried by heating in vacuum.

Metathesis reaction can be performed in organic medium (CH_2Cl_2 , acetone) and not in water from the very beginning but in this case the initial products are not completely soluble in the reaction medium. [2004Was]

An example of synthesis procedure of 1-butyl-2,3-dimethylimidazolium tetrafluoroborate [2006Ho]:

A solution of 1-bromobutane (119 ml, 1.1 equiv) was added slowly and cautiously to 1,2-dimethylimidazole (96.1 g, 1 mol) in 500 ml acetone. The mixture was gently heated at reflux under argon for 24 h. After cooling to room temperature, a white solid precipitated out and the yellowish solvent was decanted. The white solid (1-butyl-2,3-dimethylimidazolium bromide, [BMMIm]Br) was washed thoroughly with acetone (2×300 ml) and ether (2×300 ml). A 2 l round bottle flask was then charged with 1.5 l acetonitrile, [BMMIm]Br, and sodium tetrafluoroborate (120 g, 1.1 equiv). The mixture was allowed to stand at room temperature for three days with stirring. The precipitate (NaBr) that appeared was filtered off and the filtrate was concentrated under vacuum to give a colorless liquid. Further precipitation of NaBr was achieved upon the addition of dichloromethane (1 l). The crude IL was purified on a silica column using dichloromethane as eluent to give a colorless liquid. Yield: 201.6 g (84%). ^1H NMR (CDCl_3 , δ ppm): 7.32 (dd, 2H), 4.07 (t, 2H), 3.80 (s, 3H), 2.61 (s, 3H), 1.76 (m, 2H), 1.37 (m, 2H), 0.93 (t, 3H).

Preparation of ILs exhibiting high purity turned out to be a difficult task.

It is not possible to purify ILs by distillation due to their low vapor pressure. On the other hand this characteristics made it possible to separate the volatile impurities quite easily.

In general, it is better to concentrate the activities on the purity of the starting materials and choosing a synthesis mechanism that either allows easy separation of the side reaction products or keep their quantity as low as possible.

For example haloalkanes prior to use are washed with portions of concentrated sulfuric acid until no further color is removed into the acid phase, then neutralized by NaHCO_3 solution and deionized water, and finally distilled. The impurities that are removed are

neither detectable by NMR nor by CHN analysis but they are thought to be responsible for coloring the final product – IL.

Purification of the ILs formed by anion metathesis can raise a set of considerable difficulties. In this case the most common impurities are halide anions, or unwanted cations inefficiently separated from the final product. These impurities can complicate electrochemical studies as well as the other processes involving ILs i.e. catalysis (deactivation of a catalyst).

This is a problem for the ILs reacting with water, since the water stable ILs can be purified efficiently by washing with pure water.

1.1.3 Cation, anion and impurities influence on the properties of the ILs

As it has been defined in section 1.1, ILs are considered as salts with a melting point below the boiling point of water.

Generally, the physico-chemical properties of the ILs depend primarily on the nature of the anions and origin and quantity of the impurities. Commonly the use of different anions has a more dramatic and wide ranging effect on the physical and chemical properties of ILs than the variation of the cation.

Anion

Anions that form room temperature ILs are usually weakly basic inorganic or organic compounds that have a delocalized negative charge. Factors effecting viscosity of the ILs are poorly understood, but the chemical structure of the anion has a particularly strong influence – the lowest viscosity ILs are formed from the small anions that have a delocalized negative charge and do not take part in any hydrogen bonding [2004For].

Anion water stability is one of the parameters greatly influencing the properties of the resulting IL. For example, PF_6^- is much less hydrophilic than the BF_4^- anion. Hydrophobic ILs almost always involve perfluorinated anions.

Tetrafluoroborate and triflate anions require N-butyl or N-hexyl substituent before displaying hydrophobic characteristics, providing the evidence of some cation influence.

The most common anions that produce hydrophilic ILs include mesylate [2000Kit, 2002Gol], trifluoroacetate, and CH_3CO_2^- [1992Wil, 2001Sed].

Cation

Usually cations that produce ILs with low melting temperatures are organic structures with low symmetry. Figure 1.5 shows some alternatives, based on substituted 5-ring systems, to the popular imidazolium cations: pyrazolium, triazolium, thiazolium, and oxazolium [2003For]. Metathesis of these substances to salts with anions like triflate or tetrafluoroborate, lowers the melting temperature to near or below room temperature. As a rule there is a further decrease in melting points with the increase of alkyl chain in the range of 3 – 5 carbon atoms.

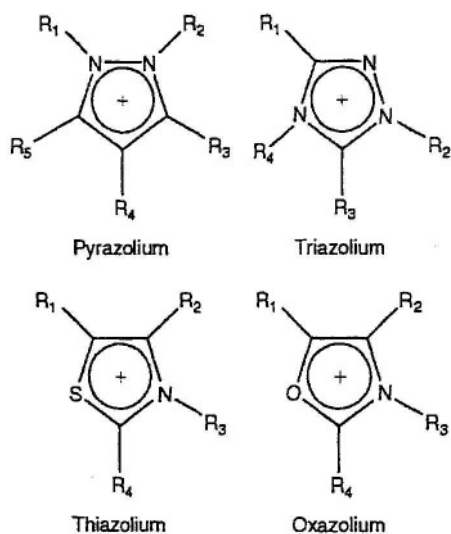


Fig.1.5 Five-membered heterocyclic cations

Figure 1.6 shows examples of “task specific” cations, designed specially to imply a desired property to the ILs.

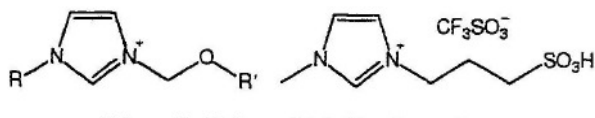


Fig. 1.6 Task specific imidazolium cations [2003For].

Impurities

The variability of data collected on the same ILs in literature shows that up to now there is no purity standard and a lot of impurities remain undetected.

Some problems arising in preparation of the water miscible ILs were studied by Seddon et al. [2000Sed] who studied the Na^+ and Cl^- concentrations in the range of the ILs formed by treatment of $[\text{EMIm}]\text{Cl}$ with $\text{Ag}[\text{BF}_4]$, $\text{Na}[\text{BF}_4]$, $\text{Ag}[\text{NO}_3]$, $\text{Na}[\text{NO}_3]$, and HNO_3 . It turned out that properties of the ILs like density and viscosity radically change with the presence

of unwanted additives. It has been shown that all preparations using Na^+ salts resulted in high residual concentrations of Cl^- , while the use of Ag^+ salts gave rise to much lower levels. The low solubility of NaCl in the ILs, however, indicated that the impurities arise from the fact that the reaction with Na^+ salts does not run with a 100% efficiency, as well as the fact, that NaCl salt is more soluble in water residues, always preset in ILs in ppm quantities.

Another example of the metal impurities is seen when $[\text{EMIm}][\text{CH}_3\text{CO}_2]$ is prepared from $[\text{EMIm}]\text{Cl}$ and $\text{Pb}[\text{CH}_3\text{CO}_2]_2$. The resulting salt contains large amount of residual lead (ca. 0.5 M) [2000Ham].

Small amounts of impurities colouring a supposedly colorless ILs are usually not detectable by ^1H NMR or CHN microanalysis. Up to now the exact origin of these impurities is not determined, but it seems likely that it comes from side reactions involving the oligomerization or polymerization of small amounts of free amine, or else from the impurities of haloalkanes.

Water still remains the most common impurity that can be present in quite high concentrations. Even water stable ILs such as $[\text{BMIM}][\text{BF}_4]$ and $[\text{BMIM}][\text{PF}_6]$ can absorb up to ca. 2 wt.% water on equilibrium with air. This is why it is recommended to heat the ILs under vacuum for several hours before use for getting rid of the residual water.

All the facts of contamination with undesirable impurities make it difficult to achieve high quality results when dealing with ILs. Depending on the quality of the ILs available, researchers get different results with the same substances. That makes the knowledge about nature and quantity of impurities even more crucial.

1.2 Physical-chemical properties

1.2.1 Phase transition behavior

ILs, consisting of totally ionized components and displaying relatively weak ion-ion pairing, have little or no measurable vapor pressure. The extent of the liquid range is limited by decomposition at elevated temperatures.

The thermal behavior of many ILs is relatively complex. For a typical IL, cooling from the liquid state causes glass formation at low temperatures; the solidification kinetics is slow. On cooling from the liquid, the low-temperature liquid region is not usually bounded by the melting point, but rather is extended down to a lower temperature limit imposed by the glass transition temperature. This tendency is enhanced by addition of lattice-destabilizing additives, including organic solvents and inorganic salts. Solidification temperatures recorded either on cooling or on heating, may not be true melting points, and may represent kinetically controlled transformations. Reliable data must be collected in the heating mode.

In many cases the glass transition temperatures are low: in the range between -70°C and -90°C .

Liquid Range

Imidazolium salts

Changes in the ring substitution patterns can have significant effects on the melting points of imidazolium salts. It can be a result of simple changes in symmetry or H-bonding interactions (i.e., substitution at C(2,4,5)-positions on an imidazolium ring affects packing and space filling of the imidazolium cations). Substitution of the C(2)-position, for example, increases the melting points of the salts. This may be caused by changes in the cation structure that can induce aromatic stacking of methyl- π interactions between cations [2004Hol].

In most cases, additional functions, such as ether groups, increase the number of interactions, and thus increase the melting point.

Imidazolium substituent with different alkyl chain length

Manipulating the alkyl chain length may produce major changes in the melting points, and also the tendency of the ILs to form glasses rather than crystalline solids on cooling, by changing the efficiency of the ion packing [2004Hol].

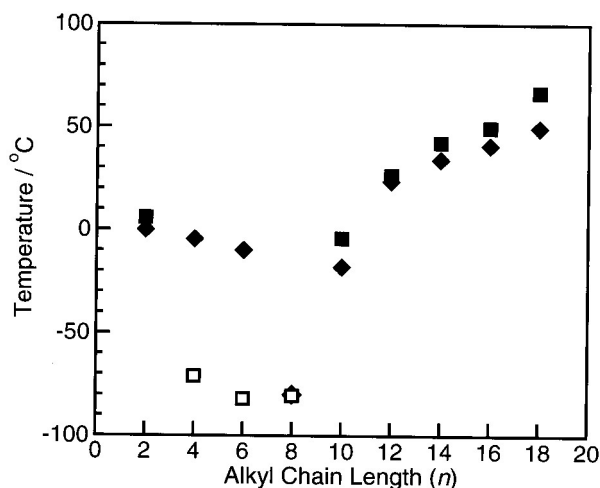


Fig. 1.7 Changes in liquification points for 1-alkyl-3-methylimidazolium tetrafluoroborate (\square) and bis(triflyl)imide ILs (\diamond) as a function of chain length, showing true melting points (solid fill) and glass transitions (open symbols) [2004Hol].

Figure 1.7 shows the changes in liquification points (either melting points or glass transitions) for a series of 1-alkyl-3-methylimidazolium tetrafluoroborate [1999Hol] and bis(triflyl)imide ILs by varying the length of the linear alkyl-substituent on the N(3)-position.

One can see from the figure that the increase of the substituent length initially reduces the melting point of the IL, with the major trend toward glass formation on cooling for $n = 4$ to 8. On extending the alkyl chain beyond a certain value (around 8 – 10 carbons for alkyl-imidazolium salts), the melting points of the salt start to increase again with increasing chain length, as van der Waals interactions between the long hydrocarbon chains contribute to the local cluster structure by induction of microphase separation between covalent, hydrophobic alkyl chains and charged ionic regions of the molecules.

The short-range structuring of the liquids is a combination of dominant Coulombic charge-charge attractions balanced against rotational and vibrational freedom of the ions. Changes of the degree of freedom and in nonparticipating portions of the cation that do not contribute to Coulombic stabilization of the crystal in salt-like lattices result in decrease of melting points and heats of formation. At longer chain lengths, amphiphilic nature

manifests itself in hydrophobic van der Waals contributions and formation of bilayer lattices.

1.2.2 Viscosity

ILs comprise a wide range of substances with various properties. Regarding the viscosity, there are two classes of fluids: Newtonian and non-Newtonian.

Most ILs now used are Newtonian fluids. Trulove and Mantz published a substantial review on the physicochemical properties of ILs covering the variety of data reported in the literature [2004Trul].

Figure 1.8 represents conductivity values plotted against viscosity for ILs listed in [2004Trul].

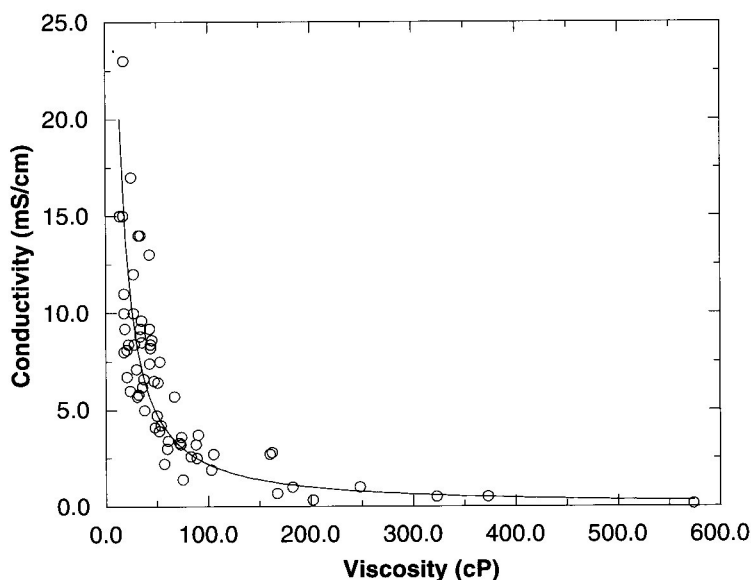


Fig. 1.8 Plot of conductivity vs. viscosity of the ILs reviewed in [2004Trul]

The conductivity and viscosity values are often combined in Walden's rule (Eq. 1.1), which states that the product of the viscosity (η) and the molar conductivity (Λ) in electrolytic solutions is a constant.

$$\Lambda\eta = \text{const} , \tag{1.1}$$

where Λ is given as:

$$\Lambda = \frac{\sigma M}{d}, \quad (1.2)$$

where σ is the ionic conductivity, M is the molecular mass of the IL and d is its density.

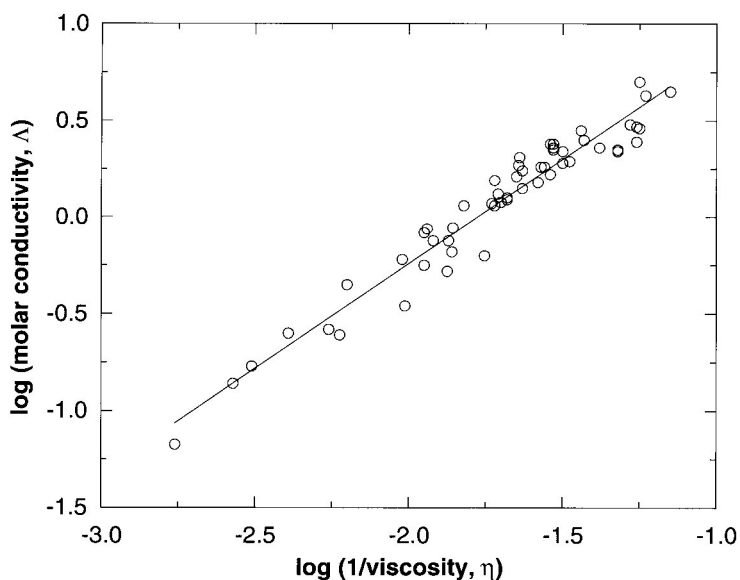


Fig.1.9 Walden plot for the ILs summarized in [2004Trul].

The literature data should be treated with care. The purity issues are not always accurately taken into account. Impurities can influence viscosity values significantly. For example contamination with chloride increases the viscosity, and contamination with water has the opposite effect [2000Sed].

1.2.3 Conductivity

The ionic conductivity of an electrolyte is of a great importance for understanding the nature of the substance as well as for a potential application. There is a variety of AC and DC methods for measuring the conductivity. For the ILs, majority of data was collected with two techniques: impedance bridge method and complex impedance method. In both methods a two-electrode cell is used to measure the impedance Z of the IL:

$$Z = \sqrt{(1/\omega C) + R_{\Omega}^2}, \quad (1.3)$$

where R_{Ω} represent the resistive contribution; C is the capacitive contribution; ω is the frequency of AC.

At higher AC frequencies the equation is reduced to $Z = R$, the resistance of the IL in the impedance cell. The conductivity can be obtained from the equation:

$$\sigma = \frac{l}{AR}, \quad (1.4)$$

where l is the distance between the two electrodes in the impedance cell and A is the area of the electrodes.

Term l/A is often referred to as a cell constant.

The conductivity of an electrolyte is a measure of the available number of charge carriers and mobility. One would expect ILs to have high conductivities as they consist entirely of ions. Unfortunately this is not completely true. ILs exhibit reasonably good ionic conductivities compared to the non-aqueous solvent/electrolyte systems (up to 10 mS cm^{-1}). The dependence of the conductivity on temperature for imidazolium-based ILs is shown in the Fig. 1.10.

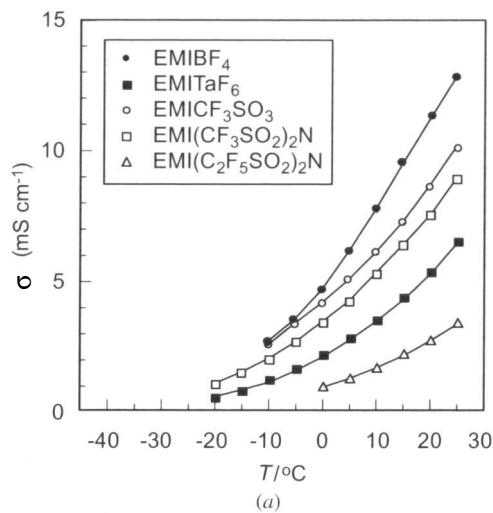
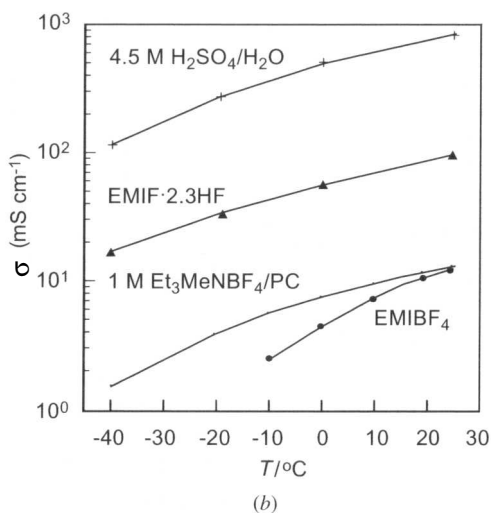


Fig. 1.10 Temperature dependence of electrolytic conductivities of ethyl-methyl-imidazolium ILs with various anions (a)



compared to conventional aqueous and non-aqueous electrolyte systems (b). [2005Ue]

However, IL conductivities are significantly lower compared to concentrated aqueous electrolytes. This effect can be attributed to the decrease in number of charge carriers due to ion pairing and/or ion aggregation and to the reduced ion mobility resulting from large ion size [2003Tru].

The conductivity – temperature relation for the ILs in some cases can be fitted by the Arrhenius equation. Some literature data on activation energies derived from Arrhenius activation are listed in the Table 1.1.

Table 1.1 Literature data on Arrhenius activation energies for some imidazolium ILs

IL	E_A / kJ mol ⁻¹	Reference
EMImTf	17.6	[1998Ful]
EMImTf	15.9	[2000Eve]
EMImNTf ₂	14.0	[2000Eve]
EMImBF ₄	18.0	[1998Ful]
EMImPF ₆	25.5	[1998Ful]
OMIm[PF ₆]	48.6	[2002McL]
BuMMIm[NTf ₂]	29.7	[2002McL]

M – methyl; E – ethyl; Bu - buthyl; O- octyl; Im – imidazolium; Tf – trifluoromethylsulfonate; NTf₂ - bis(trifluoromethylsulfonyl)imide.

In most cases, conductivity of the ILs in the vicinity of the glass transition temperatures can be described by an empirical Vogel-Tamman-Fulcher (VTF) equation:

$$\ln \sigma = \ln \sigma_0 + \frac{-k}{T - T_0} \quad (1.5)$$

where σ_0 and k are constants and T_0 is the ideal glass transition temperature.

Figure 1.11 shows some examples of Arrhenius plots of temperature dependence of conductivity data [1999McEwen, 2001Nod, 2004Trul]. Solid lines represent the best fit with VTF equation.

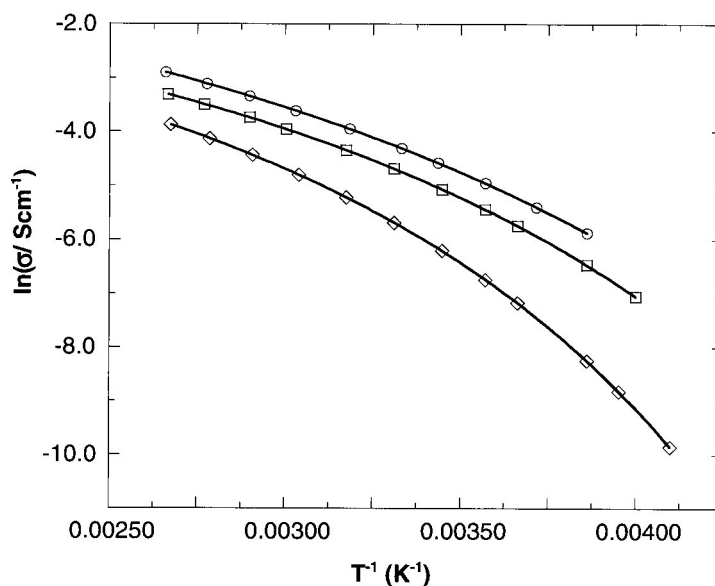


Fig. 1.11 Examples of Arrhenius plots for [EMIm]BF₄ (○), [EMIm][(CF₃SO₂)₂N] (◇) and [PMMIm][(CF₃SO₂)₂N] (□) [2004Trul].

The temperature dependence of conductivity is a result of a complex interaction of short- and long-range forces that is strongly influenced by the type of the cation and anion [2004Tru]. Up to now there is no accurate way of predicting the conductivities in relation to structure of the ILs.

1.2.4 Temperature stability

The upper limit of the liquid range is usually defined by the thermal decomposition of the IL. In contrast to molten salts, which form tight ion-pairs in the vapor phase, the reduced Coulombic interactions between ions energetically restrict ion-pair formation required for volatilizing the salts, producing low vapor pressures.

The nature of the ILs, containing organic cations, restricts upper stability temperatures. Pyrolysis generally occurs between 350°C to 450°C if no other lower temperature decomposition pathways are possible. Grimmet et al. have studied the decomposition of imidazolium halides [2005Grim] and identified the degradation pathway as E2 elimination of the N-substituent, essentially the reverse of the S_N2 substitution reaction used for the formation of ILs.

If we compare the decomposition temperatures for ILs with different anions, the stability of the IL will be inversely proportional to the capability for the stable alkyl-X species

formation. As can be seen from TGA decomposition data for a range of [RMIm] salts (Fig. 1.12), the decomposition temperatures vary with the anion type in the following order, $\text{Cl}^- < [\text{BF}_4]^- \sim [\text{PF}_6]^- < [\text{NTf}_2]^-$, so that ILs containing weakly coordinating anions are most stable to high temperature decomposition.

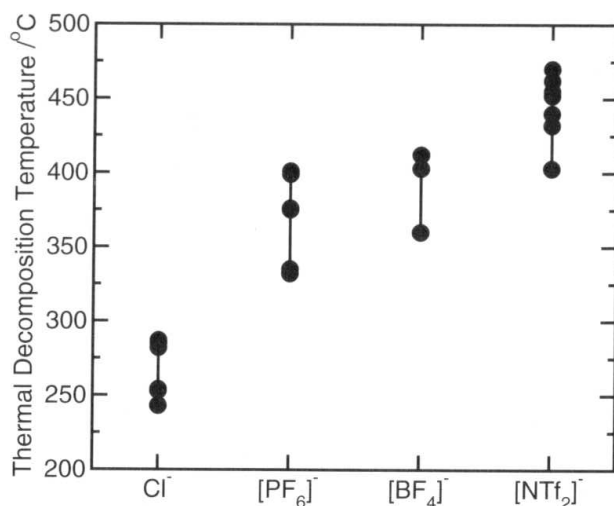


Fig. 1.12 Thermal decomposition temperatures for ILs containing 1-alkyl-3-methylimidazolium cations [2004Hol].

Ngo et al. [2000Ngo] have shown that the thermal decomposition of the ILs, measured by TGA, depends also on the sample pans used. Increased stabilization of up to 50°C was observed in some cases on changing from aluminum to alumina sample pans.

1.3 Electrochemical behavior of ILs

Electrochemical stability of the ILs is an important issue for understanding the reaction mechanisms in this medium as well as for considering the potential application.

Chloroaluminate systems have been studied extensively over the last decade. The most significantly different feature of these systems is that the mole ratio between the organic chloride and AlCl_3 varies. Usually the mole fraction of AlCl_3 is denoted as N ($=[\text{AlCl}_3]/([\text{AlCl}_3]+[\text{RCl}])$). The chloroaluminate systems are categorized by the N values: $N > 0.5$ – acidic, $N = 0.5$ – neutral and $N < 0.5$ – basic melts.

The potentials in these systems are often measured against the Al/Al^{3+} couple.

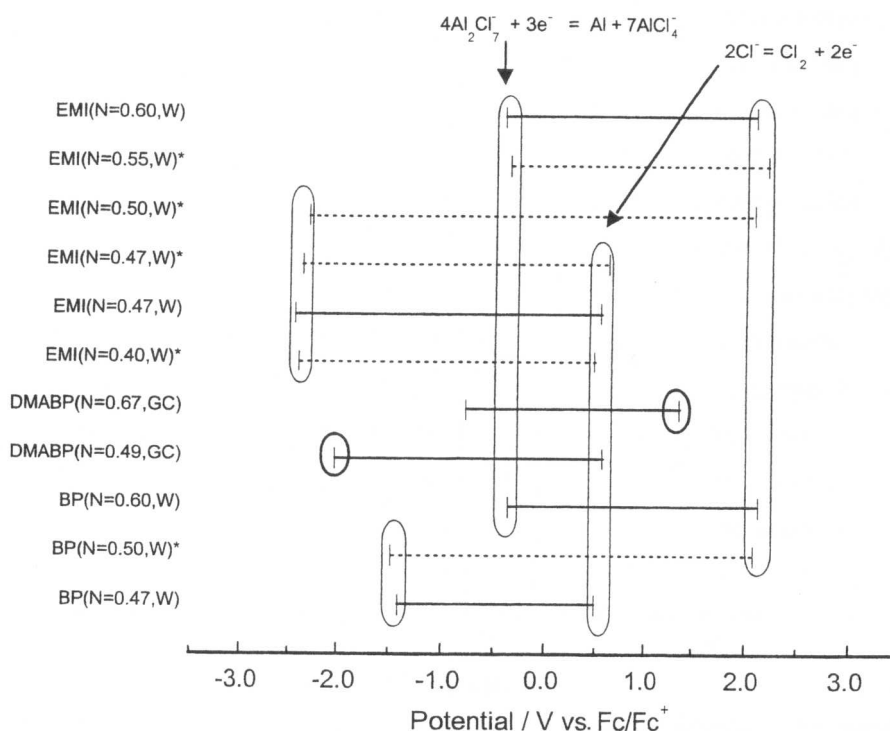
Table 1.2 shows the ions involved in the potential determining reactions.

Table 1.2 Ionic species associated with a cathodic and anodic limiting potential of chloroaluminate melts [2005Mat].

Composition (N^*)	Anions in melts	Species limiting the	
		Cathodic potential	Anodic potential
$N > 0.5$ acidic	Al_2Cl_7^- , AlCl_4^-	Al_2Cl_7^-	AlCl_4^-
$N = 0.5$ neutral	AlCl_4^-	Cation	AlCl_4^-
$N < 0.5$ basic	AlCl_4^- , Cl^-	cation	Cl^-

* mole fraction of AlCl_3

Figure 1.13 shows the electrochemical windows of various chloroaluminate systems. One can see that the electrochemical window is dependant on the melt composition.



EMI (1-ethyl-3-methylimidazolium), DMABP (p-dimethylamino-N-butylpyridinium), BP (N-butylpyridinium)

Fig.1.13 Electrochemical windows of chloroaluminate systems. Working electrodes: GC(glassy carbon); W (tungsten); the potential was measured against ferrocene couple (Fc/Fc⁺) [2005Mat].

The instability on air and relative low electrochemical stability of the chloroaluminate systems pushed the researchers to studies of the non-chloroaluminate. Fluoroanions were extensively studied [2000Har].

The electrochemical stability windows reported so far are reviewed in [2005Mat].

The measured values of the cathodic and anodic decomposition potentials obviously differ because of the type of the reference electrode. The ranges of current densities used for determining the limiting potentials were different. For these reasons comparison of the electrochemical windows for different ILs is complicated, even if we do not take into consideration the errors caused by varying other experimental parameters (potential sweep rate, purity).

The cathodic limit of the electrochemical window is generally governed by the cation reduction and the anodic – by anion oxidation. However, the anodic limit of EMI⁺ is determined by the cation, since it is independent on the anion.

It has been proven that EMIm^+ has not only inferior cathodic stability to Et_3MeN^+ but also inferior anodic stability to BF_4^- [2005Ue]. It follows from the comparison of electrochemical window of EMImBF_4 (Fig. 1.14a) and those of 0.5 M $\text{EMImBF}_4/\text{PC}$ and 0.5M $\text{Et}_3\text{MeNBF}_4/\text{PC}$ (Fig. 1.14b) [2002Ue].

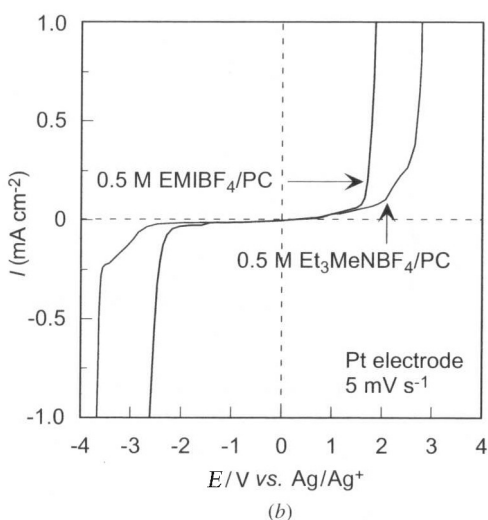
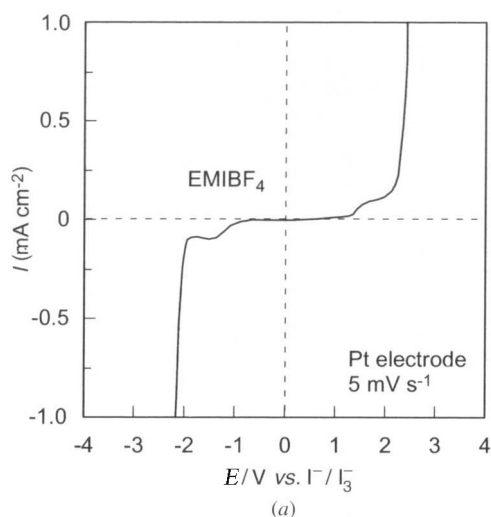


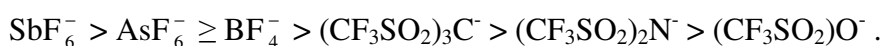
Fig. 1.14 Linear sweep voltammograms on Pt electrode

(a) EMImBF_4 , $\text{EMImBF}_4/\text{PC}$

(b) $\text{Et}_3\text{MeNBF}_4/\text{PC}$ [2002Ue].

This narrower electrochemical window indicates that EMIm^+ is more sensitive not only to reduction but also for the oxidation due to existence of a π -electron conjugated system.

Concerning the stability of the anions, it has been shown by ab initio molecular orbital and density functional calculations that the ionization energies of the MF_n^- type anions are larger than those of the $(\text{CF}_3\text{SO}_2)_n\text{X}^-$ anion (organic fluoranions). The order of anion stability observed in PC solutions was found to be applicable to IL systems [1997Ue]:



Electrochemistry of 1-butyl-3-methyl-1H-imidazolium tetrafluoroborate (BMImBF₄) IL was studied in detail by the group of Johnson [2003Xia].

The cyclic voltammetry with Pt electrodes yielded an electrochemical window of 4.9V (+2.9V to -2.0V vs. Ag/AgBF₄) (Fig. 1.15), wider than that of EMImBF₄ (4.5, +2.5V to -2.0V vs. Ag/AgCl).

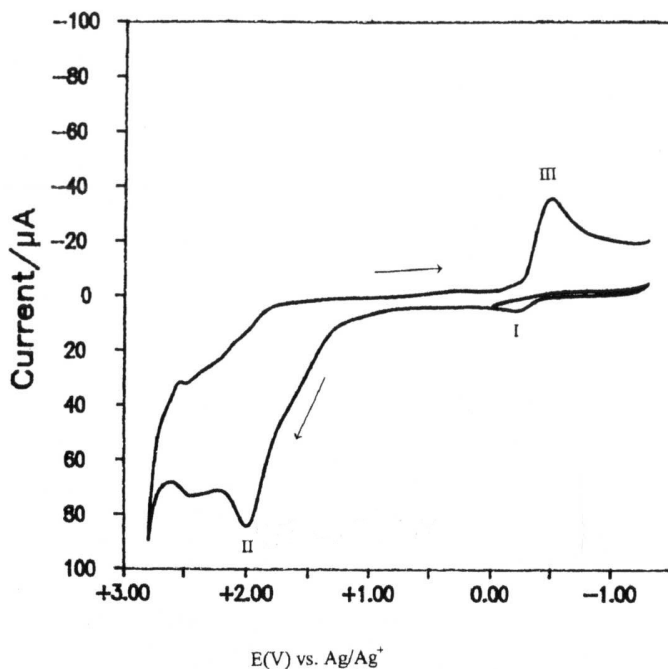


Fig. 1.15 Cyclic voltammogram of BMMImBF₄ on 1mm Pt electrode at room temperature, scan rate 100 mV/s [2003Xia].

When sweeping negatively from 0V, there was no reduction peak up to -2V but after reversal at -2V, there appeared an oxidation peak at -0.13V (peak I) which was dependant on the previous reduction potential. When the cathodic end potential moved from -2 to -1.5V, peak I was reduced in size from 150 to 8 μ A, and the peak potential shifted from +0.2 to -0.13V. It is concluded from the above observation, that the peak I is due to the oxidation of the reduction product of 1-butyl-3-methyl-1H-imidazolium cation, which is in accordance with previous reports. [1994Ful, 2001Kat]. The oxidation peak at 2V (peak II) is due to the chlorine impurity in the IL, which is confirmed by additional dissolution of Cl⁻ containing reagents (1-butyl-3-methyl-1H-imidazolium chloride or HCl gas). The increase of peak II was visible in both cases.

On sweeping in the negative direction from 0V, there was no peak at -0.9V but upon reversal at the second cycle there was a reduction peak at -0.9V (peak III). This showed that the peak III was related to the oxidation limit, but did not originate from the initial IL.

The higher is the oxidation potential, the larger the reduction current of peak III is. Hence it was the reduction either of the oxidation product of BF_4^- or oxides on the Pt electrode [2003Xia].

Based on the spectroscopic and chromatography studies of the electrolyte decomposition products, the authors propose mechanisms of the cathodic and anodic decomposition reactions (Fig.1.16).

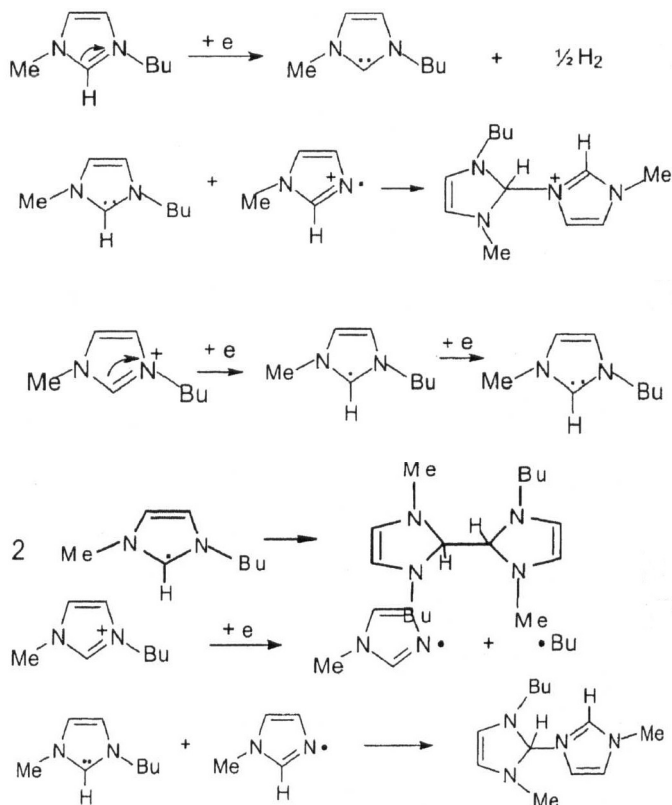


Fig.1.16 Mechanism of the cathodic decomposition of the BMIm⁺ cation [2003Xia].

Anodic process:



The authors conclude that BF_4^- oxidizes to BF_3 and fluorocarbons at the anode, while Bmim^+ undergoes dimerization and dealkylation reactions at the cathode after being reduced to a carbene.

The mechanism of the reaction has been proven by the NMR and gas chromatography studies of the decomposition products.

1.4 Electrochemical behavior of Ti in different media.

1.4.1 Aqueous solutions

The values of the standard electrode potentials are as follows [1975Dob]:



As we can see, the standard reduction potentials are far more negative than the one for hydrogen evolution. Hence, the Ti deposition in aqueous solutions became a challenging task.

The idea of shifting the Ti deposition potential to more positive values by simultaneous alloying with the substrate material is discussed in [1963Kud]. The authors report metallic films (3-4 μm) on lead, copper and platinum. The X-Ray analysis showed TiCu_3 - TiCu_4 phases in the deposit on copper.

Tyurin and co-workers [1990Tur] studied the Pourbaix diagram for the Ti- H_2O system. On the basis of the calculated diagrams, the authors were able to deposit thin Ni-Ti, Fe-Ti and Zn-Ti alloys.

Ti electrodeposition from the hexafluorotitanate anion was also reported in [1959Mach].

None of the authors managed to obtain a thick crystalline deposit. Titanium was always deposited in very small quantities and alloyed with the substrate. Generally, the deposition stopped when the surface alloy reached its maximum stoichiometry regarding Ti.

1.4.2 Organic solvents

Although some groups of scientists (see section above) reported reduction of Ti to a metal state in water, the task is complicated by the rapid electrolyte decomposition.

The search for a more electrochemically stable medium led to organic solvents. A lot of them have much higher cathodic stability than water. For example, propylencarbonate does not decompose to potentials -2.5V vs SCE (standard calomel electrode), tetrahydrofuran – up to -4.0V vs. SCE [1979Tih]. The problem was widely investigated in the former Soviet Union.

The solutions of titanium halogenides in alcohols, ethers and mixtures of these solvents with addition of small quantities of oleoresin and toluene were proposed for the Ti deposition.

Ti deposition is reported from a solution of TiF_4 in alcohol, with small quantity of toluene. The deposition was carried out on the freshly deposited copper layer. Similar electrolyte (mixture of ethanol, toluene and acetone), but with addition of TiCl_3 was used for deposition of Zn-Ti alloy on Cu. The alloy contained 12.8% Ti [1964Fer]. The authors state, that Na^+ and F^- ions have a negative influence on the deposition, because on addition of these ions, the Ti quantity in the alloy decreases.

The deposition of the pure radioactive Ti^{44} is reported [1973San] from the solution of TiCl_3 in dimethylsulfoxide. The authors claimed to receive Ti layers with 1 to 75 μm thickness. The temperature was 22°C, current density -0.42 A/dm², pH=2.5. The presence on 5 vol. % of water did not have any influence on the current efficiency. Inactive Ti deposits can be obtained from a solution containing 0.15 ml of saturated TiCl_3 solution in HCl and 5ml dimethylsulfoxide (DMSO). The authors propose to use these electrolytes for deposition of zirconium, hafnium, niobium, cobalt, manganese and other metals. The authors suggest, that the Ti deposition takes place from the simple ion. Sodium and fluorine ions interfere with the deposition. In the presence of these ions, the deposit quality is decreased and the colour becomes black and dull.

The Ti deposition from DMSO solution with TiCl_4 was studied in [1977Lev]. Beside the pure DMSO, the mixture with ethyl alcohol was used. The authors report a very thin deposit (0.02 μm).

Reid et al. [1957Reid] supposed that the chlorides are not the best choice for Ti deposition. The authors suggest using solutions of organometallic, hydride and borane complexes of Ti. The deposition proceeds from the complex ions, but pure Ti is not obtained.

The kinetic of Ti deposition from the solution of TiCl_4 in formamide and dimethylformamide was studied by voltammetry method [1977Levin]. The authors suggested a mixed Ti deposition kinetics. Two electrons participate in the cathodic process. The following mechanism of the cathodic process is proposed:



In dimethylformamide the formation of the donor-acceptor complex of TiCl_4 with dimethylformamide is described. The ratio is 2:1. The deposition takes place from the complex ion.

1.4.3 Electrochemical behavior of Ti in high temperature molten salts

1.4.3.1 Electrochemical behavior titanium in chloride electrolytes

Widely accepted stepwise mechanism for the reduction of Ti^{III} in chloride melts is as follows:



This behavior was found, as an example, when TiCl_3 was dissolved in NaCl-KCl equimolar melt [1992Tar]. The experiment was performed at 700°C .

Fig. 1.17 shows the voltammetric curves for a $[\text{TiCl}_3] = 8.3 \times 10^{-5} \text{ mol cm}^{-3}$ at various scan rates:

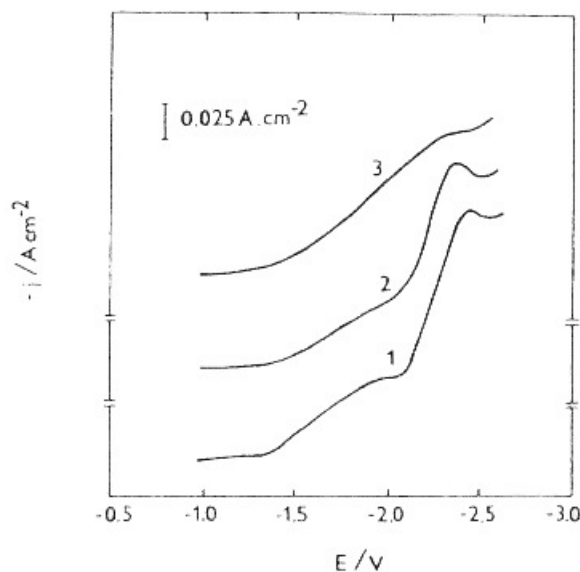


Fig. 1.17 Voltammetric curves of the reduction of Ti^{III} in the system NaCl-KCl- TiCl_3 , at different scan rates. Curve 1: $\nu = 1.0 \text{ V s}^{-1}$; curve 2: $\nu = 0.1 \text{ V s}^{-1}$; curve 3: $\nu = 0.05 \text{ V s}^{-1}$, tungsten working electrode, 700°C [1992Tar].

All curves at $\nu > 0.05 \text{ V s}^{-1}$ exhibit two clear peaks starting at potentials around -1.42V and -2.10V respectively (the potential values are referred to the chlorine electrode). The ratio of peak current densities $i_p^{\text{I}}/i_p^{\text{II}}$ approaches the value of $1/2$ at the given conditions, and their concentration dependences are linear within the concentration range $(2.5 \text{ to } 100) \cdot 10^{-5} \text{ mol cm}^{-3} \text{ TiCl}_3$, which supports the two-step mechanism mentioned above.

The presence of Ti^0 was detected at the cathode by X-Ray diffraction when potentiostatic electrolysis was carried out [1999Shap] at the second reduction wave potential, in order to confirm the correct assignment of that voltammetric curve to the final reduction step, $Ti^{II} \rightarrow Ti^0$.

The wave corresponding to the first reduction step, $Ti^{III} \rightarrow Ti^{II}$, disappears gradually when the scan rate is decreased, eventually merging with the peak for $Ti^{II} \rightarrow Ti^0$. This effect might account for the discrepancies found in the existing literature on the reduction mechanism of titanium in chloride melts.

For the $Ti^{III} \rightarrow Ti^{II}$ process Taranenکو et al. [1992Tar] proposed, based on the analysis of the voltammetric dependences of the type $i_p^{1/2} vs. v^{1/2}$, that a possible disproportionation reaction for Ti^{II} is:



This interpretation is supported by Shapoval et al. [1999Shap], calculating the disproportionation rate constant as $(2.2 \pm 0.2) \cdot 10^4 \text{ cm}^2 \text{ mol s}^{-1}$. The authors indicate two strategies for the elimination of disproportionation reactions:

- addition of cations with greater polarisability than K^+ or Na^+ ;
- addition of anions with stronger basic properties than Cl^- .

Both strategies proved to be successful.

The $TiCl_4$ reduction was investigated in the $BaCl_2$ - $CaCl_2$ - $NaCl$ system [1984Din]. The suggested mechanism is:



There is, though, no agreement on the details of these cathodic processes. Some authors even suppose the involvement of reduced alkali ions in the final reduction of titanium ions to titanium metal [1992Tar].

1.4.3.2 Electrochemical behavior of titanium in all-fluoride electrolytes

Makyta et al. [1989Mak, 1993Mak] studied the behavior of titanium and boron by adding K_2TiF_6 and KBF_4 to a LiF-KF eutectic mixture and to FLINAK (LiF-NaF-KF eutectic mixture), at different titanium salt concentrations while varying the working temperature as well (500°C, 600°C, and 750°C).

Figure 1.18 shows the voltammogram of the supporting electrolyte, an equimolar LiF-KF mixture, at 750°C, with a scan rate of 1 V s^{-1} .

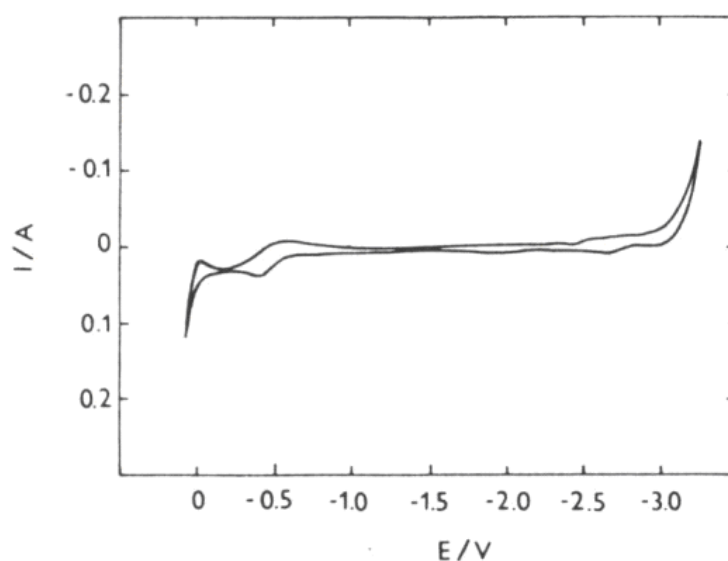


Fig. 1.18 Cyclic voltammogram of the pure supporting electrolyte, LiF-KF, at 750°C, $\nu = 1 \text{ V s}^{-1}$, Pt quasi-reference electrode [1989Mak].

Fig. 1.19 shows three different voltammetric curves, obtained in melts of different compositions.

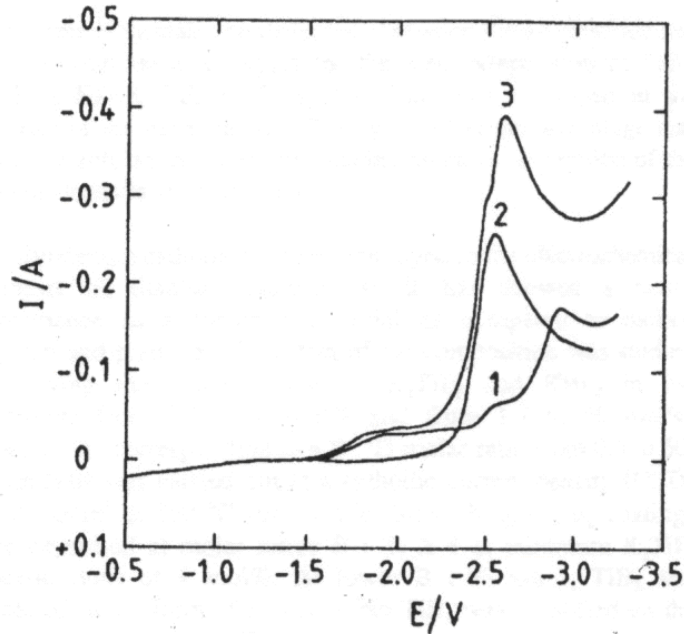


Fig. 1.19 Voltammetric curves from different melt compositions, scan rate of 1 V s^{-1} , 750°C , Pt quasi-reference electrode [1993Mak].

- (1) LiF-KF electrolyte with addition of K_2TiF_6 (concentration of 0.3 mol%)
- (2) LiF-KF electrolyte with addition of KBF_4 (concentration of 0.5 mol%)
- (3) LiF-KF electrolyte with K_2TiF_6 0.3 mol% and KBF_4 0.6 mol%.

Curve 1 shows the reduction of Ti^{IV} to metallic titanium. The mechanism for this reduction is:



where the first reduction step, $\text{Ti}^{\text{IV}} \rightarrow \text{Ti}^{\text{III}}$, occurs at -1.70 V , and the second step, $\text{Ti}^{\text{III}} \rightarrow \text{Ti}^0$, at -2.70 V (all the potential values are referred in this case to the potential of platinum “quasireference” electrode).

Comparing with Fig. 1.18, the last reduction process occurring at -3.0 V is the deposition of the alkali metal.

Curve 2 shows a single maximum at approximately -2.3 V , which can be assigned to the 3-electron reduction:



The position of this maximum is independent of the concentration of the electrochemically active species and the scan rate.

1.4.3.3 Electrochemical behavior of titanium in mixed chloride-fluoride electrolytes

Makyta et al. [1999Mak] studied the influence of fluoride content on the reduction behavior of titanium in the system NaCl-KCl-NaF-TiCl₃ at 700°C.

Fig. 1.20 shows the corresponding voltammetric curves, for a [TiCl₃]=1.55 · 10⁻⁴ mol cm⁻³ melt, for different [Ti]:[F] molar ratios, at a scan rate of 1 V s⁻¹.

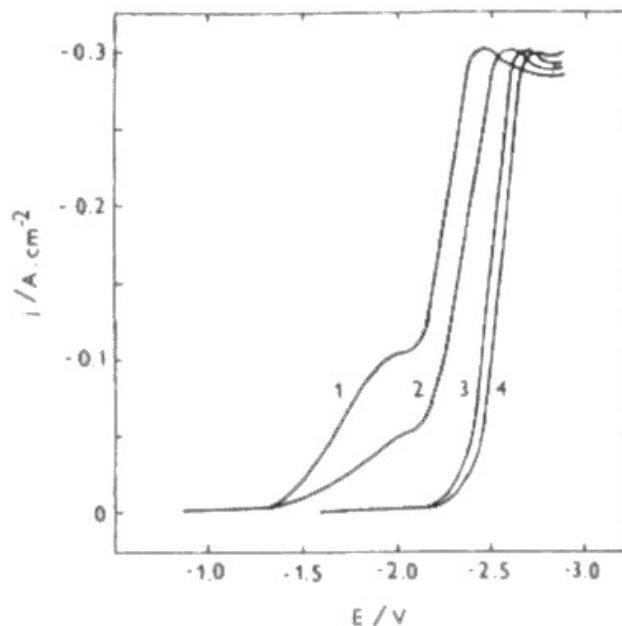


Fig. 1.20 Voltammetric curves for the reduction of Ti^{III} in the system NaCl-KCl-NaF-TiCl₃ at 700°C: curve 1 - [Ti]:[F]= 1:0; curve 2 - [Ti]:[F]= 1:1; curve 3 - [Ti]:[F]= 1:2; curve 4 - [Ti]:[F]= 1:100 [1992Tar].

As can be seen in Fig. 1.20, the reduction of Ti^{III} to Ti⁰ proceeds in two steps for molar ratios [Ti]:[F] > 1:2. However, with the increase of the fluoride concentration, the wave corresponding to Ti^{III} → Ti^{II} disappears. Thus, with [Ti]:[F] ≤ 1:2, the reduction occurs directly from Ti^{III} to Ti⁰:



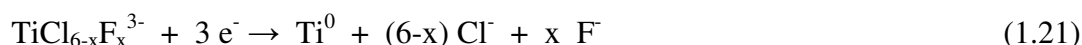
The decrease in molar ratios also shifts the peak potential towards more negative values.

In the same publication, it is stated that the potential difference between cathodic peak current density and anodic peak current density varies with the scan rate, from 0.3 V to 1.1 V, pointing to the irreversibility of the Ti^{III} → Ti⁰ electrode process. Besides, the concentration dependence of the peak current density for the reduction Ti^{III} → Ti⁰ in the

electrolyte with [Ti]:[F]= 1:100 is linear within the concentration range: $(2.5 \cdot 10^{-5}$ to $50 \cdot 10^{-5})$ mol cm⁻³ TiCl₃.

Thus, the formation of mixed chloro-fluoride complexes of titanium of the type TiCl_{6-x}F_x³⁻ is responsible for suppressing the disproportionation reaction and modifying the reduction mechanism for the Ti species [1992Tar, 1999Mak]. The following reaction was proposed:

The electrochemical reaction for the Ti(III) reduction this salt melt is:



1.4.3.4 Diffusion coefficients for titanium species in molten salt systems

The values reported for the system, have been calculated by Kaptay et al. [1997Dev], and are shown in Table 1.3:

Table 1.3 Diffusion coefficients of titanium species in the melt NaCl-NaF-KCl-KBF₄-K₂TiF₆ and its subsystems, at 700°C [1997Dev].

Melt	Cations	αv_α	D (10 ⁻⁵ cm ² /s)
NaCl-KCl-K ₂ TiF ₆ -NaF	Ti (III)	0.95 ± 0.02 *	3.00 ± 0.05 *
NaCl-KCl-NaF-KBF ₄ -K ₂ TiF ₆	Ti (III) + 2 B (III)	n~ 9 **	0.89 ± 0.05 **

*Irreversible charge transfer: αv_α (α is the transfer coefficient and v_α is the number of electrons taking part in irreversible electrochemical reaction) was calculated by the equation of Matsuda-Ayabe, and D, the diffusion coefficient, was determined by Delahay's equation.

**Reversible charge transfer with insoluble product: n, the number of electrons, was calculated using the Mamontov-Manning-Dale equation, and D was determined through the Berzins-Delahay equation.

Table 1.4 shows other values for the diffusion coefficients reported in the literature for titanium species in different molten salts systems:

Table 1.4 Diffusion coefficients of titanium species in different salt melts.

Melt - Temperature	Species	D (cm ² /s)	Ref.
KCl-NaCl-TiCl ₃ – 700°C	Ti ³⁺	$3.72 \cdot 10^{-5}$	[1999Shap]
KCl-NaCl-TiCl ₄ – 700°C	Ti ⁴⁺	$1.94 \cdot 10^{-5}$	[1999Shap]
LiCl-KCl * – 500°C	Ti ²⁺	$(1.54 \pm 0.17) \cdot 10^{-5}$	[1999Shap]
NaCl-KCl-TiCl ₃ – 727°C	Ti ³⁺	$(3.5 \pm 0.3) \cdot 10^{-5}$	[1999Shap]
NaCl-KCl-NaF-TiCl ₃ – 700°C	Ti ³⁺	$(3.0 \pm 0.4) \cdot 10^{-5}$	[1999Shap]

* The titanium salt used is not specified in the reference.

1.4.4 Electrochemical behavior of Ti in ILs

In previous years there have been some efforts in studying Ti electrochemistry in ILs especially in chloride melts [1990Car, 2003Tsu].

Osteryoung and coworkers have studied the Ti(IV) electrochemistry on Pt working electrode in the Lewis acidic molten salts (1-ethyl-3-methyl imidazolium chloride with AlCl₃) [1990Car]. As a reference electrode the authors used aluminium wires immersed in acidic 1.5:1.0 melts separated via a fritted tube. The authors note the variable behavior of the Ti(IV) electrochemistry and explain this phenomena by influence of the electrolyte aging, electrode history and so on.

The staircase voltammetry was employed to examine the Ti electrochemical couples. A staircase voltammogram of 40 mM Ti(IV) in 1.5:1.0 AlCl₃ – ImCl molten salt at a Pt electrode is shown on the Fig. 1.21.

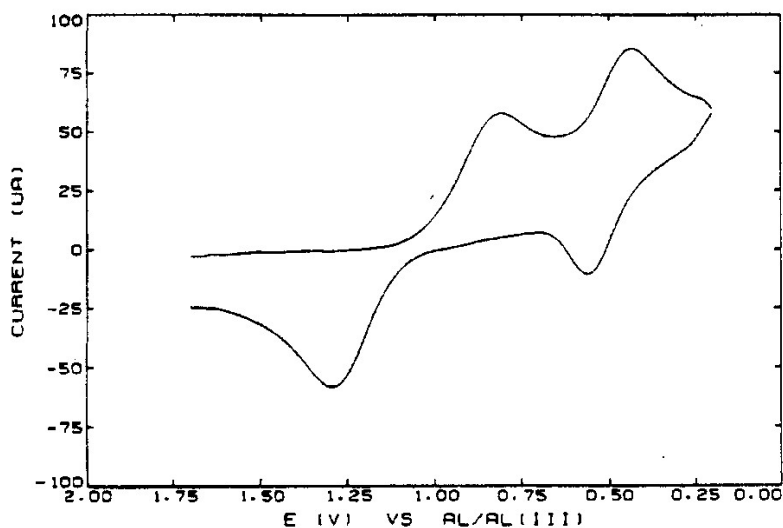


Fig. 1.21 Staircase cyclic voltammogram for reduction of 40 mM Ti(IV) in 1.5:1.0 AlCl₃ – ImCl molten salt at a Pt electrode at ambient temperature, scan rate 250 mV s⁻¹ [1990Car].

The two redox couples, Ti(IV)/Ti(III) and Ti(III)/Ti(II), are apparent. The Ti(III)/Ti(II) couple possesses a large peak potential separation with a cathodic peak potential near 0.8V and anodic peak potential at approx. 1.3V. The Ti(IV)/Ti(III) couple demonstrates more reversible behavior with cathodic and anodic peak potentials 0.4 and 0.55V respectively. They admit, that in this medium it is not possible to reduce Ti(III) species to Ti(0) state. Al – Ti alloys were deposited from Lewis acidic aluminum chloride 1-ethyl-3-methylimidazolium chloride melt [2003Tsu]. TiCl₂ was used for introducing Ti into the melt 60.0 – 40.0% mol fraction.

Anodic behavior of the Ti electrode was studied (Fig.1.22). On the anode at low current densities oxidation of Ti(0) did not lead to dissolved Ti(II), but to an insoluble passivating film of TiCl₃. At high current densities or very positive potentials, Ti(0) was oxidized directly to Ti(IV); however, the electrogenerated Ti(IV) vaporized from the melt as TiCl₄.

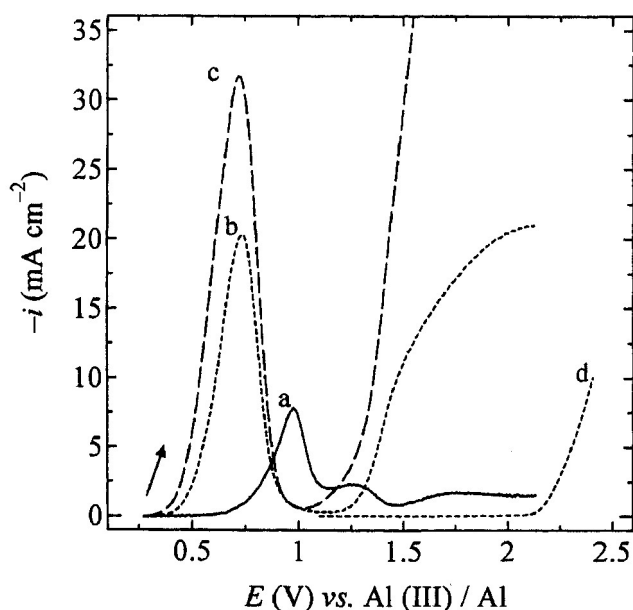


Fig. 1.22 Linear Sweep Voltammograms recorded as a function of temperature in the 66.7 m/o AlCl₃ – EMImCl melt: (a) Ti disk electrode, room temperature; (b) Ti disk electrode, 353.2 K; (c) Ti disk electrode, 373.2 K and (d) Pt disk electrode at room temperature. The potential sweep rates were 0.01 V s⁻¹ [2003Tsu].

Electrodeposition was investigated at a Cu rotating disk and wire electrodes out of saturated solution of Ti(II) in the 66.7-33.3% mol fraction at low current densities [2003Tsu]. Authors obtained Al-Ti layers with 19% atomic fraction of Ti and the Ti content in the alloy was decreasing with the increase of the current density.

There has been reported a Ti deposition on highly oriented pyrolytic graphite from 1-butyl-3-methyl imidazolium bis((trifluoromethyl)sulfonyl)amide (BMIm[BTA]) [2003Muk]. The nucleation process has been monitored by *in situ* electrochemical scanning tunneling microscopy (EC-STM).

Up to six wires grow at constant potential over a period of about 20 min.

The wires exhibit a narrow width distribution of 10 ± 2 nm and have a length of more than 100 nm.

The same authors [2005Muk] have reported electrodeposition of Ti from TiCl_4 in the IL 1-methyl-3-butyl-imidazolium bis (trifluoro methyl sulfone) imide at room temperature. As working electrode, Au(1 1 1) single crystal surface evaporated on Cr was used.

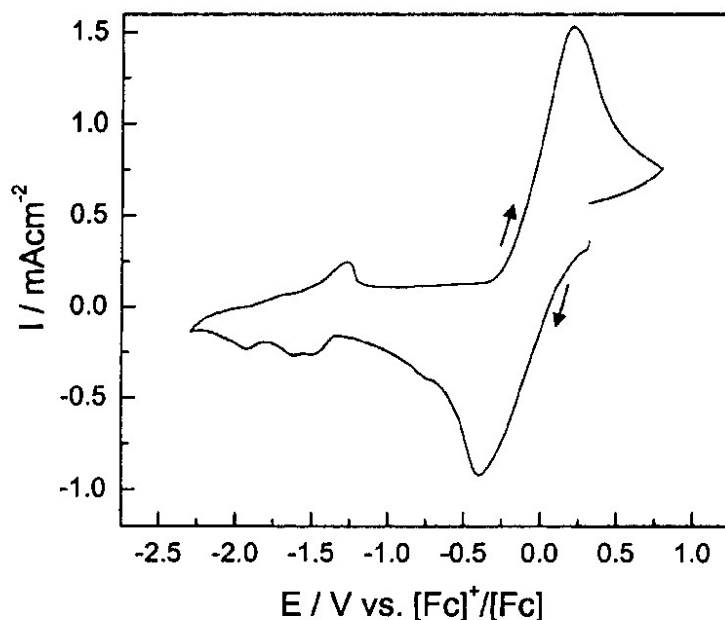


Fig. 1.23 Cyclic voltammogram of 0.24 M TiCl_4 in 1-butyl-3-methyl imidazolium bis((trifluoromethyl)sulfonyl)amide on Au(1 1 1) substrate vs. $[\text{Fc}]^+ / [\text{Fc}]$ obtained at a sweep rate of 10 mVs^{-1} at room temperature [2005Muk].

The first cathodic peak at -0.39 V (Fig. 1.23) is attributed to the Ti(IV) to Ti(II) reduction process. It has been observed that Ti(IV) generally is reduced to Ti(II) in two one electron steps at higher temperature in alkali chloride or chloride-fluoride mixtures [1981Cha, 1993Har]. There is a shoulder around -0.8 V , which the authors assign to Ti(III) reduction. The hump in the CV at -1.45 V is assigned to the underpotential deposition of Ti metal from Ti(II) state. With the small hump at -1.61 V , another underpotential deposition

process can possibly be correlated to the formation of a binary alloy of Au – Ti. The peak at -1.9V is attributed to 3D growth of Ti clusters in the overpotential deposition. The low current density in the CV in this potential range presumably is due to a thin passivating layer on the electrode.

At the anodic side at -1.27V a relatively broad peak is observed, which authors assign to stripping of Ti and oxidation to Ti (II). A quasi reversible peak of oxidation of Ti(II) to Ti(IV) appears at the anodic potential of approx. $+0.22\text{V}$.

1.5 Short description of some industrial processes of Ti production

Kroll process (1940) [1940Kroll]

The schematic drawing of the reactor is presented in Fig. 1.24:

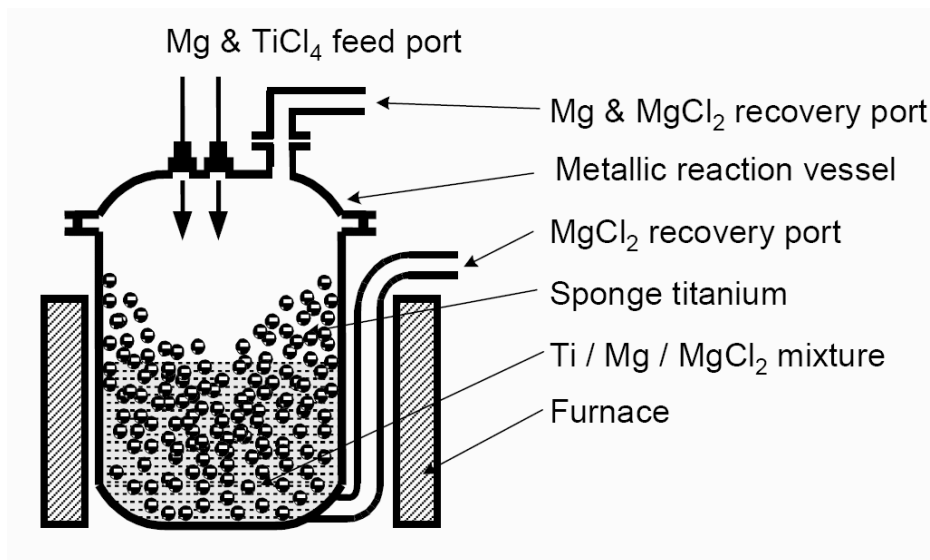


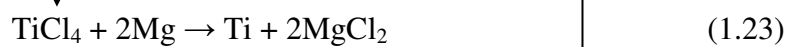
Fig. 1.24 Schematic drawing of the reactor for titanium reduction by the Kroll process.

Reactions that take place:

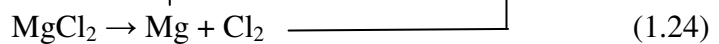
Chlorination:



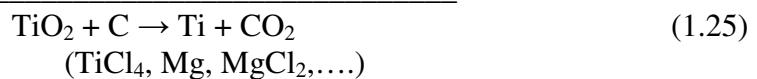
Reduction:



Electrolysis:



Overall reaction:



The most widespread process.

It requires several days to produce Ti in “ton” scale.

The product (titanium sponge) contains up to 500 – 1000 ppm of oxygen.

FFC Cambridge process (Farthing-Fray-Chen process, 2000) [2000Chen]

The schematic drawings of the electrolyzer are presented in Fig. 1.25.

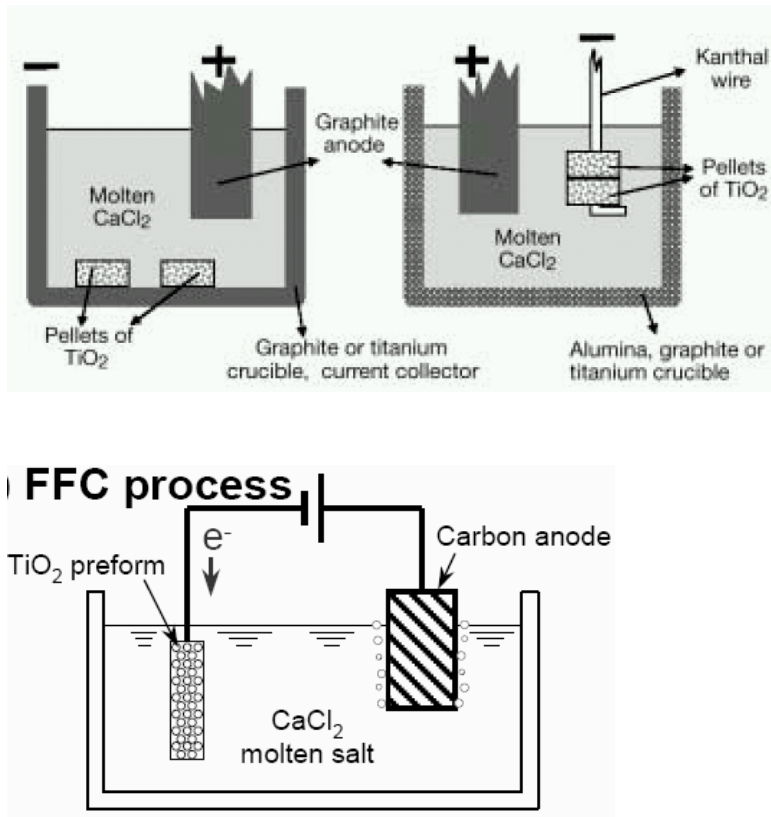
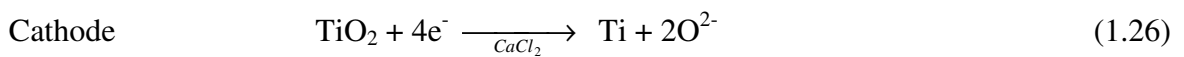


Fig. 1.25 Schematic drawing of the electrolyzer used in the FFC process [2000Chen].

Direct electrochemical reduction of TiO_2 and simultaneous deoxidation of obtained titanium was achieved in the process.

Reactions at the electrodes:



Oxide reduction process (OS Process, Ono and Suzuki, 2002) [2002Ono, 2002Suz]

The schematic drawing of the electrolyzer is presented in Fig. 1.26:

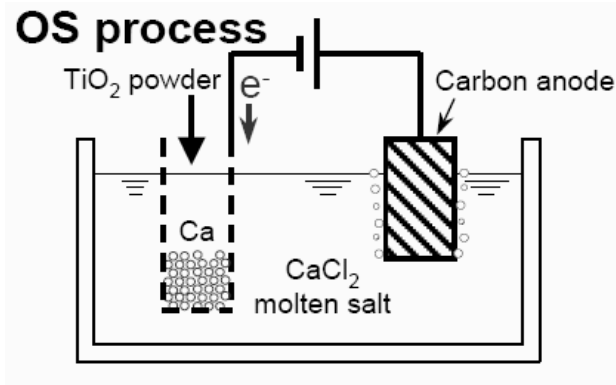
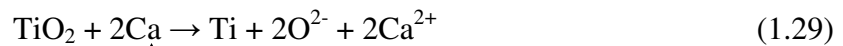


Fig. 1.26 Scheme of the electrolyzer used in the OS Process.

Reactions on the electrodes:

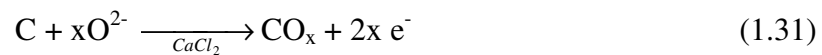
Calciotermic reduction of TiO_2



Cathode



Anode

Electronically mediated Reaction (Okabe and Sadoway, 1998) [1998Okab, 2001Tan]

EMR/MSE Process

The electrochemical reaction is applied during metallothermic reduction.

Schematic drawing of the reactor is presented in the Fig. 1.27.

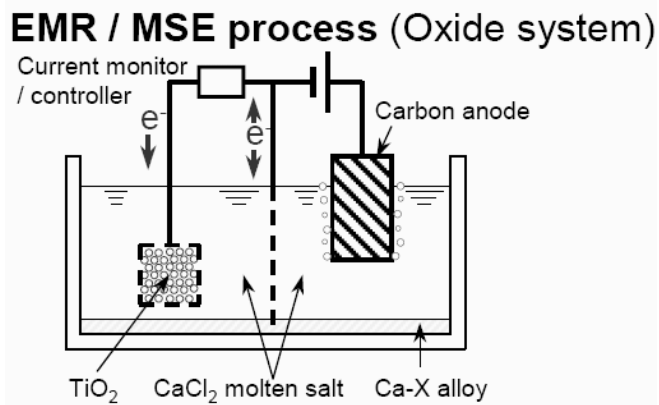
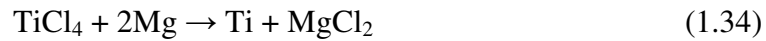


Fig.1.27 Schematic drawing of the electrolyzer used in the EMR process [2001Tan].

Cathode



Anode

**Table 1.5** Comparison of the Ti production processes [2002Okab]

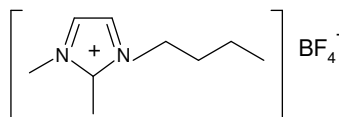
Advantages	Disadvantages
Kroll process	
<ul style="list-style-type: none"> • High purity Ti available • Easy metal/salt separation • Established chlorine circulation • Utilizes efficient Mg electrolysis • Reduction and electrolysis operation can be carried out independently 	<ul style="list-style-type: none"> ○ Complicated process ○ Slow production speed
FFC Process	
<ul style="list-style-type: none"> • Simple process • Semi-continuous 	<ul style="list-style-type: none"> ○ Difficult metal/salt separation ○ Reduction and electrolysis have to be carried out simultaneously ○ Sensitive to carbon and iron contamination ○ Low current efficiency
OS Process	
<ul style="list-style-type: none"> • Simple process • Semi-continuous 	<ul style="list-style-type: none"> ○ Difficult metal/salt separation ○ Sensitive to carbon and iron contamination ○ Low current efficiency
EMR/MSE Process	
<ul style="list-style-type: none"> • Resistant to iron and carbon contamination • Semi-continuous process • Reduction and electrolysis operation can be carried out independently 	<ul style="list-style-type: none"> ○ Difficult metal/salt separation when oxide system ○ Complicated cell structure ○ Complicated process

2. Experimental part

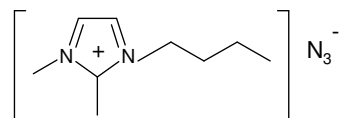
2.1 Chemicals

Structures of ILs investigated in the present work:

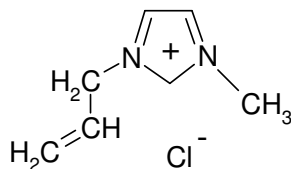
The ILs studied obtained from Prof. H. Schottenberger, University of Innsbruck, Institute of General, Inorganic and Theoretical Chemistry, Austria:



1-butyl-2,3-dimethylimidazolium tetrafluoroborate (BMMImBF₄)

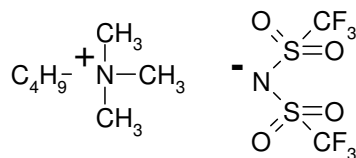


1-butyl-2,3-dimethylimidazolium azide (BMMImN₃)

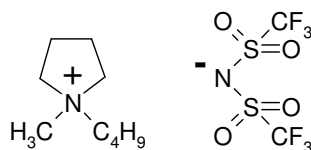


1-allyl-3-methylimidazolium chloride (AllMImCl)

ILs obtained from IOLITEC/D:



N-butyl-N-trimethyl-ammonium bis(trifluoromethylsulfonyl)imide (BuMe₃Am[NTf₂]).



N-butyl-N-methyl-pyrrolidinium bis(trifluoromethylsulfonyl)imide (BuMePy[NTf₂])

Titanium tetrachloride (99.9%) and Titanium tetrahydrofuran (99.9%) were obtained from Aldrich and used as received.

All ILs were dried under vacuum (ca. 0.01 mbar) at 80°C overnight.

The water content was checked by Karl-Fischer titration (Metrohm 756 KF Coulometer).

The water content was in the range 7 to 15 ppm.

To avoid the risk of contamination, all the operations with ILs were performed in a dry glove-box (MBraun Labstar). Oxygen and water concentration in the glovebox was always less than 5 ppm.

After handling in the glove-box, the samples exhibit the same water content, measured again by KF-titration.

Titanium tetrafluoride (99.9%) was obtained from Aldrich and used as received.

2.2 Conductivity

Conductivity and cyclic voltammetry measurements were done outside after preparing the cell by sealing and filling it with Argon in the glove box.

Conductivity measurements were carried out in a temperature range between 30°C and 95°C (Qcond 2400 VWR international). The heating rate was approximately 0.5°C/min.

2.3 Cyclic voltammetry and chronopotentiometry

Cyclic voltammetry and chronopotentiometry of the studied electrolytes were performed in a standard three electrode electrochemical cell (see drawing in the Appendix). Before the experiments, the cell was thoroughly washed and dried. As a working electrode Pt-disk (area 0.031 cm²) was used, a glassy carbon rod served as an auxiliary electrode.

Reference electrode.

In the present work, a Ag/AgCl electrode in oversaturated AgCl in BMMImBF₄ solution was used as a reference. The reference electrode compartment was separated from the electrolyte by means of Vycor® glass frit (see drawing in the Appendix).

All the electrochemical measurements were carried out using a Voltalab PGZ301 system (Radiometer Analytical).

2.4 Viscosity and density

The temperature dependence of the density and viscosity (range 40°C to 100°C) were measured using an SVM 3000 viscosimeter (Anton Paar/A).

For some experiments a rolling ball viscometer AMV200 (Anton Paar/A) was used. The capillary was filled with a IL in the glove-box, sealed, then taken out and inserted into the viscometer.

2.5 IR spectroscopy

FTIR-internal reflection spectra were recorded in the range 200 - 4000 cm^{-1} , using a Bruker FTIR spectrometer Equinox 55 with a MKII Golden Gate Single Reflection ATR System with diamond top plate and KRS-5 lenses (Specac) and a MCT nitrogen-cooled detector.

2.6 Surface analysis

For characterisation of the surface and deposited layers a scanning electron microscope (Philips XL-30 ESEM) equipped with an energy-dispersive X-ray spectrometer (EDX) was used. Optical microscopy was performed using an Olympus GX51 optic microscope.

2.7 Deposition experiments

All the deposition experiments were carried out in the same cell as the cyclic voltammetry. The substrate was a Pt rod or a Pt chip. As an auxiliary electrode, glassy carbon rod was used. The melt was stirred during the deposition process.

Titanium tetrachloride was added to the melt by means of Hamilton syringe.

Titanium tetrahydrofuran and tetrafluoride (powders) were added in the dry glove-box.

3. Results and discussion

3.1 Physical chemical properties of trialkyl substituted imidazolium based ILs (IL).

3.1.1 Density and molar volume

Unlike viscosity or conductivity, density is not a property that is very sensitive to structural changes. It depends linearly on the temperature (Fig. 3.1). As expected, BMMImBF₄, has a higher density than BMMImN₃, since tetrafluoroborate is the heavier anion.

In the mixtures, the two different anions do not seem to interact with each other in a different way than they would interact within the same anionic species. Therefore, densities change almost linearly with the composition of the ILs.

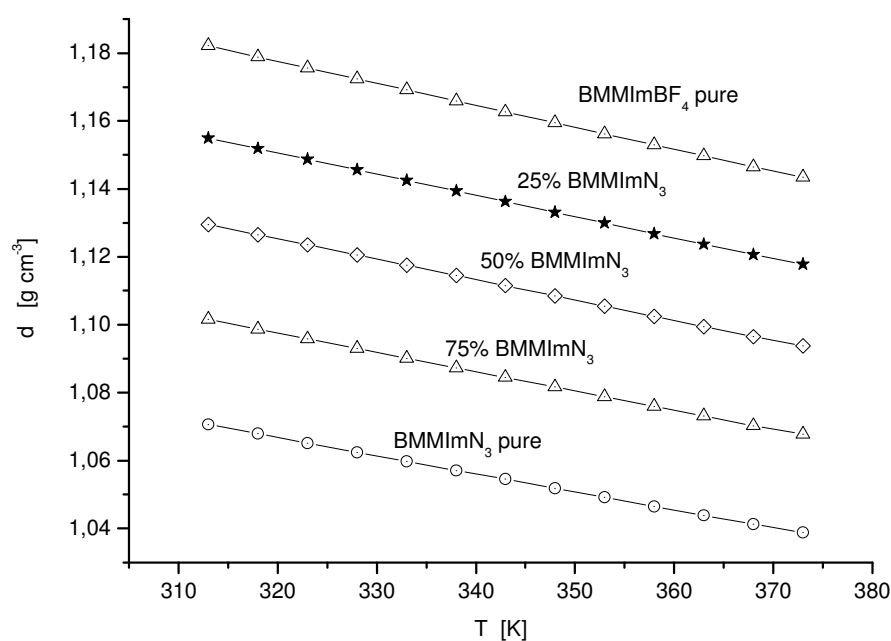


Fig. 3.1 Density dependence of pure ILs and the mixtures on the temperature.

Molar volumes of the mixtures were calculated from density data using the equation

$$V_{molar} = \frac{M}{d} \quad (3.1)$$

where V_{molar} is the molar volume of the mixture at a given temperature and composition [$\text{cm}^3 \text{mol}^{-1}$], M is the molar mass of the mixture [g mol^{-1}] (calculated according to the molar ratios of the components), and d is the density of the mixture at given temperature and composition [g cm^{-3}].

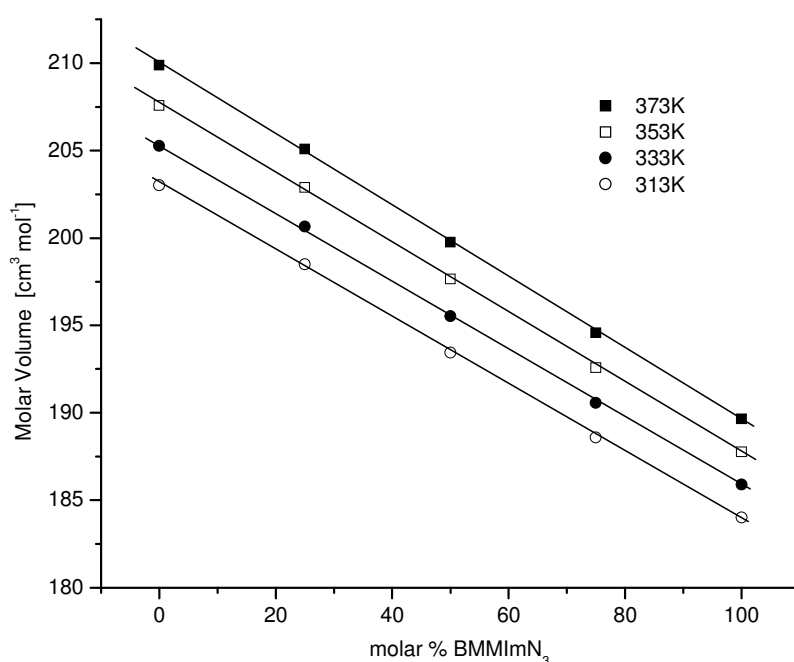


Fig. 3.2 Dependence of molar volume on the composition at various temperatures.

Fig.3.2 shows the isotherms of molar volumes, which are linear. Thermodynamically, it means that no additional interactions exist, and the mixtures behave as the ideal ones.

3.1.2 Viscosity

The most dramatic influence on viscosities has the nature of the cation [1996Bon, 2004Was]. While keeping the cation the same, the impact of two different anions on the viscosities was studied. Fig. 3.3 shows the dependence of viscosity of the investigated pure ILs and mixtures on the temperature. The viscosity is determined by van der Waals interaction and hydrogen bonding [1996Bon, 2001Huang]. As expected, the viscosity of the ILs is decreasing with increasing temperature. The viscosity of BMMImN₃ is always higher than the viscosity of BMMImBF₄. The difference in the viscosity values of the pure ILs is decreasing with increasing temperature. At 100°C, no difference in viscosities was observed. Adding 25% BMMImN₃ to BMMImBF₄ has a negligible effect on the viscosity

of the resulting IL. A further increase of the BMMImN₃ content in the mixture leads to increasing viscosities mainly at temperatures <70°C.

Both, the structure and charge density of the anion effect the viscosity significantly at temperatures lower than 70°C. Van der Waals interaction decreases with the decrease of the anion size but the electrostatic interaction increases. The second factor is likely to dominate in this case, exhibiting higher viscosities of the mixtures with higher concentration of the azide anion.

At higher temperatures (>70°C), the viscosity is mainly determined by the mobility of the cation and the influence of the size of the anion is negligible.

Although significant work in the field has already been done, the influence of the chemical structure on the viscosity of the IL is not yet clear [2000Sed, 2004Was, 1986Hus].

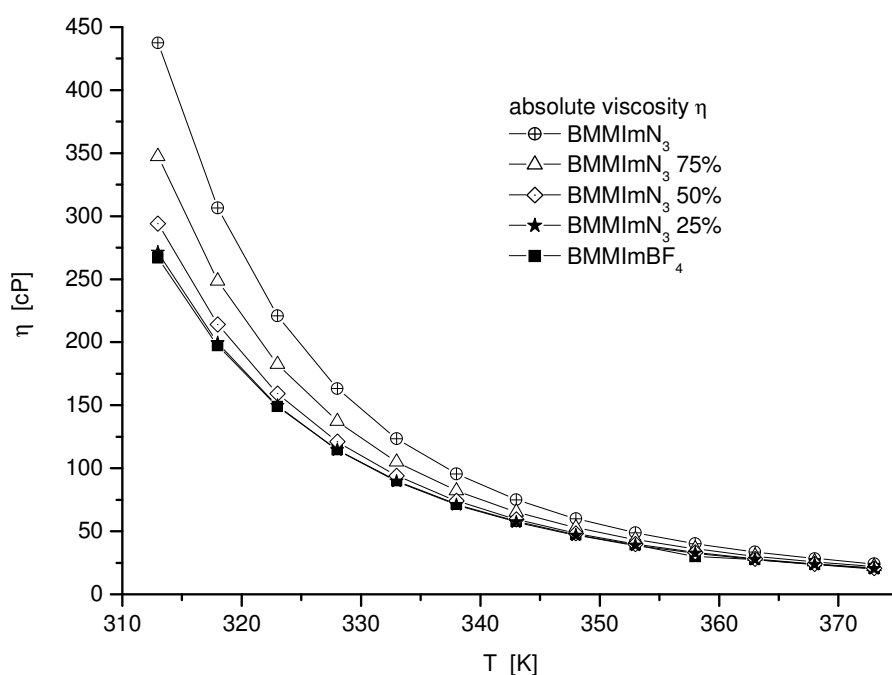


Fig. 3.3 Viscosity dependence of pure BMMIm BF₄, BMMImN₃, and the mixtures of BMMImBF₄ with 75, 50 and 25% BMMIm N₃ on temperature.

Viscosity data was fitted with Arrhenius and Vogel-Tamman-Fulcher (VTF) equations (see Fig.3.4). Best fit was achieved in terms of VTF equation (correlation coefficient $R^2=0.999 \div 1.000$). The VTF equation has been previously successfully used to interpret the temperature behaviour of imidazolium substituted ILs [1999McEwen, 2005Mat, 2004Eve].

The three parameter fit has been performed with the VTF equation. For viscosity data it is adapted as follows:

$$\ln \eta = \ln \eta_0 + \frac{k}{T - T_0} \quad (3.2)$$

where η_0 , and k are constants and T_0 is the ideal glass transition temperature (Fig.3.4).

Fig. 3.5 represents the viscosity data plotted in terms of the Arrhenius equation.

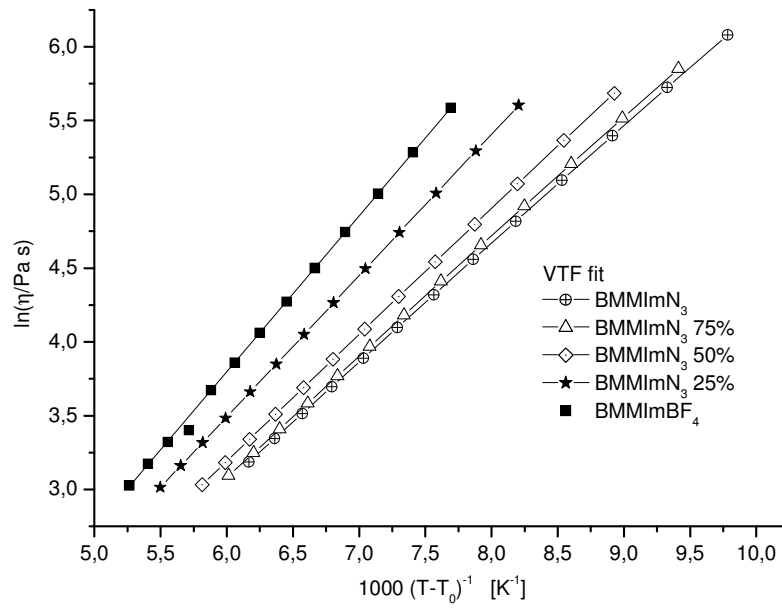


Fig. 3.4 $\ln(\eta/\text{mPa s})$ vs. temperature linearization in terms of VTF equation (Eq. 3.2).

The activation energies E_a of the viscous flow have been calculated using the Arrhenius equation:

$$\ln \eta = \ln \eta_0 + \frac{E_a}{RT} \quad (3.3)$$

where η is the viscosity at temperature T [Pa s], η_0 the limiting viscosity [Pas], E_a the activation energy of viscous flow [J mol^{-1}], R is the gas constant [$\text{J mol}^{-1} \text{K}^{-1}$] and T is the temperature [K] (Fig.3.5).

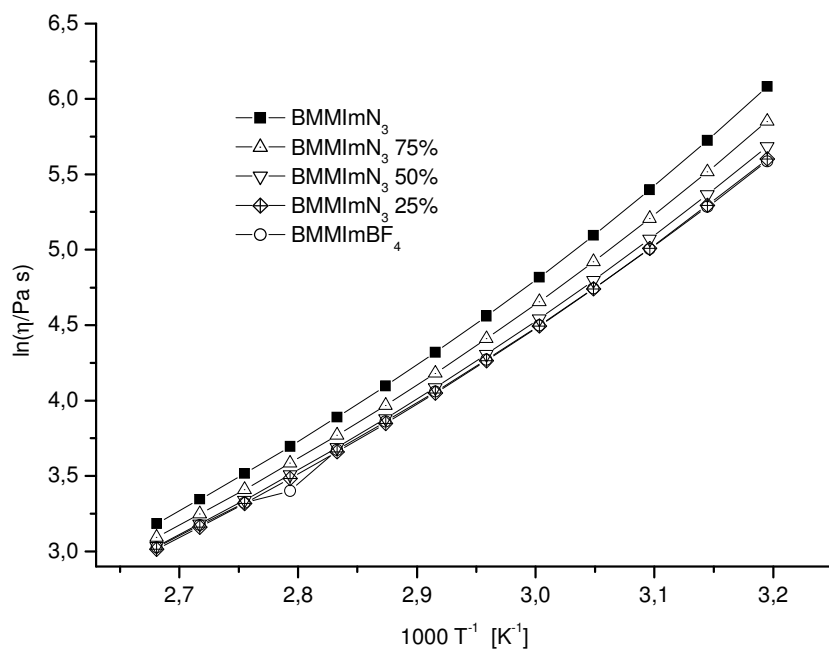


Fig. 3.5 $\ln(\eta/\text{mPa s})$ vs. T^{-1} (Eq. 3.3).

The results are summarized in Table 3.1.

Table 3.1 Results of VTF and Arrhenius fit for viscosity data

	$\ln\left(\frac{\eta}{\text{mPas}}\right)$	k [K]	T_0 [°C]	R^2 (for VTF fit)	Activation energy E_a [kJ mol ⁻¹]
BMMImN ₃	-1.76	805	-66	0.999	46.4
BMMImN ₃ 75%	-1.79	813	-66	0.999	44.3
BMMImN ₃ 50%	-1.92	852	-72	0.999	42.6
BMMImN ₃ 25%	-2.55	957	-82	1.000	41.6
BMMImBF ₄	-2.55	1050	-90	0.999	41.5

3.1.3 Conductivity

The dependence of conductivity on temperature for pure ILs and their mixtures is presented in Fig. 3.6.

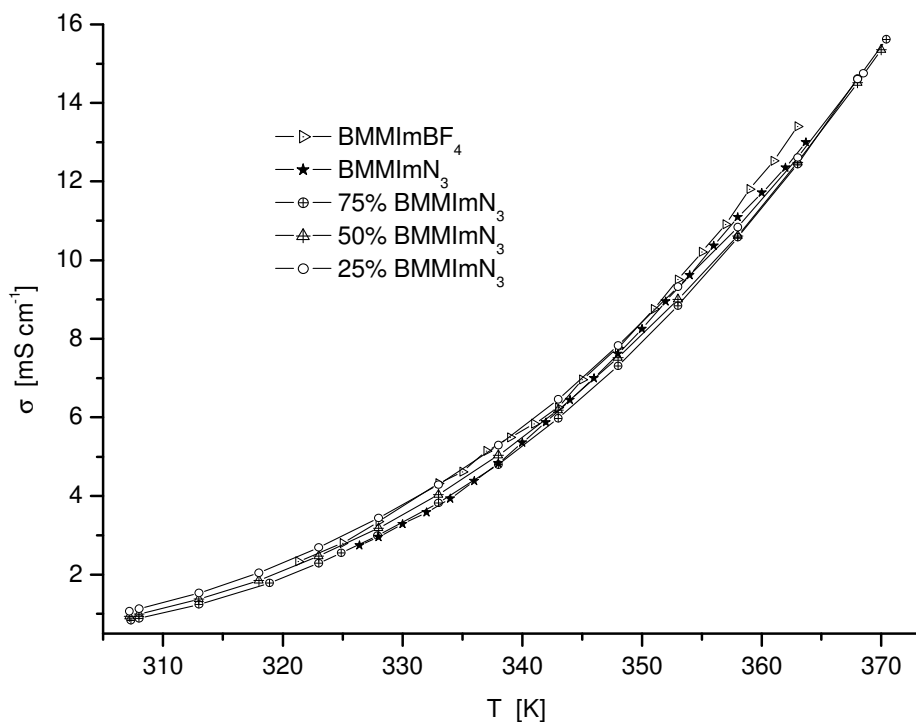


Fig.3.6 Conductivity vs. temperature

We do not observe large variation of the conductivity values with the change of composition. This indicates that the effect of the two anions on conductivity is similar.

The Vogel-Tamman-Fulcher (VTF) equation was also used for the analysis of the conductivity data [1999McEwen] (Fig.3.8). Arrhenius equation was used for the estimation of activation energies from the data of Fig. 3.7.

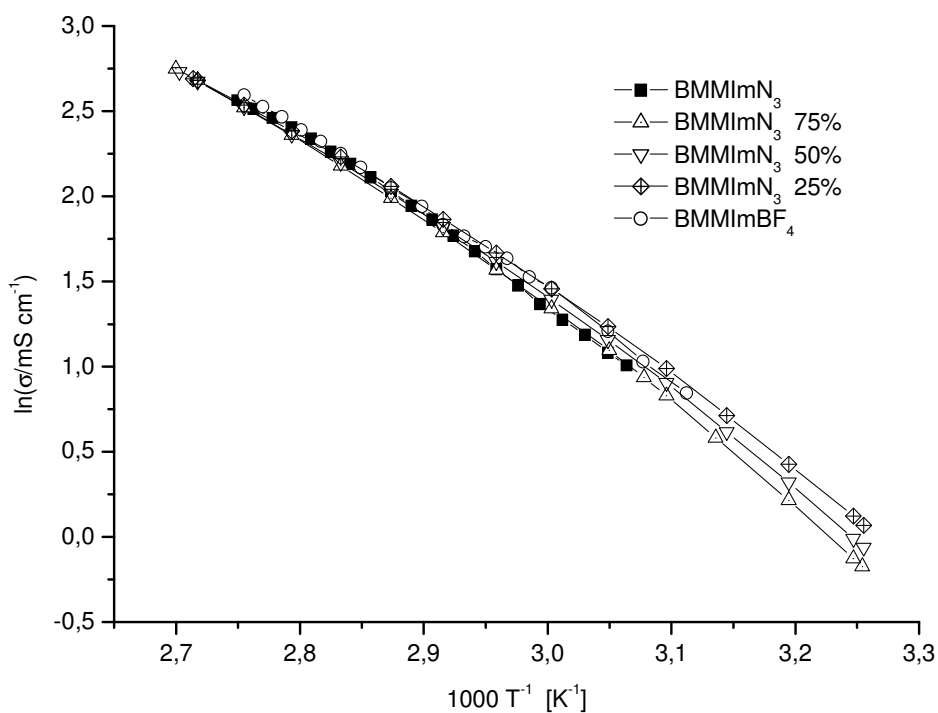


Fig. 3.7 $\ln(\sigma/\text{mS cm}^{-1})$ vs. T^{-1} (Arrhenius-type plot).

The conductivity data was fitted with Function (3.2).

The conductivity data are linearized with VTF – type function:

$$\ln \sigma = \ln \sigma_0 + \frac{k}{T - T_0}, \quad (3.4)$$

shown in Fig. 3.8.

The results of both Arrhenius and VTF fit are shown in Table 3.2.

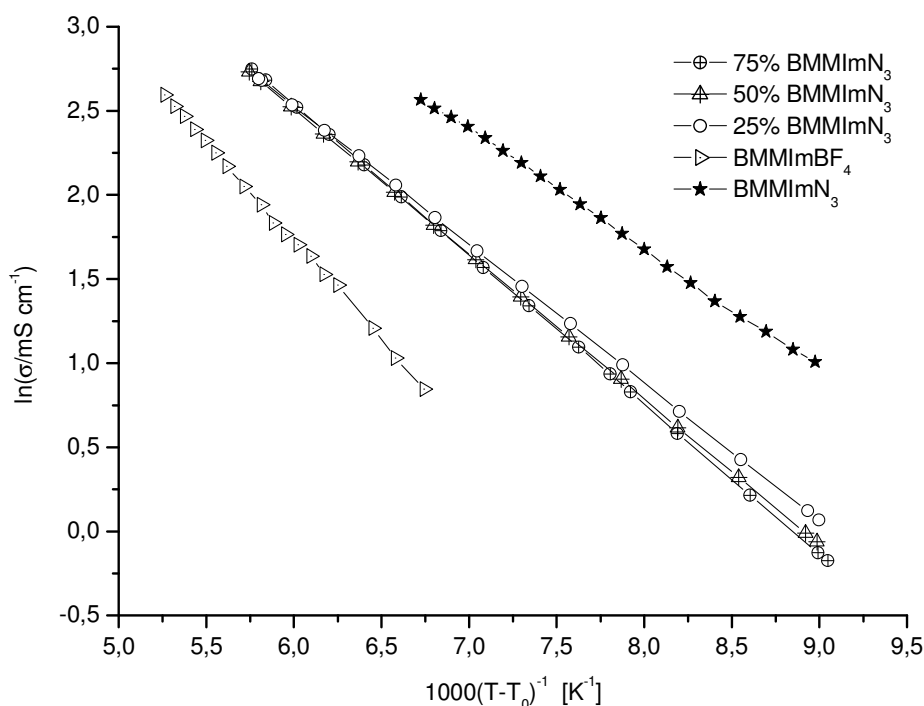


Fig. 3.8 $\ln(\sigma/\text{mS cm}^{-1})$ vs. temperature linearization in terms of VTF equation.

The ideal glass transition temperature (T_0) for each IL as well as for their mixtures has been derived from the three parameter fit of conductivity vs. temperature curves. The linear character of the curves depicted in the Fig. 3.8 proves the validity of the VTF equation for the approximation of the conductivity for this type of ILs.

Conductivity and viscosity of an IL are often combined into what is called Walden rule, which is also valid for ILs [2004Was].

$$\Lambda\eta = \text{const}, [\text{cm}^2 \text{ mPa s } \Omega^{-1} \text{ mol}^{-1}] \quad (3.5)$$

where η is the viscosity [mPa.s] and Λ is the molar conductivity of the IL given by the expression:

$$\Lambda = \frac{\sigma M}{d}, [\text{cm}^2 \Omega^{-1} \text{ mol}^{-1}] \quad (3.6)$$

where σ is the ionic conductivity [S cm^{-1}], M is the molar weight [g mol^{-1}], and d is the IL density [g cm^{-3}].

The Walden product ($\Lambda\eta$) is frequently constant over a range of temperature for a given IL. Results of the Walden product calculations for the ILs and their mixtures studied in this work are presented in Table 3.2.

For now, no clear correlation of Walden product with respect to the anion size was found.

Table 3.2 Results of VTF and Arrhenius fit for conductivity data.

	VTF equation			Arrhenius eq.	
	$\ln\sigma_0$	$-k$	T_0 [°C]	Walden product, $\Lambda\eta$	$-E_a$ [kJ mol ⁻¹]
BMMImN ₃	7.33	701.3	-57	84.9	42.2
BMMImN ₃ 75%	7.88	890.0	-76	74.4	43.7
BMMImN ₃ 50%	7.97	907.3	-77	71.1	41.9
BMMImN ₃ 25%	7.46	822.0	-77	75.1	40.1
BMMImBF ₄	8.74	1164.6	-99	77.6	40.1

In both, viscosity and conductivity data analysis with Arrhenius equation, activation energies tend to increase with increasing concentration of the azide anion. As the activation energy proved to be related to structural effects of the ions [2002Ohn], we believe the tendency can be explained with prevailing of electrostatic interaction over the input of van der Waals forces.

Some literature data on activation energies derived from conductivity data for imidazolium ILs are compiled in the Table 3.3. Due to the more complicated structure of the ILs studied, E_A is higher than the activation energies of most of the ILs mentioned in literature so far. Larger disubstituted imidazolium cations, as in the case of OMImPF₆ (octyl, methyl imidazolium hexafluorophosphate), exhibit a higher activation energy of conductivity [2002McL].

Table 3.3 Literature data on activation energies for some imidazolium ILs

IL	$-E_a$ [kJ mol ⁻¹]	Reference
EMImTf	17.6	[1998Ful]
EMImTf	15.9	[2000Eve]
EMImNTf2	14.0	[2000Eve]
EMImBF ₄	18.0	[1998Ful]
EMImPF ₆	25.5	[1998Ful]
OMImPF ₆	48.6	[2002McL]
BuMMImNTf2	29.7	[2002McL]

a M – methyl; E – ethyl; Bu - butyl; O- octyl; Im – imidazolium; Tf – trifluoromethylsulfonate; NTf2 - bis(trifluoromethylsulfonyl)imide.

3.1.4 Electrochemical stability of the ILs

The purity of the IL is of a great importance for getting reproducible results. Prior to the experiments, voltammetry of the ILs has been performed. After establishing a constant potential of the Pt electrode in the melt, cathodic and anodic curves were recorded consequently. The anodic sweep was started from the equilibrium potential as well.

It was found that the pure BMMImBF₄ is electrochemically stable in the range of –1.85V to +2.05V (Fig. 3.9, curve 2) and BMMImN₃ - in the range of –1.9V to +0.5V (Fig. 3.9, curve 1) vs. Ag/AgCl reference electrode.

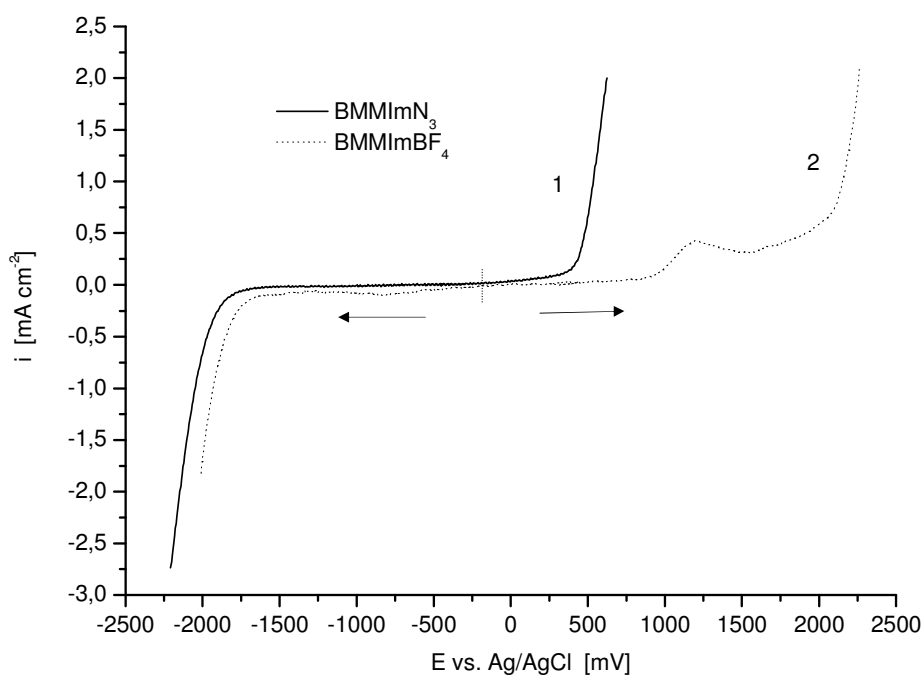


Fig. 3.9 Voltammetry of the pure 1-butyl-2,3-dimethyl imidazolium ILs with (1) azide and (2) fluoroborate cations; sweep rate 100mV s^{-1} , temperature 65°C , Pt working electrode.

The cathodic limit for both ILs is caused by reduction of the imidazolium based cation. In the anodic direction, oxidation of tetrafluoroborate anion (curve 2), with BF_3 and fluorocarbons formation, is limiting the electrochemical window of the BMMImBF_4 [2003Xia, 2003Tru]. The anodic peak at $+1.2\text{V}$ is attributed to the chloride anion oxidation [2003Xia]. The impurity of Cl^- results from the synthesis.

A slightly higher cathodic stability of BMMImN_3 is probably related to the lower water content compared to the BMMImBF_4 IL (7 and 15 ppm measured by Karl Fischer Titration).

Using azide anion instead of tetrafluoroborate decreases the anodic stability by 1.5V .

Their mixtures show, even with low amounts of BMMImN_3 , a behavior quite similar to pure BMMImN_3 with an anodic decomposition potential of $+0.5\text{V}$ (Fig.3.10). The anodic region of the mixtures is limited by the oxidation of the azide anion. In the case of addition of 25% of BMMImN_3 , the effects on the cathodic and anodic stability are eliminated. Table 3.4 summarizes the electrochemical stabilities for the ILs tested.

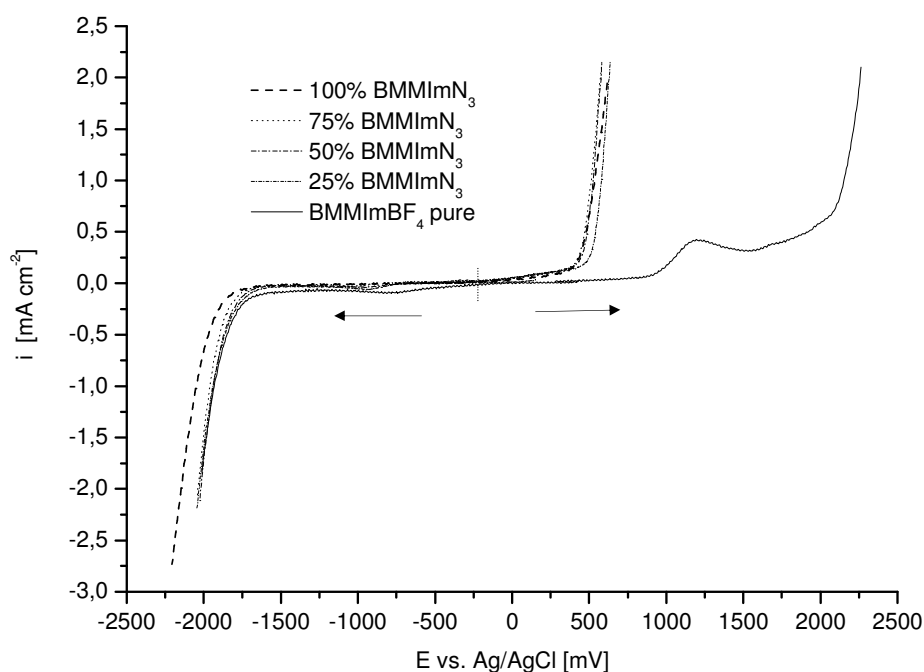


Fig. 3.10 Cyclic Voltammograms of the pure ILs and their mixtures (molar ratios).

Table 3.4 The electrochemical stability of BMMImBF₄ and BMMImN₃ and their mixtures, Pt working electrode, Ag/AgCl reference electrode, 65°C.

Compound	Electrochemical stability [V]	
	cathodic	anodic
BMMImN ₃	-1.9	0.5
3:1	-1.85	0.5
1:1	-1.85	0.5
1:3	-1.85	0.5
BMMImBF ₄	-1.85	2.05

Physical and electrochemical properties of two trisubstituted imidazolium salts as well as their mixtures with molar ratios 3:1; 1:1, and 1:3 have been studied. For BMMImBF₄ the cathodic stability is -1.9V and the anodic is +2.05V vs. Ag/AgCl reference electrode. If azide anions are added to the IL-mixture, the anodic decomposition potential decreases by 1.5V. The azide anion exerts therefore a great influence on the electrochemical stability and limits the anodic part of the electrochemical window. This is probably due to the anodic oxidation of the azide anion, according to the reaction



The conductivity values do not differ significantly by changing the composition of the mixture.

At room temperature, the mixtures reveal viscosity values of approximately 250 to 450 mPa s. As usual, it decreases with increasing temperature. Higher viscosity values are observed in the mixtures with greater amount of IL containing an azide anion. This is due to the increased electrostatic interactions of the azide anions and the BMMIm cations.

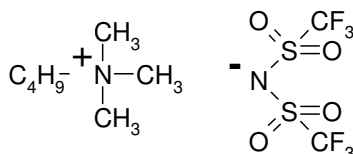
Both, conductivity and viscosity dependencies on the temperature are approximated with the VTF equation. The differences in values of ideal glass transition temperatures, derived from VTF fit of conductivity and viscosity data, lies in the range of several degrees, which proves the right choice of the model used for interpretation.

Walden product which is thought to be constant over the range of temperatures was determined to be in the range of (70 to 80) $\text{cm}^2 \text{mPa s } \Omega^{-1} \text{mol}^{-1}$.

Density depends linearly on temperature and composition. The influence of the composition on the density is rather small. The influence of the anion structure on the conductivity is also very small, both anions seem to contribute equal amounts to the conductivity.

3.2 Physical-chemical properties of some alternative ILs

3.2.1 N-butyl-N-trimethyl-ammonium bis(trifluoromethylsulfonyl)imide (BM₃Am[NTf₂]).



dried under vacuum 0.003 mbar for 5 hours

Density and conductivity were determined at 25°C:

$$d_{25^{\circ}\text{C}} = 1.47 \text{ g cm}^{-3}; \sigma_{25^{\circ}\text{C}} = 2.08 \text{ mS cm}^{-1}$$

Cyclic voltammetry:

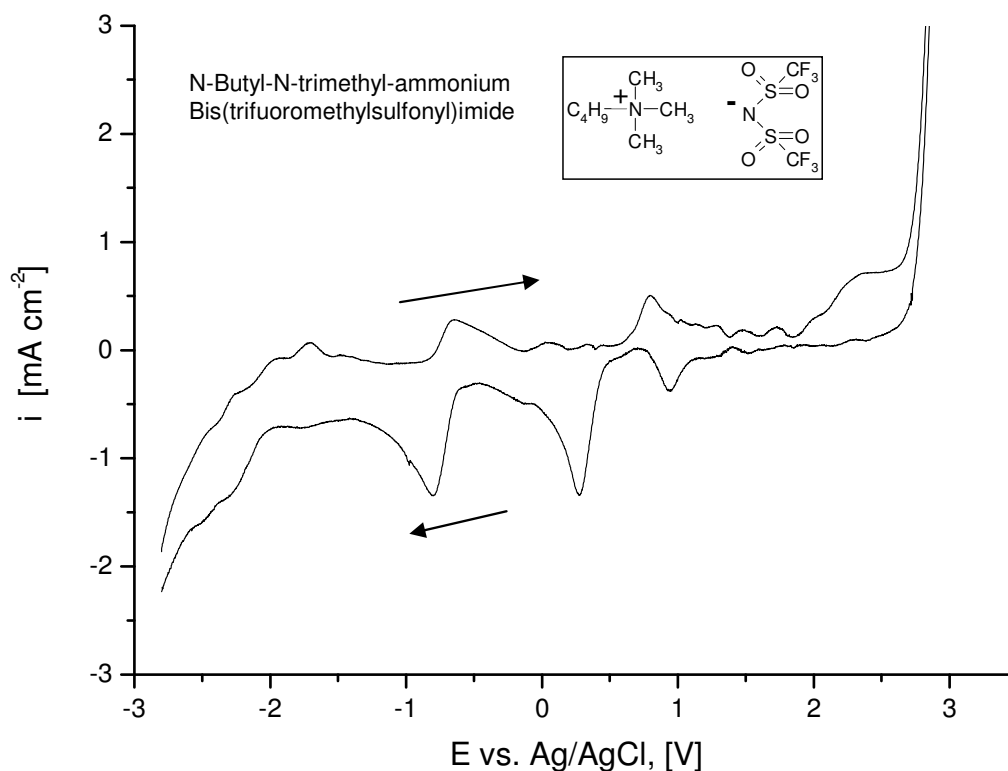


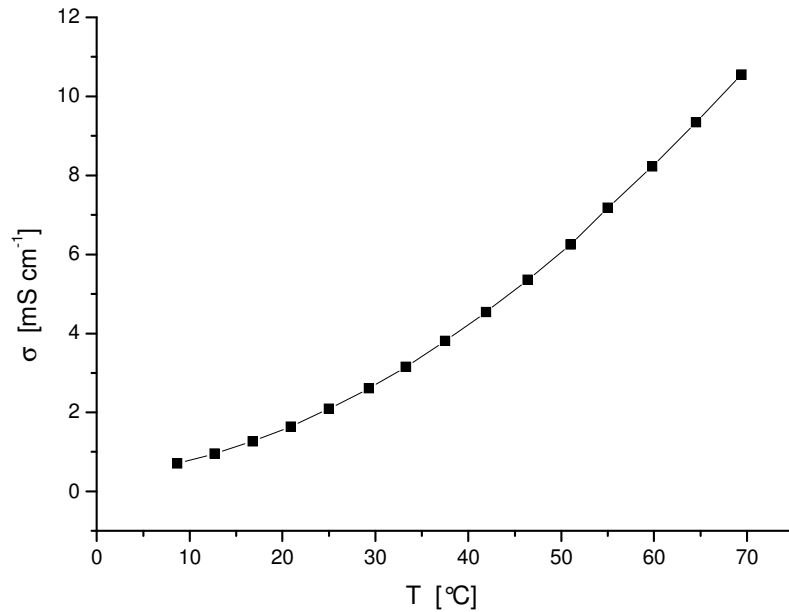
Fig. 3.11 Cyclic voltammetry of BM₃Am[NTf₂], Pt working electrode, $\nu=100 \text{ mV s}^{-1}$, 65°C.

Different peaks are seen on the cyclic voltammetry curve (Fig.3.11).

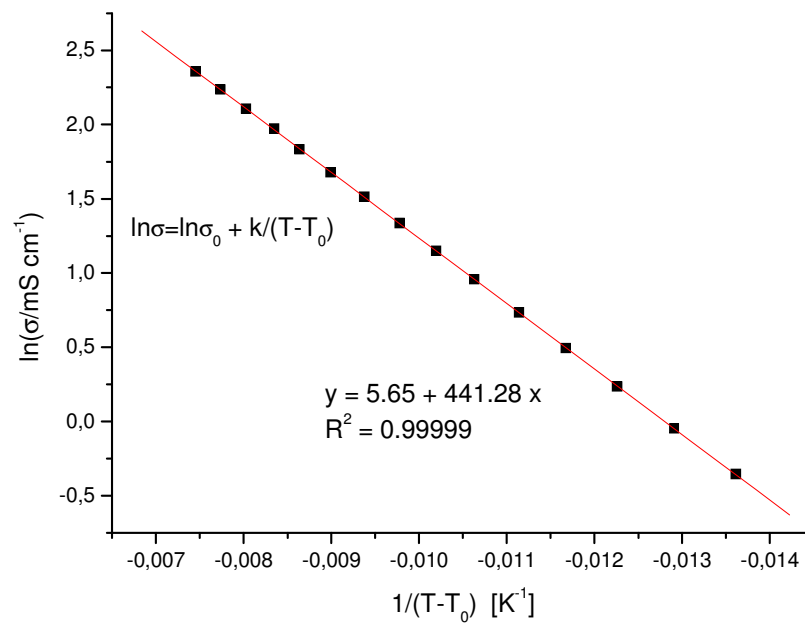
The most probable reason for this behavior is contamination of the IL with some electrochemically active impurities. The electrochemical window of the IL is 5.6V.

Because of the complicated electrochemical behavior, the deposition experiments in this IL were not performed.

Conductivity Measurements



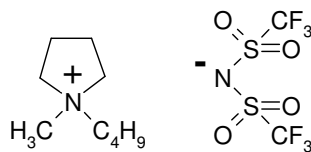
(a)



(b)

Fig. 3.12 a) conductivity vs. temperature; b) linearisation in terms of VTF equation.

3.2.2 N-butyl-N-methyl-pyrrolidinium bis(trifluoromethylsulfonyl)imide (BMPy[NTf₂])



dried under vacuum 0.003 mbar overnight

Density and conductivity were determined at 25°C:

$$d_{25^{\circ}\text{C}} = 1.61 \text{ g cm}^{-3}; \sigma_{25^{\circ}\text{C}} = 2.74 \text{ mS cm}^{-1}$$

Cyclic voltammetry:

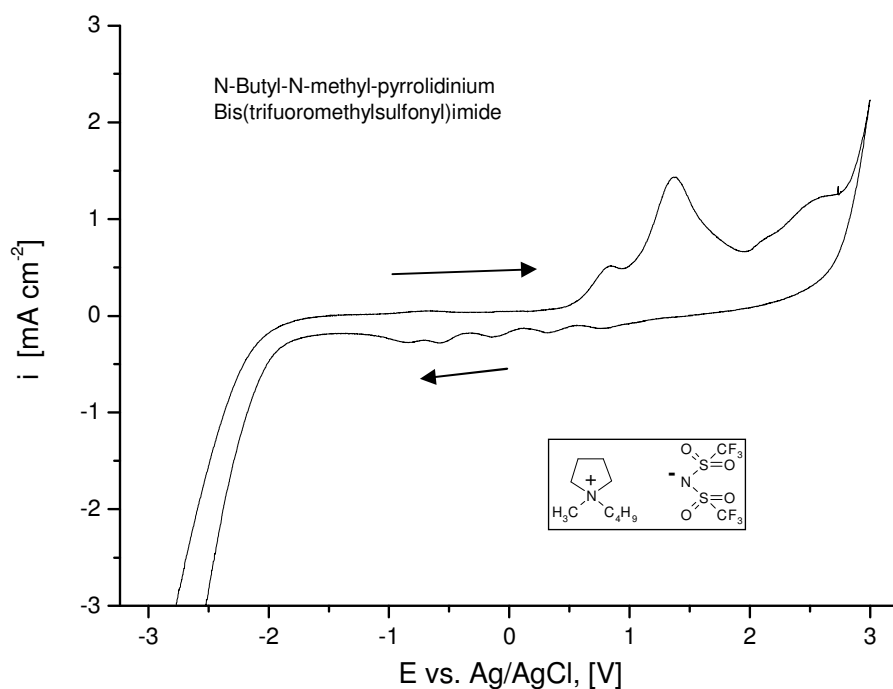
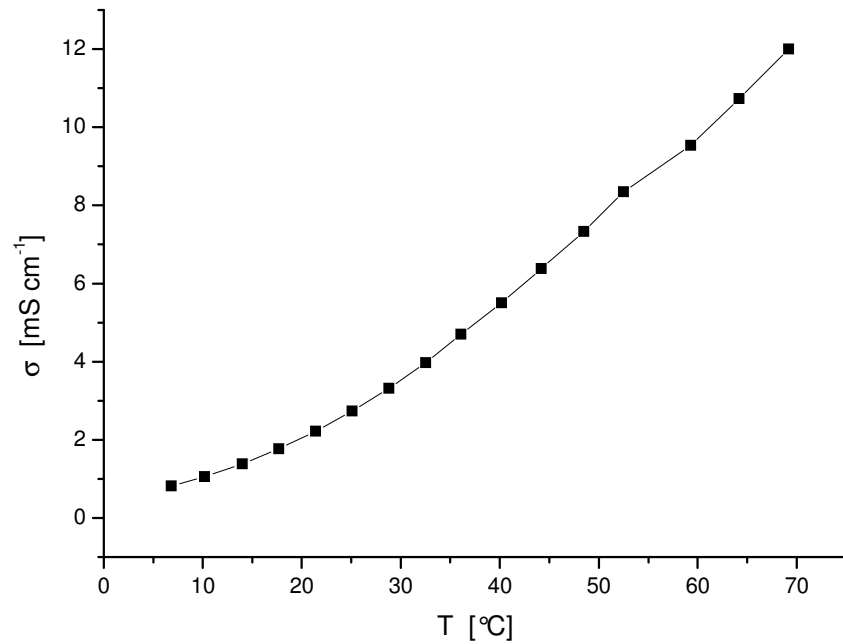


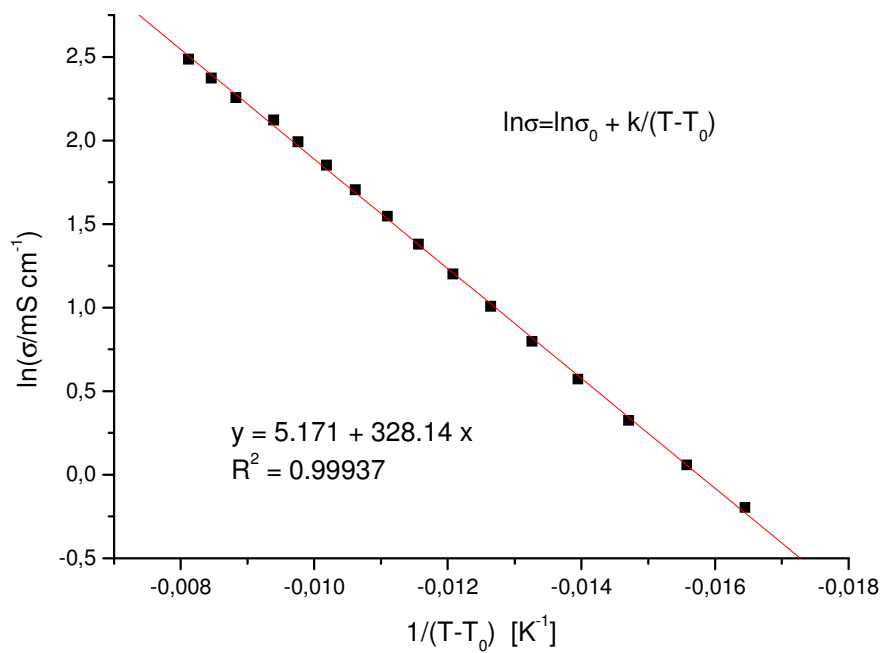
Fig. 3.13 Cyclic voltammetry of BMPy[NTf₂], Pt working electrode, $\nu=100 \text{ mV s}^{-1}$, 65°C.

The small waves on the cathodic scan are most probably due to impurities. Anodic peaks at +0.8V and +1.2V are likely to correspond to organic components oxidation.

The cathodic stability of the IL studied is slightly lower than of the BM₃Am[NTf₂] and is comparable to BMMImBF₄. The electrochemical window is 5V.

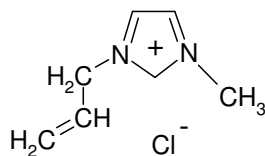
Conductivity measurements

(a)



(b)

Fig. 3.14 a) conductivity vs. temperature; b) linearisation in terms of VTF equation.

3.2.3 1-allyl-3-methyl Imidazolium chloride (AllMImCl)

dried under vacuum 0.003 mbar overnight

Density and conductivity were determined at 25°C:

$$d_{25^{\circ}\text{C}} = 1.35 \text{ g cm}^{-3}, \sigma_{25^{\circ}\text{C}} = 0.35 \text{ mS cm}^{-1}$$

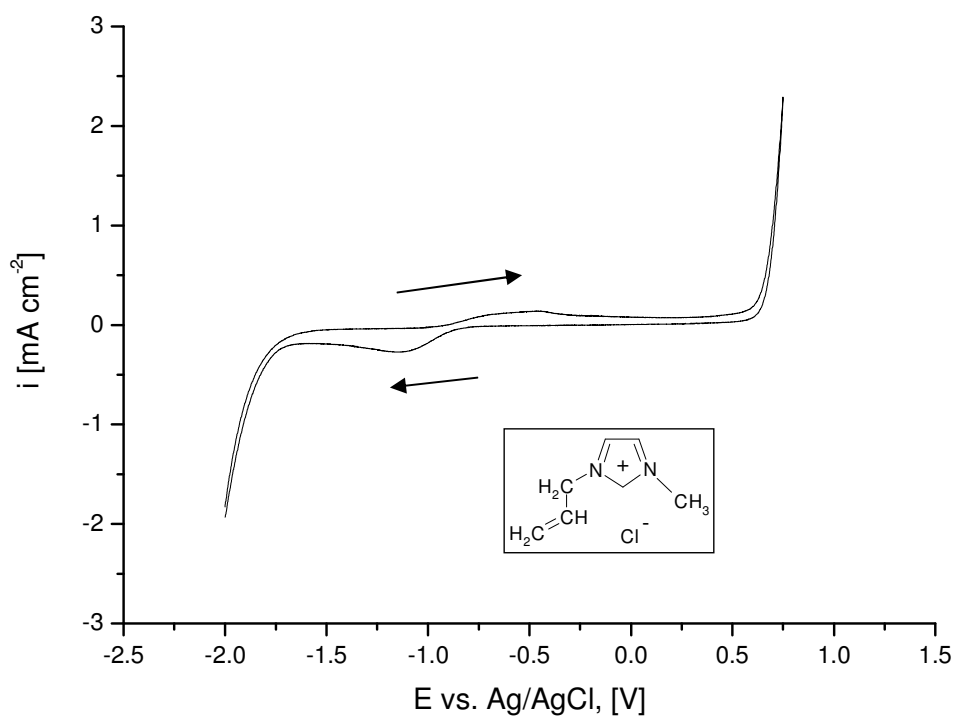
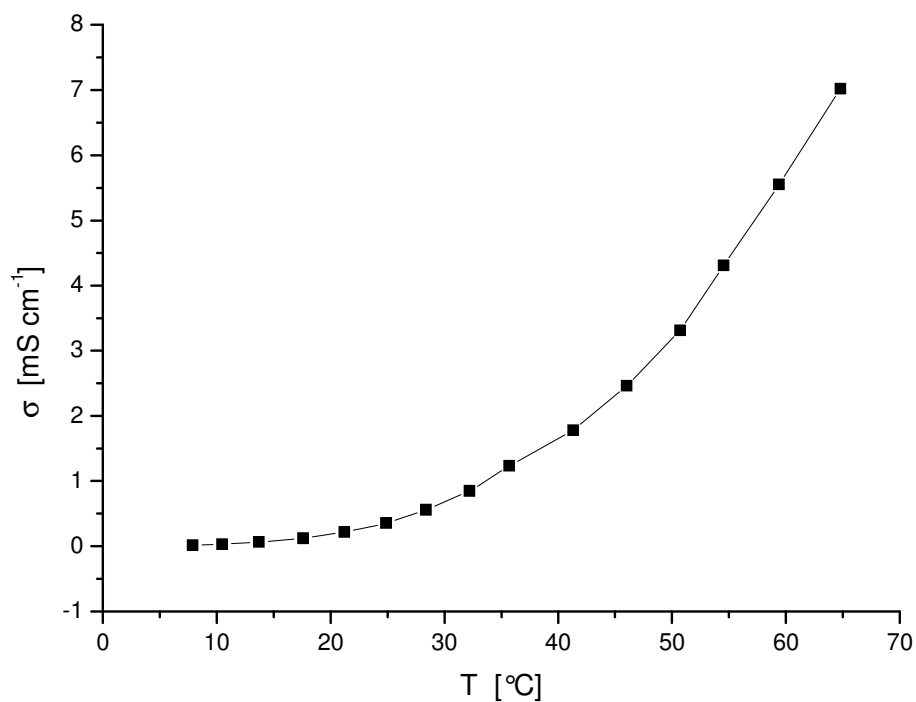


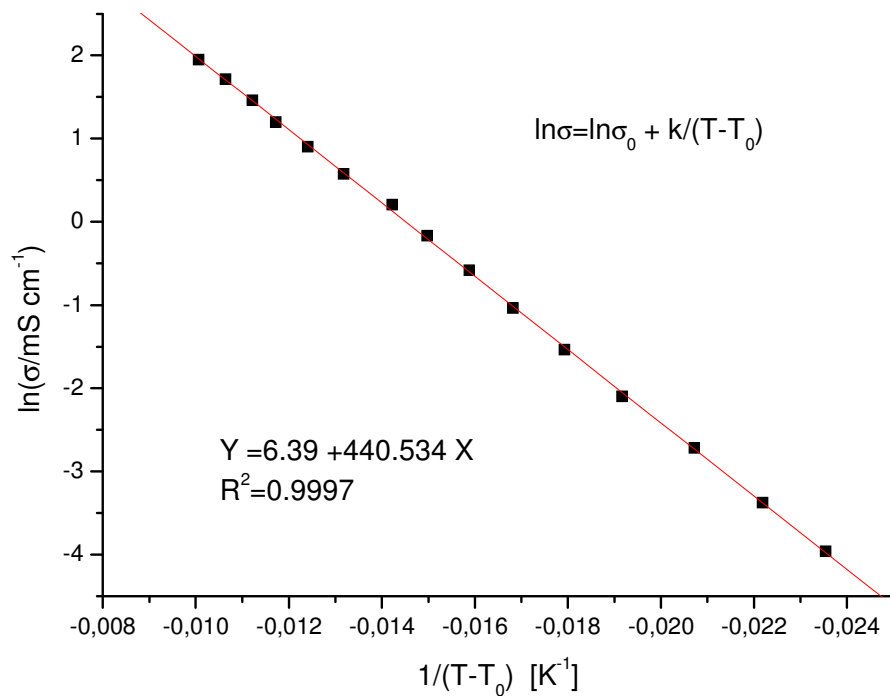
Fig. 3.15 Cyclic voltammetry of AllMImCl, Pt working electrode, $\nu=100 \text{ mV s}^{-1}$, 65°C.

We see some peaks which might be due to the rest halide impurities from the synthesis.

Conductivity measurements



(a)



(b)

Fig. 3.16 a) conductivity vs. temperature; b) linearisation in terms of VTF equation.

Table 3.5 Conductivity and density values for studied ILs

	Conductivity data				density	
	VTF equation				$\sigma_{25^{\circ}C}$ [mS cm ⁻¹]	$d_{25^{\circ}C}$ [g cm ⁻³]
	$\ln\sigma_0$	$-k$	T_0 [K]	T_0 [°C]		
BM ₃ Am[NTf ₂]	5.65	441.3	208.4	-64.7	2.08	1.47
BMPy[NTf ₂]	5.17	328.1	219.1	-54.0	2.74	1.61
AllMImCl	6.39	440.5	238.4	-34.75	0.35	1.35

The nature of ILs being liquid can be explained with the packing difficulties of asymmetric organic cations. In present case, the IL with the biggest cation (BuMe₃Am[NTf₂]) has the lowest ideal glass transition temperature ($T_0 = -67.7^{\circ}C$ in Table 3.5) derived from the three parameter fit of the conductivity data with VTF equation. The most structured IL – AllMeImCl - has the highest T_0 ($-34.7^{\circ}C$).

Table 3.6 Comparison of the phys-chem. properties the ILs.

Formula	Name	Electrochemical stability [V] (decomposition potentials vs. Ag/AgCl)			conductivity at 65°C [mS cm ⁻¹]	T_0 [°C]
		E_{cath}	E_{an}	ΔE		
	1-butyl-2,3-dimethylimidazolium tetrafluoroborate (BMMImBF ₄)	-1.85	2.05	3.90	5.2	-99
	1-butyl-2,3-dimethylimidazolium azide (BMMImN ₃)	-1.9	0.5	1.95	4.8	-57
	N-butyl-N-trimethylammonium bis(trifluoromethylsulfonyl) imide (BM ₃ Am[NTf ₂])	-2.0	2.8	4.8	8.5	-64.7
	N-butyl-N-methylpyrrolidinium bis(trifluoromethylsulfonyl) imide (BMPy[NTf ₂])	-1.9	2.7	4.6	10.7	-54.0
	1-allyl-3-methylimidazolium chloride (AllMImCl)	-1.7	0.7	2.4	7.0	-34.7

Such term as “electrochemical window” is not quite appropriate with regard to the electrochemical stability of the ILs. One must consider both cathodic and anodic stability. The first is essential for application of the ILs in the reductive media or for cathodic electrochemical processes to be carried out (electrodeposition, for example). The second is important when using ILs in oxidative media or for anodic oxidation processes

Nature of the cation determines the cathodic stability. Dialkylsubstituted imidazolium is less stable than the trisubstituted. Among the cations, dialkylpyridinium seems the same as trisubstituted imidazolium. Most stable is tetraalkylammonium, less stable – the disubstituted imidazolium.

Nature of the anion determines the anodic stability. The trifluoromethylsulfonyl imide is much more stable than others. The salts with this anion would be preferable for oxidative processes (anode treatment of metals, for example). The anodic stability of ILs with different anions decreases in the order: $\text{NTf}_2^- > \text{BF}_4^- > \text{Cl}^- \geq \text{N}_3^-$.

3.3 Electrochemistry of titanium (IV) in 1-butyl-2,3-dimethyl imidazolium tetrafluoroborate.

The description of the pure ILs cyclic voltammetry is given in chapter 3.1.4.

The addition of TiCl₄ to pure BMMImBF₄ results in cathodic and anodic peaks, increasing with the concentration of TiCl₄ (Fig.3.17).

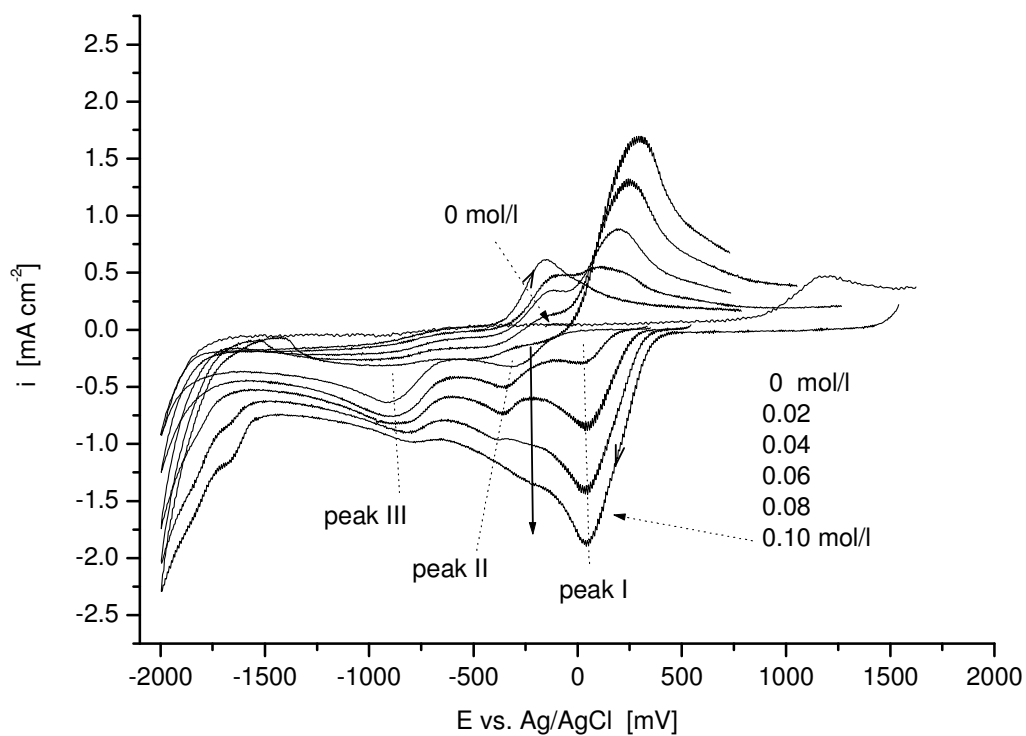


Fig. 3.17a

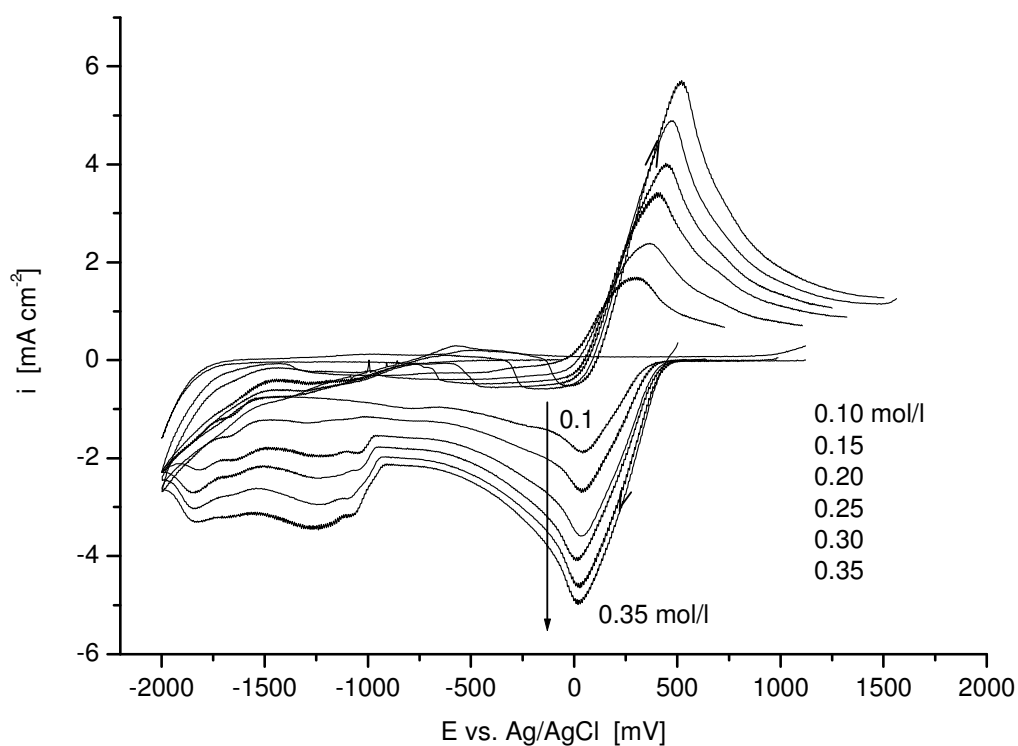


Fig.3.17b

Fig.3.17 Cyclic voltammograms of TiCl₄ solutions in BMMIm-BF₄ at concentrations: a) 0 to 0.1 mol/l in concentration steps 0.02 mol/l; b) 0.1 to 0.35 mol/l in concentration steps 0.05 mol/l. Scan rate 0.1 V s⁻¹.

The observed pattern differs depending on the concentration. The CV of diluted solutions (Fig.3.17a) shows a first cathodic peak within the range -0.36V to -0.38 V. At concentrations higher 0.02mol/l, an additional cathodic peak appears at +0.03V to 0.05V. These two cathodic peaks gradually merge with increasing concentration. Up to a concentration of 0.1 mol/l, a third cathodic peak is observed at -0.9V (Fig.3.18, circles). The dependency of the peak current density on the concentration for the first cathodic peak (I) consists of two linear branches (Fig.3.18, squares). In addition, the peak at -0.9V vanishes and, instead, a broad irregular cathodic wave appears at approx. -1.25V.

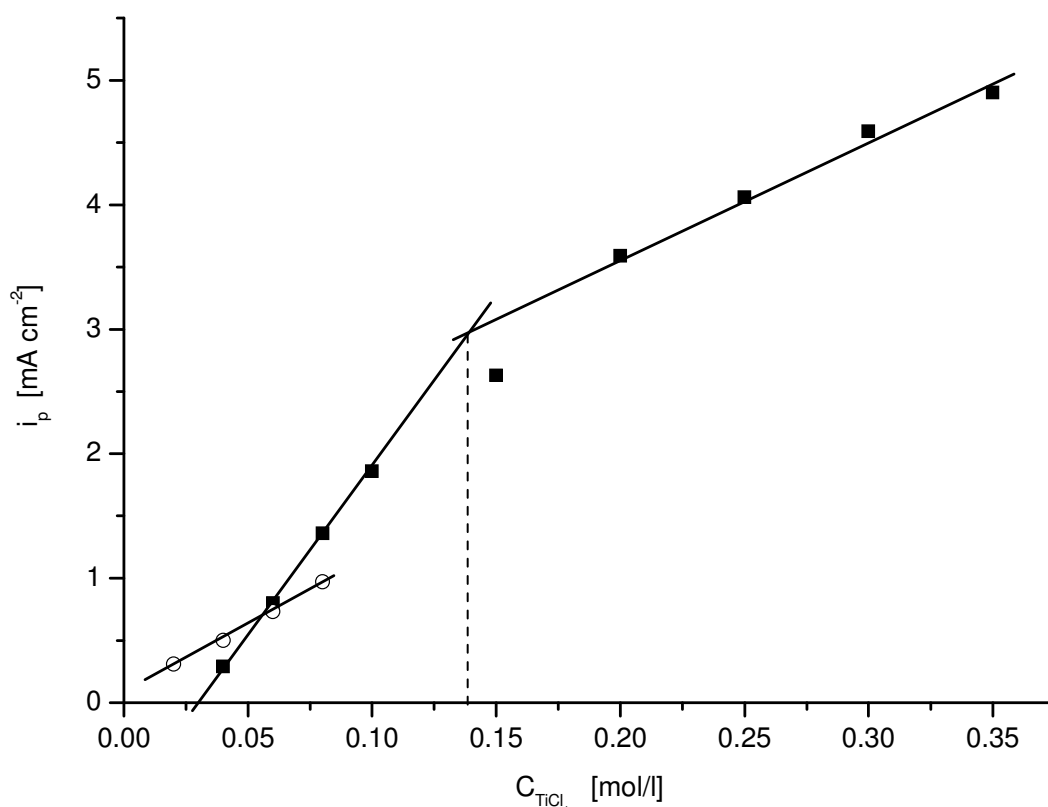


Fig.3.18 Current of cathodic peak I (■) and peak III (○) vs. concentration.

Thus, the preliminary study of TiCl₄ - BMMIm-BF₄ system by cyclic voltammetry revealed at least three concentration regions where the electrochemical behaviour of dissolved TiCl₄ is essentially different: 1) “dilute”, $C < 0.03 \text{ mol/l}$; “medium”, $0.03 < C < 0.14 \text{ mol/l}$, and 3) “concentrated”, $C > 0.14 \text{ mol/l}$. The reduction processes in these 3 concentration regions were studied with of CV and chronopotentiometry methods.

Dilute solution (0.025 mol/l TiCl₄ in BMMImBF₄)

Cyclic voltammograms at different sweep rates were recorded, as well as chronopotentiograms for a range of transition times starting at 0.3s up to 14s.

Two cathodic waves are distinctly observed, both in CV and chronopotentiograms, in this concentration region (Fig.3.19; 3.20).

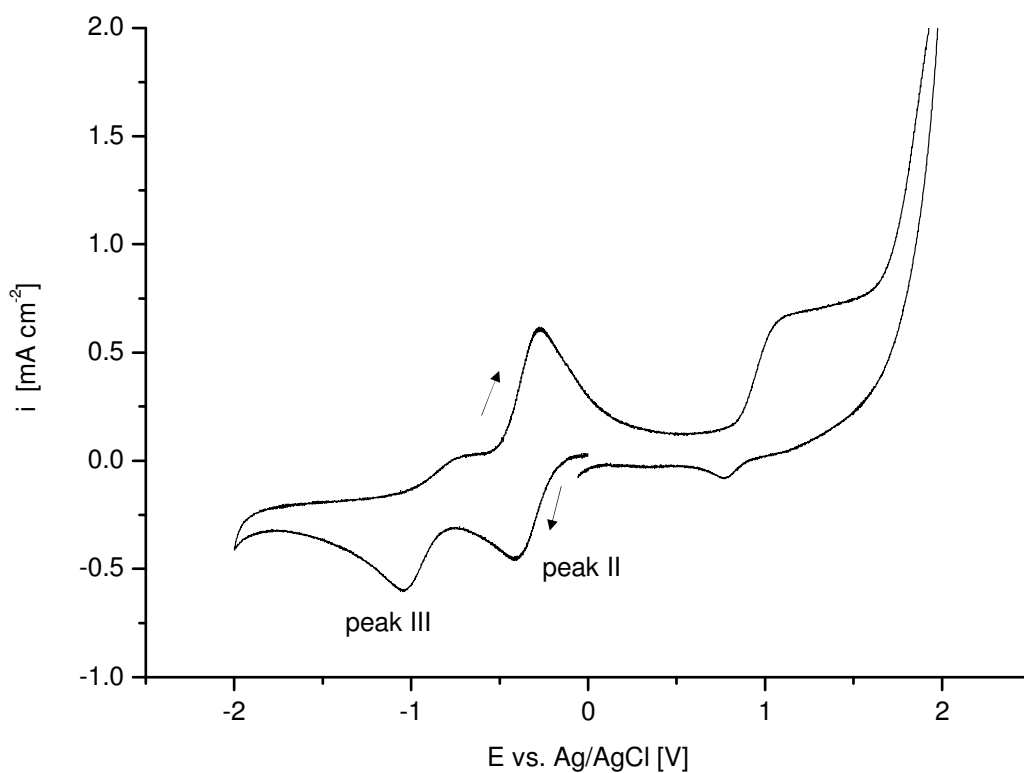


Fig.3.19 Cyclic voltammetry curve of 0.025 mol/l TiCl₄ in BMMImBF₄ at 0.1 V/s.

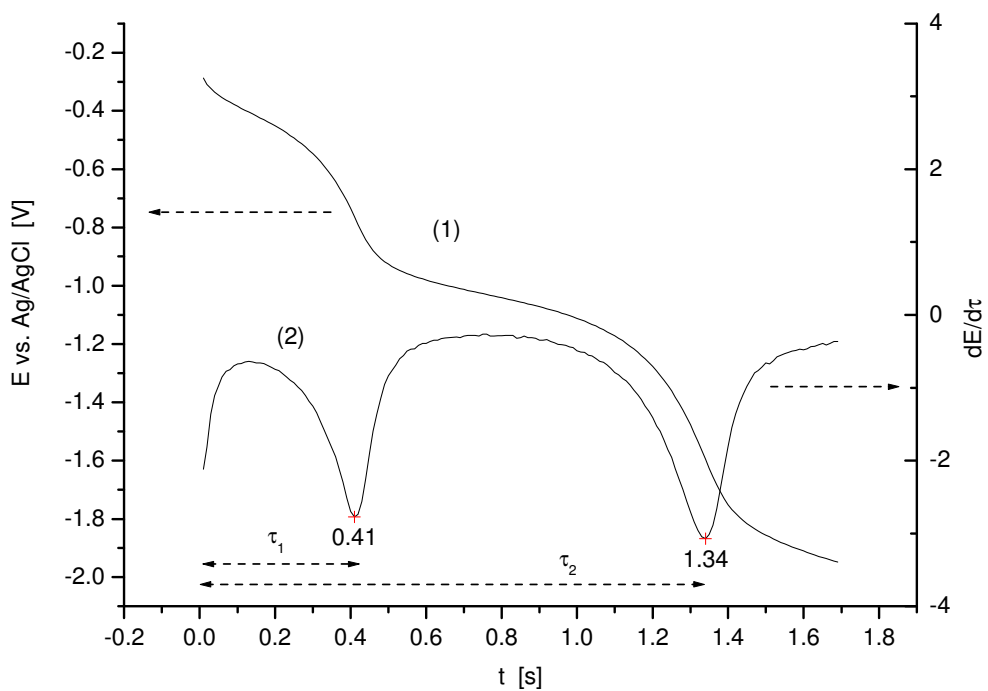


Fig.3.20 Potential response to a current step -1.45 mA cm^{-2} (curve 1) and its 1st derivative (curve 2).

Voltammetry data were analysed in terms of the Sevcik – Randles equation [2001Bar]:

$$\frac{i_p}{\nu^{1/2}} = 0.4463 \cdot \left(\frac{F^3}{RT}\right)^{1/2} n^{2/3} A D_o^{1/2} C_o^* \quad (3.8)$$

where i_p is the peak current, ν is the sweep rate, n is the number of electrons involved in the reaction and A is the area of the electrode, D_o is the diffusion coefficient and C_o^* is the bulk concentration of the depolarizer.

Peak currents were determined for the two cathodic peaks and $\frac{i_p}{\sqrt{\nu}}$ was plotted as a function of $\sqrt{\nu}$ (see Fig. 3.21). For analysis of CP data, the Sand equation was applied [2001Bar]:

$$i \cdot \tau^{1/2} = \frac{1}{2} \pi^{1/2} F n A D_o^{1/2} C_o^* \quad (3.9)$$

where i is the applied current, τ is the transition time, n is a number of electrons involved in the reaction.

Analysis of transition times and peak currents show that the reduction processes have some kinetic complications and are different for the two peaks, where peak II indicates a diffusion controlled reaction (Fig.3.21; 3.22).

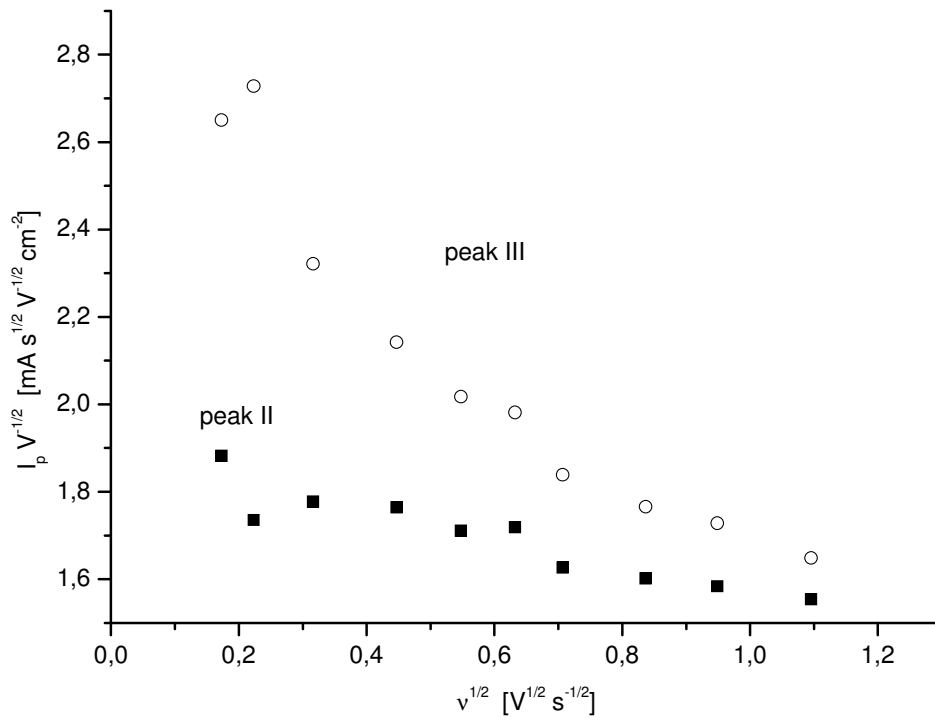


Fig.3.21 Voltammetry peak current analysis.

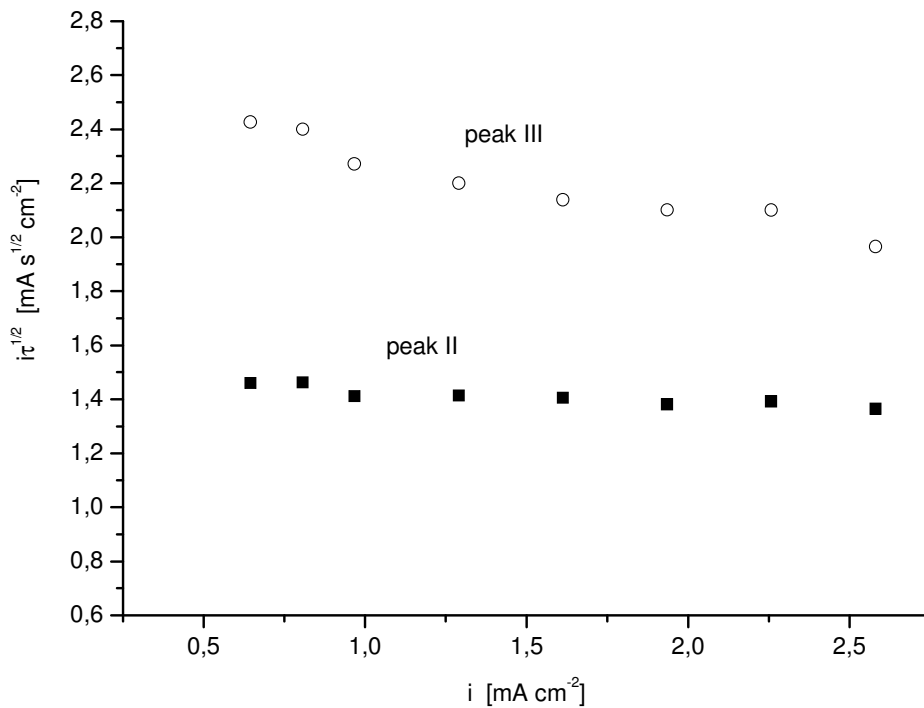


Fig.3.22 Transition time analysis.

Analysis of the shape of potential – time curves is given in terms of Karaoglanov equation (3.10) in Fig.3.23.

$$E = E_{\tau/4} + \frac{RT}{nF} \ln \frac{\tau^{1/2} - t^{1/2}}{t^{1/2}} \quad (3.10)$$

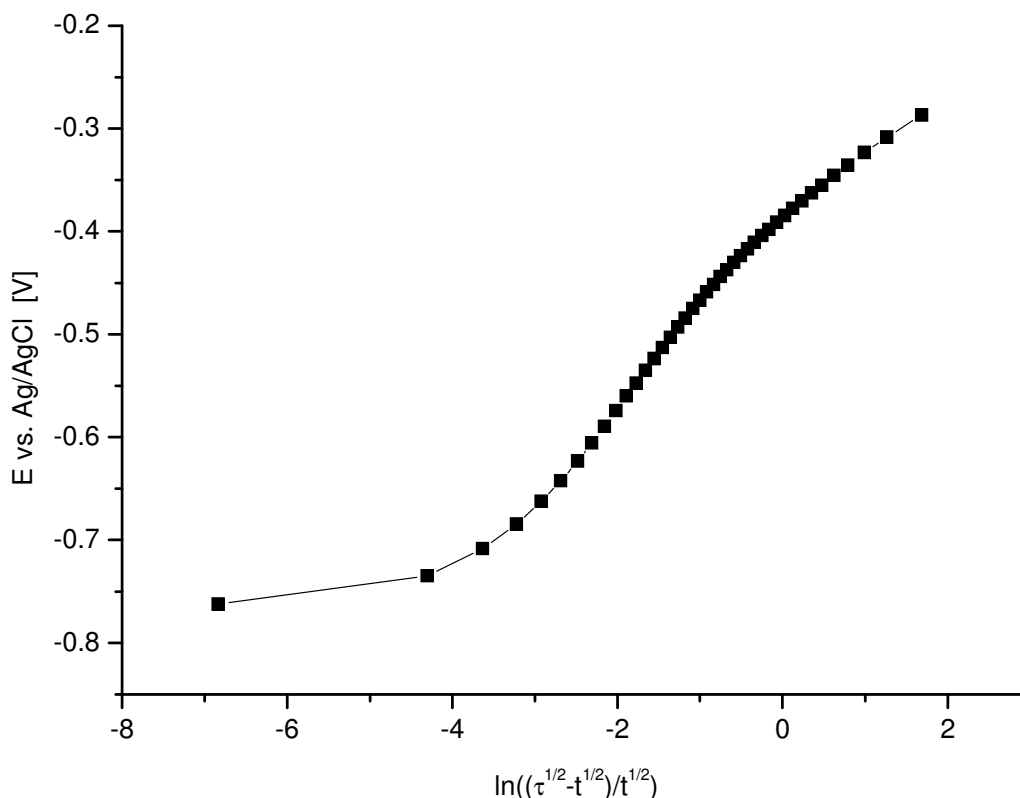
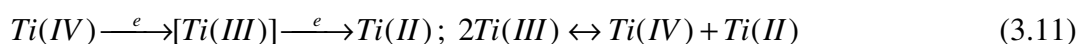


Fig.3.23 Karaoglanov plot of the potential – time curve in potential range of peak II.

This plot is S-shaped, which can be attributed to a 2-electron process with formation of thermodynamically unstable intermediate in equilibrium with the initial reactant and the product of the first visible peak [1980And]. A proposed process for peak II is shown in (3.11):



Assuming the first wave process (peak II) as (3.11), the diffusion coefficient of Ti(IV) was calculated from Sand equation (3.9), resulting for $n=2$ in $D_{Ti(IV)} = (1.09 \pm 0.03) \cdot 10^{-7} \text{ cm}^2 \text{ s}^{-1}$. This value is in a good agreement with studies of titanium (IV) chloride in strongly Lewis

acidic ILs [1990Car]. In water and DMSO solutions, studies of Ti(IV)/Ti(III) couple have shown a diffusion coefficient to be an order of magnitude higher ($10^{-6} \text{ cm}^2 \text{ s}^{-1}$) [1994Kis]. The second wave (peak III) corresponds to a process with some kinetic complications. Following general criterions are useful for the determination of the character of kinetic complications [1981Del].

Provided the conditions for semi-infiniteness and linearity of diffusion are obeyed,

- the derivative $\frac{d(i\tau^{1/2})}{di} > 0$, if the conjugated reactions of depolariser's inactivation (auto-inhibiting) take place or the diffusion process is partially overlapped with the discharge process of a surface layer (slow adsorption);
- the derivative $\frac{d(i\tau^{1/2})}{di} < 0$, if the depolarizer is partially replenished by antecedent or subsequent (auto-catalytic) chemical reactions.

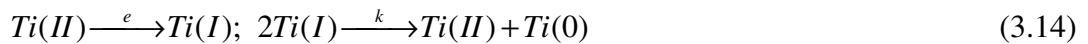
The negative slope of the plot $i\sqrt{\tau}$ vs. i (Fig.3.22) evidences a chemical reaction with partial replenishment of the depolariser. Since the first reduction step (peak II) is practically pure diffusion-controlled, the chemical reaction cannot be related to a pre-dissociation of some inactive complex of Ti(IV). Most probably, it is a disproportionation of the product according to the general scheme, which was theoretically considered by Fischer and Dračka [1959Fisch]:



According to their theory, the chronopotentiometric function $i\sqrt{\tau}$ should depend linearly on $i^{2/3}$ according to the equation:

$$i\tau^{1/2} = C_0 F \pi^{1/2} D_A^{1/2} - \left(\frac{3}{16}\right)^{1/3} \pi^{1/2} D_A^{-1/2} D_B^{2/3} F^{1/3} k_r^{-1/3} i^{2/3} \quad (3.13)$$

Fig.3.24 shows the dependency of the function $i\sqrt{\tau} = i\sqrt{\tau_{\text{peakIII}}} - i\sqrt{\tau_{\text{peakII}}}$ on $i^{2/3}$. It is linear, which confirms the validity of general reaction mechanism (3.12) for the second reduction wave (peak III). Obviously, in such case A is $Ti(II)$ and B is $Ti(I)$, and the 2-nd step mechanism is



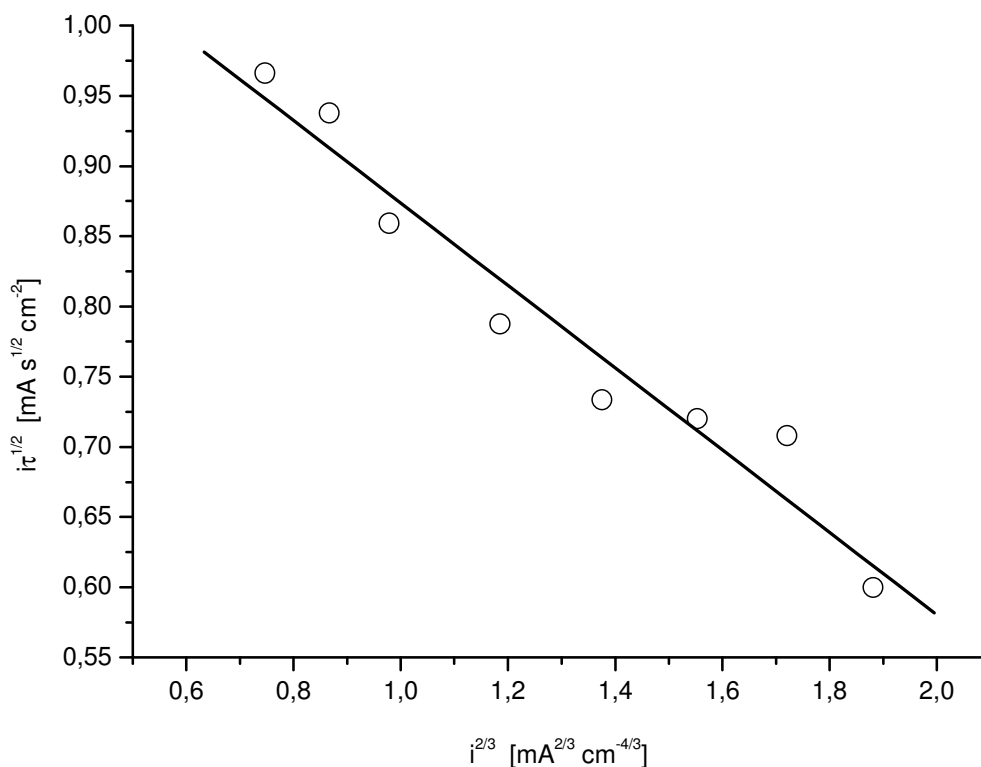


Fig.3.24 Transition times analysis in terms of Fischer - Dračka theory [1959Fisch].

Considering the chemical reaction (3.14) as totally irreversible, the diffusion coefficient of Ti(II) and the rate constant of (3.14) were calculated from fitting of the experimental data with equation (3.13) (Fig.3.24).

$$D_{Ti(II)} = (7.45 \pm 0.2) \cdot 10^{-8} \text{ cm}^2 \text{ s}^{-1}$$

$$k_r = (1.95 \pm 0.05) \cdot 10^6 \text{ cm}^3 \text{ mol}^{-1} \text{ s}^{-1}$$

Medium concentration (0.05 mol/l TiCl₄ in BMMIm-BF₄)

Three consecutive separated waves are observed in the “medium” concentration range (Fig.3.17a). The first wave (peak I) appears at more positive potentials (~0V), corresponding to the formation of the first intermediate, Ti(III), which becomes more stable as the concentration increases (the relative height of the peak is growing). Fig.3.25 shows the potential response to a current step in the electrolyte with 0.05 mol/l TiCl₄.

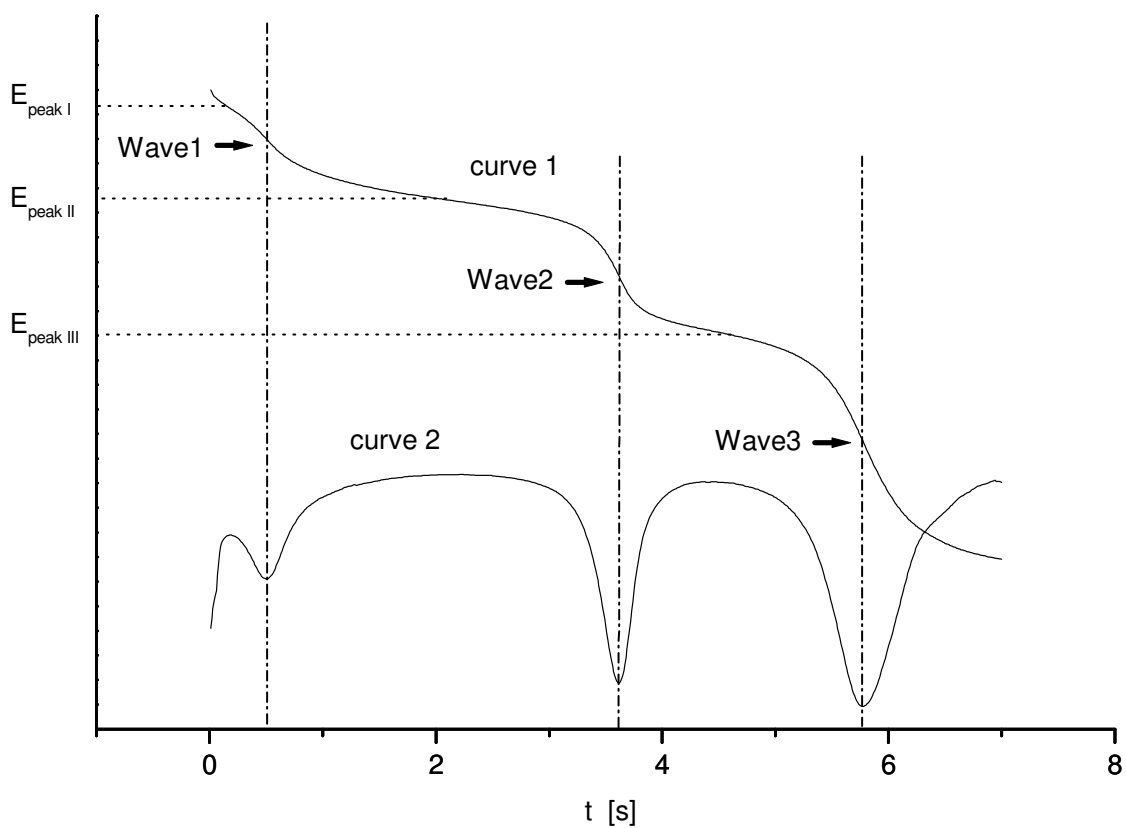


Fig.3.25 Potential response to a current step -0.97 mA cm^{-2} (curve 1) and its 1st derivative (curve 2).

The independency of the $i \cdot \tau^{1/2}$ on the current density is an evidence of a diffusion controlled reaction (see Fig.3.26).

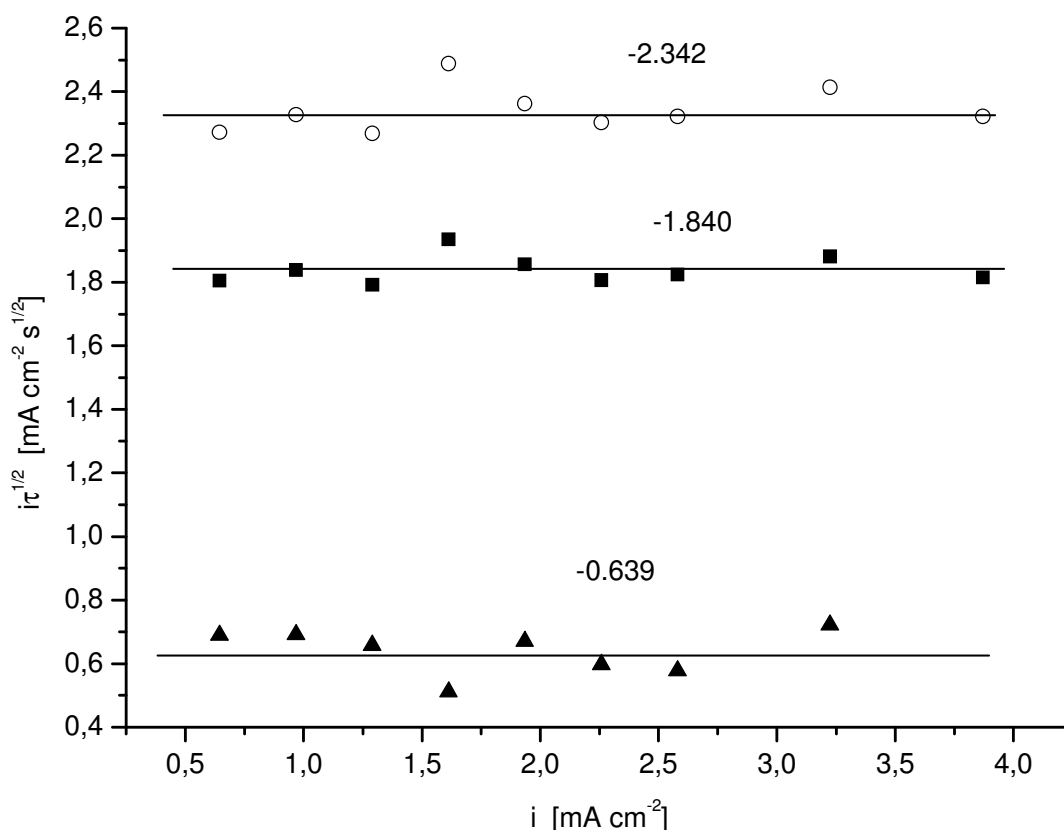


Fig.3.26 Transition time analysis in terms of Sand equation for three consecutive cathodic waves: \blacktriangle – peak I at 0.03V; \blacksquare – peak II at -0.4V and \circ – peak III at -0.9V.

The $i\tau^{1/2}$ ratios are approximately equal to: $i\tau^{1/2}_1 : i\tau^{1/2}_2 : i\tau^{1/2}_3 = 1:3:4$, which could be attributed to the formation of $Ti(III)$, $Ti(I)$ and $Ti(0)$ reduction products at the end of each reduction step. A similar pattern is observed at a concentration 0.1 mol/l.

Using equation (3.9), the diffusion coefficient for Ti(IV) species was calculated from the CP data.

The value in this intermediate concentration region is somewhat lower:

$$D_{Ti(IV)} = (6.9 \pm 0.2) \cdot 10^{-8} \text{ cm}^2 \text{ s}^{-1}.$$

“Concentrated” solutions

Further increase of the concentration, results in a phase separation in the melt: small drops of undissolved $TiCl_4$ are clearly visible on the surface and in the bulk of the electrolyte.

Accordingly, the reduction pattern becomes much more complicated at potentials more negative -1V mol/l. Series of poorly resolved waves appear in potential region about -1 to -2V in the CVs (Fig.3.17b) and up to 5 peaks are observed in the derivative curve of the CP data (Fig.3.27).

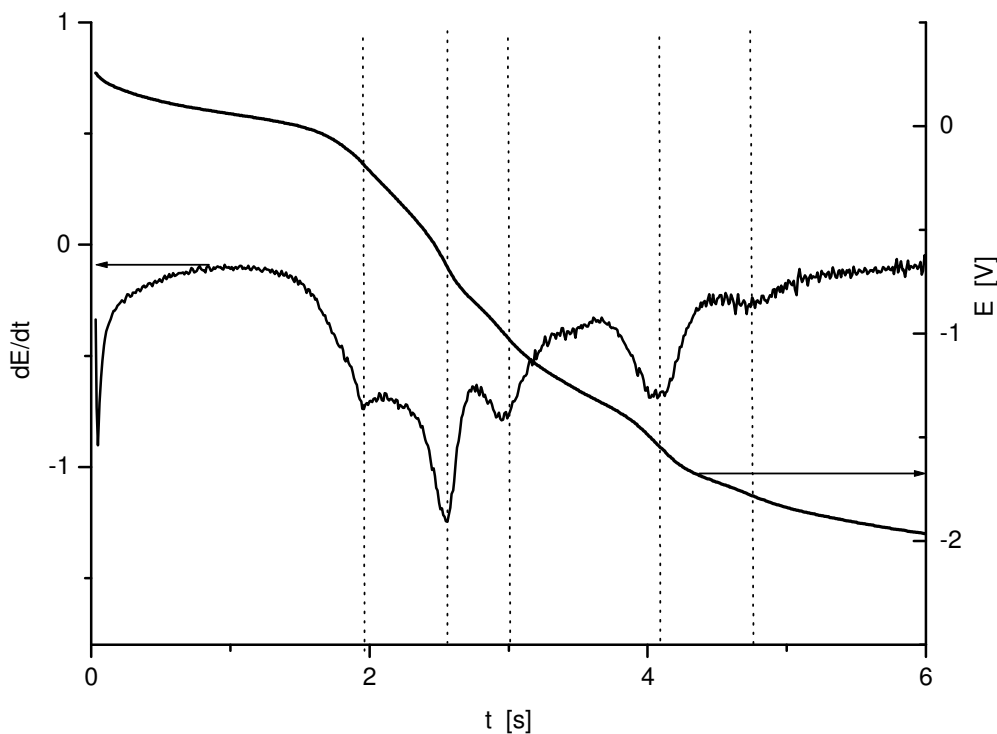


Fig.3.27 Potential response to a current step (-3.0 mA cm^{-2}) and its 1st derivative for $C_{\text{TiCl}_4} = 0.2 \text{ mol/l}$.

Transition time analysis for these peaks is given in Fig.3.28. One can see that these transition times can hardly be interpreted in terms of simple stepwise reduction mechanism.

The reason of such behaviour can be related to the phase separation, which is observed in „concentrated“ solutions. In fact, the electrochemical process takes place in heterogeneous system containing two liquid phases – IL saturated with TiCl_4 and vice versa. There are no theoretical studies of this case in the literature yet.

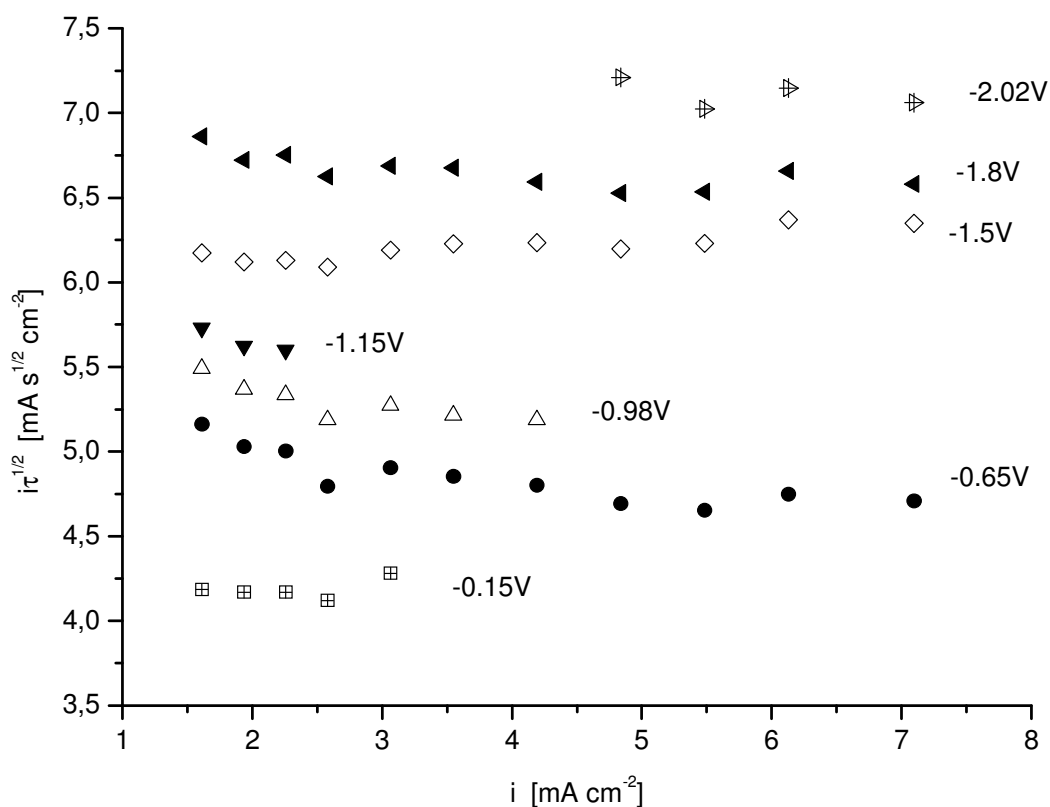


Fig.3.28 Transition time analysis in terms of Sand equation, $C_{\text{TiCl}_4} = 0.2 \text{ mol/l}$. Potentials in the plot correspond to potentials of the process transition times.

As follows from the investigations, the overall electrochemical reduction mechanism can be represented in terms of general scheme, which was first proposed in [1981Del]: sequence of one-electron reduction steps with accompanying disproportionation reactions $2\text{Ti}(i) \rightleftharpoons \text{Ti}(i+1) + \text{Ti}(i-1)$, with possible formation of each species in the intermediate oxidation states. In diluted solutions, the Ti(II) intermediate is more stable, and also the disproportionation kinetics of Ti(I) can be detected. Total 4-electron reduction to Ti(0) is observed with the formation of Ti(III) and Ti(I) as the relatively stable intermediates. At concentration higher than 0.14mol/l the limit of TiCl₄ solubility in the IL influences significantly the reduction mechanism, resulting in a very complicated reduction patterns. Theoretical explanation of the electrochemical processes in such heterogeneous system is still to be found.

3.4 Anodic dissolution of Ti in BMMImBF₄.

The studies of the anodic reaction of the titanium electrode are of a great importance for establishing in future the deposition process.

To study the titanium electrode behavior in the ILs, three pretreatments were used: etching, polishing under ambient air, polishing under Ar.

Anodic curves were recorded with a following setup:

Three electrode scheme (WE – Ti wire, REF – Ag/AgCl in BMMImBF₄, AUX – GC. Potential sweep rate – 100mV/s, t=65°C; electrolyte: BMMImBF₄).

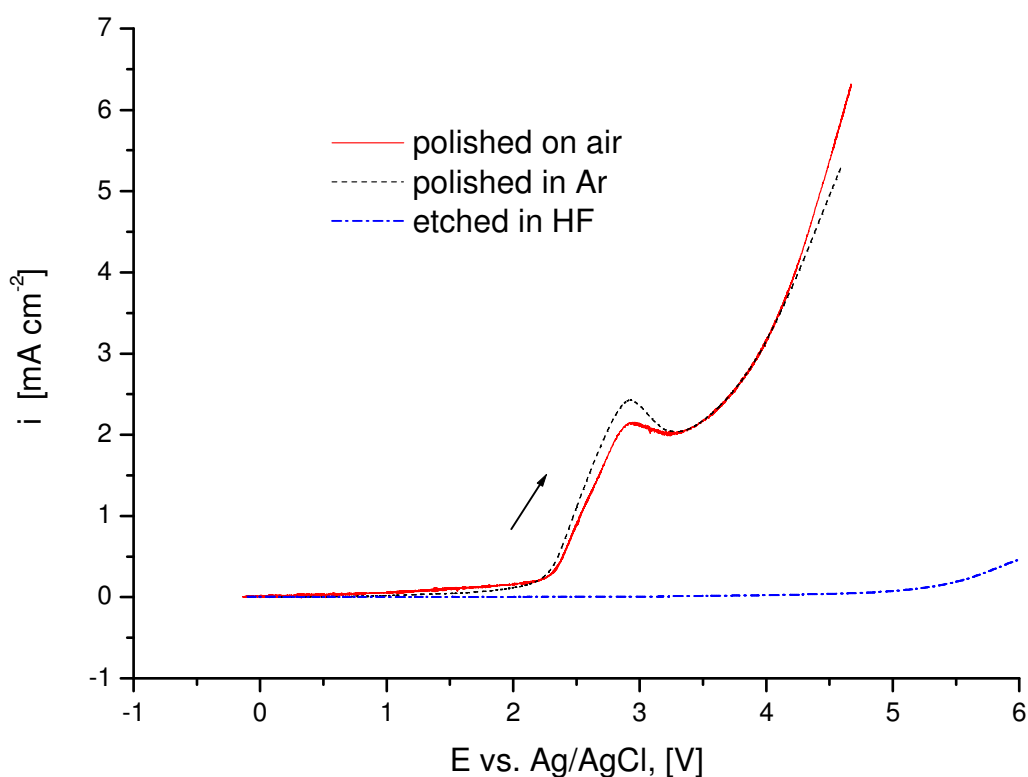


Fig. 3.29 Anodic curves of Ti electrodes with different pretreatments in BMMImBF₄

Etched Ti (Fig. 3.29 blue line) shows negligible current over a wide range of potentials – the surface is passive. The surface must be covered with the stable products of etching in HF (fluoride compounds). In two other cases – polished under Ar (black line) and polished under ambient air (red line) we see typical anodic curve for metals inclined to passivation. Active dissolution in the region 2.3V – 2.8V followed by passivation and IL decomposition.

Dissolution of Ti

Coulometry on polished Ti electrode has been performed in several steps with weighting the Ti wire before and after the experiment.

Experimental setup:

two electrode scheme - Ti wire – WE, GC – AUX; t = 65°C.

Weight of Ti electrode before the experiment:	92.21	mg
Weight of Ti electrode after the experiment:	92.072	mg
Δm	0.138	mg

Table 3.7 Sequence of currents and charge passed through the system

Current I [mA]	Time [min]	Charge Q [C]
0.5	32.4	0.972
0.2	16	0.192
-0.01	60	-0.036
0.2	3.6	0.043
Total charge:		1.171

Amount of electrons:

$$n_e = \frac{Q}{F} \quad (3.15)$$

$$n_e = \frac{1.171}{96490} = 1.214 \cdot 10^{-5} \text{ [mol]}$$

$$n_{Ti} = \frac{\Delta m}{M_{Ti}}, \quad (3.16)$$

where, Δm - weight loss of the Ti anode [g]; M_{Ti} – titanium molar weight [g].

$$n_{Ti} = \frac{0.138 \cdot 10^{-3}}{47.867} = 0.288 \cdot 10^{-5} \text{ [mol]}$$

Valence of Ti dissolved:

$$z = \frac{n_e}{n_{Ti}} \quad (3.17)$$

$$z = \frac{1.214 \cdot 10^{-5}}{0.288 \cdot 10^{-5}} = 4.21$$

The surface became passivated quite fast. For this reason a cathodic polarization was applied with a small current in order to reduce the formed passive layer.

The surface of Ti wire was etched after the experiment (see Fig.3.30).

Considering the results of weight loss of Ti electrode and the amount of the electrode that has passed through the system, the number of electrons participating in the dissolution reaction was derived ($n = 4.21$).

Possible sources of error:

- the oxidized Ti was left on the electrode in the passive film;
- weighting.

Anodized Ti electrode:

(Pretreatment: polished under ambient air)

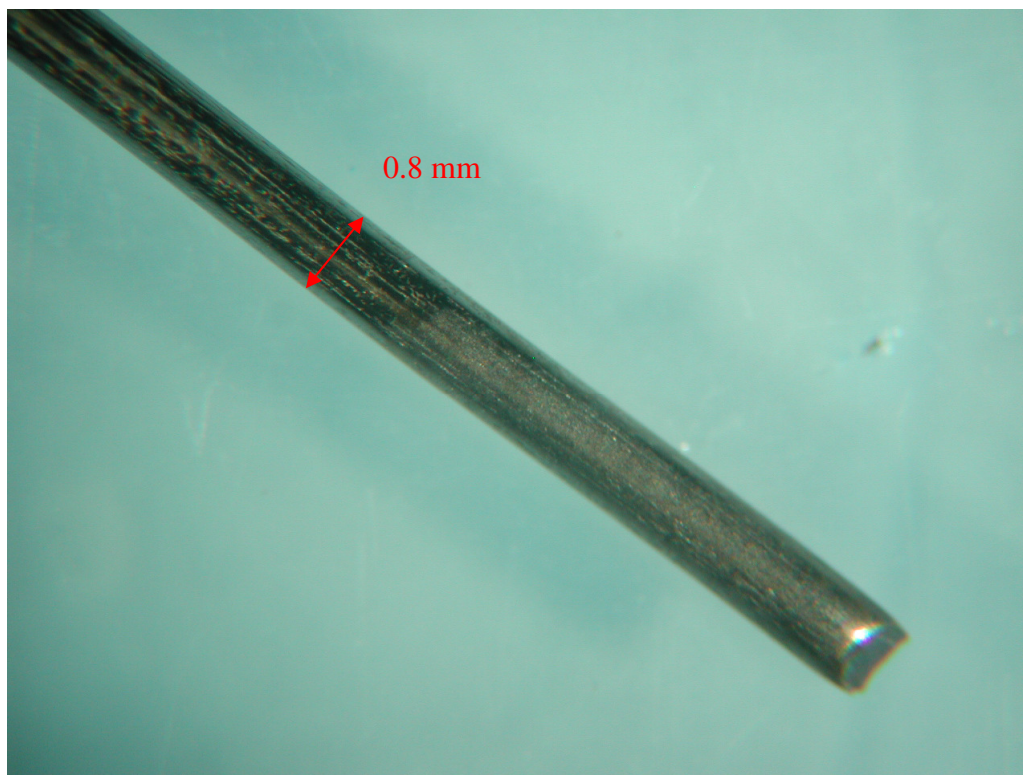


Fig.3.30 Ti wire after anodizing in BMMImBF₄.

In order to study the interface on the surface of the Ti anode, the Ti wire was anodized in the BMMImBF₄ with 0.1 mol/l TiCl₄·2THF. Glassy carbon rod was used as an auxiliary electrode. After applying anodic current of 0.2 mA for 20h, analysis of the surface has been performed.

The electrolyte decomposition was visible during the electrolysis.

For the analysis of the anodised surface, Philips XL-30 Environmental Scanning Electron Microscope (ESEM) equipped with an energy-dispersive X-ray spectrometer (EDX) was used.

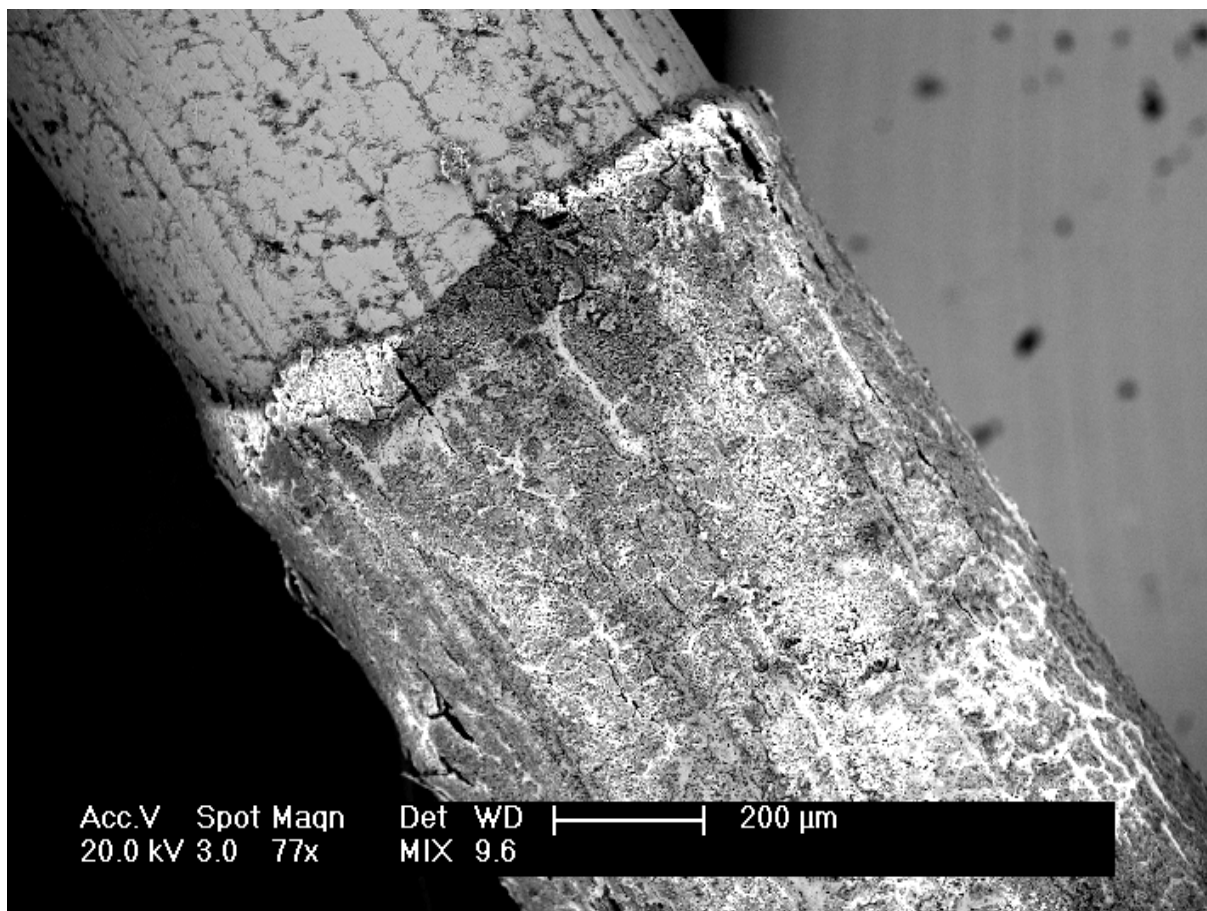


Fig. 3.31 ESEM picture of the Ti wire after applying 0.2mA for 20h, temperature 65°C.

The EDX analysis:

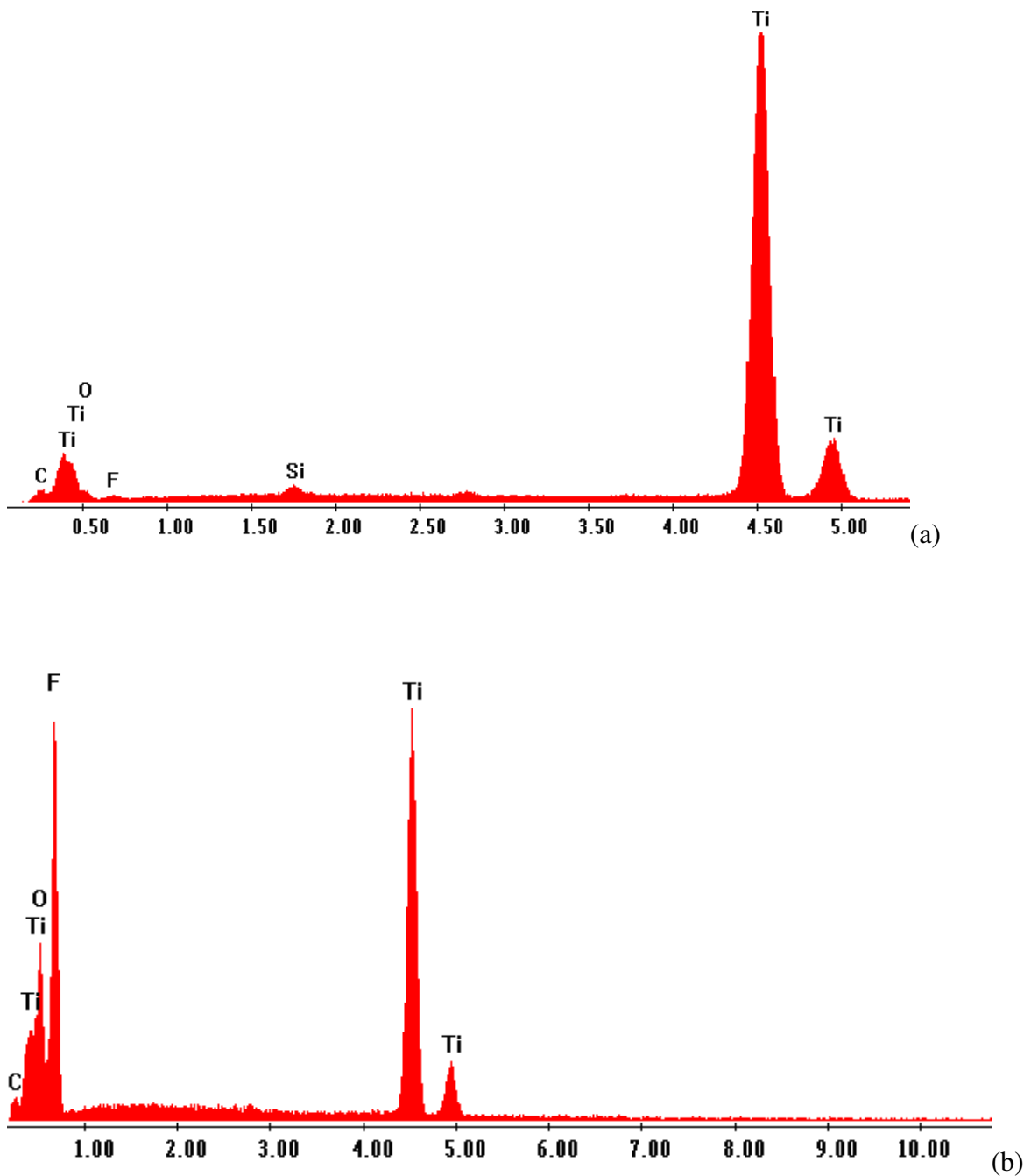


Fig. 3.32 EDX spectra of the Ti wire (a) not immersed, (b) immersed in the melt.

The surface layer consists mostly of titanium fluoride. The oxide has formed as a result of the exposure to air after the experiment.

The anodic dissolution of Ti is overlapped with the electrolyte decomposition as described in [2003Xia].





The released fluorine reacts with the active Ti anode surface with the fluoride formation.

3.5 Electrochemistry of Ti(IV) in 1-butyl-2,3-dimethyl imidazolium azide.

3.5.1 Electrochemical behaviour of TiCl₄·2THF in BMMImN₃

Linear Sweep Voltammetry of 0.12 mol/l TiCl₄·2THF in BMMImN₃ has been performed at different potential sweep rates (Fig. 3.33).

Non- stationary curves

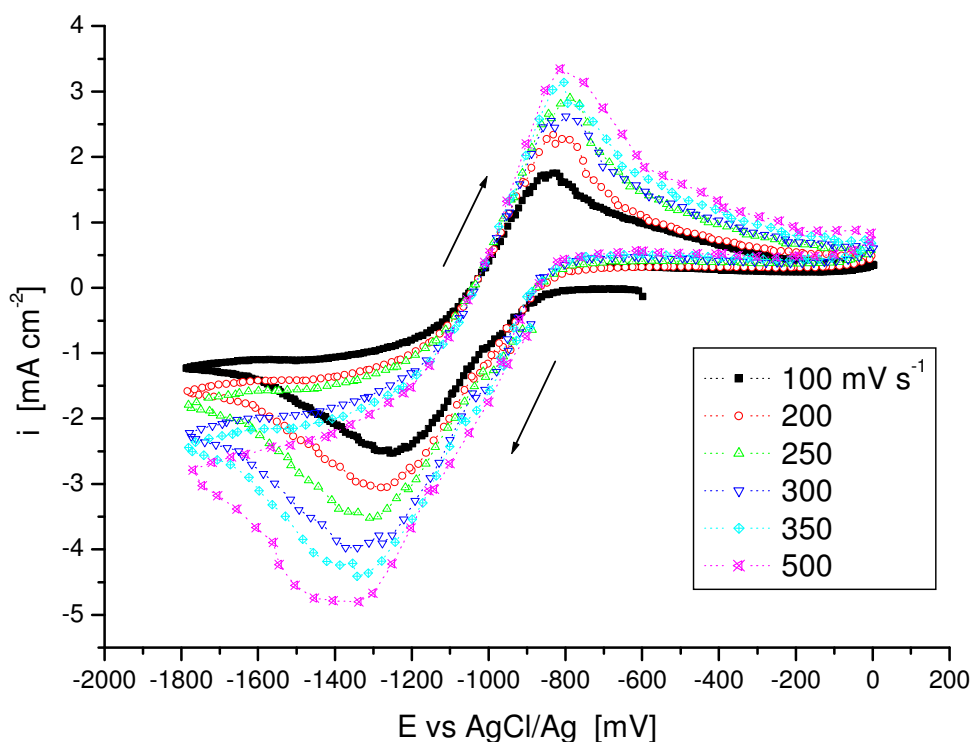


Fig.3.33 CV studies of 0.12 mol/l TiCl₄·2THF in BMMImN₃ at different potential sweep rates.

Reduction – oxidation wave has been studied in a narrower range (-1.8V – 0V) to avoid electrolyte reduction/oxidation products interference with the electrode reaction. The process does not show a clear Nernstian (reversible) behavior.

Diagnosis for Nernstian process at 65⁰C [2001Bar]:

$$|E_p - E_{p/2}| = 2.20 \frac{RT}{nF} = 64/n \text{ mV at } 65^{\circ}\text{C}$$

For the waves shown on the Fig.3.33 at 65⁰C

- $|E_p - E_{p/2}| \approx 200 - 250 \text{ mV}$
- The peak potential depends on the rate;

This indicates a non-reversible process, probably some chemical reaction overlapping.

“Half-stationary” curve

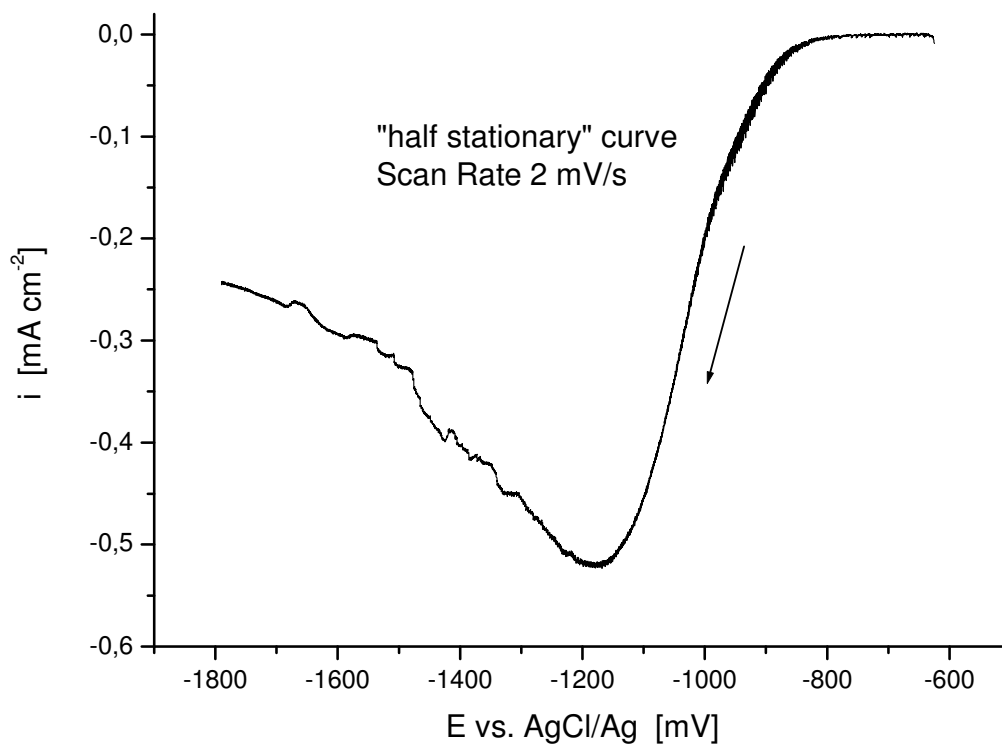


Fig. 3.34 Current – potential curve on Pt electrode; 0.12 mol/l $\text{TiCl}_4 \cdot 2\text{THF}$ in BMMImN_3 ; potential sweep rate 2 mV s^{-1} ; temperature 65°C .

- The initial part of this curve in Tafel plot:

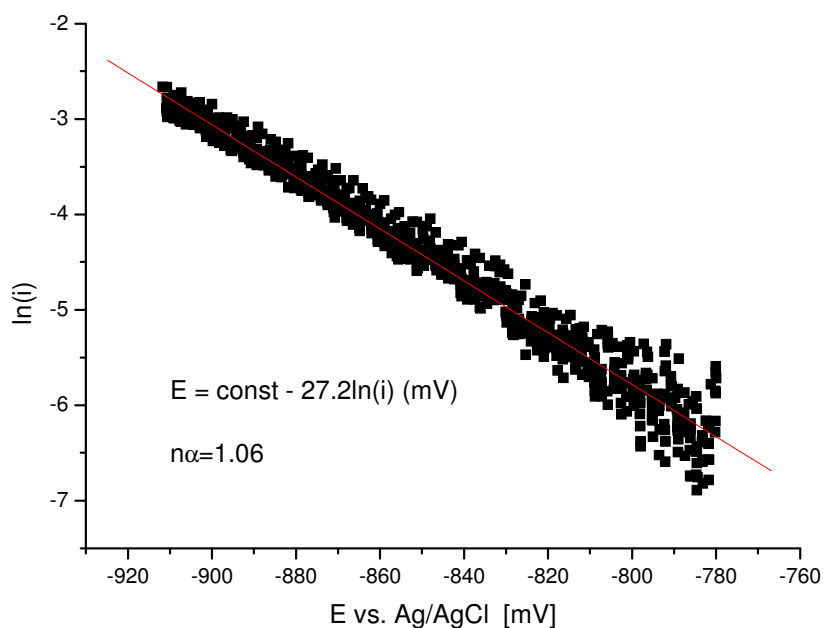


Fig. 3.35 Part of the half-stationary curve, Fig. 3.34, fitted with Tafel equation.

Assuming the Tafel dependency

$$E = const + \frac{RT}{\alpha n F} \ln|i|, \quad (3.21)$$

we get $n\alpha=1.06$.

Applying Frumkin-Bagotsky equation:

$$E = const + \frac{RT}{\alpha n F} \ln \frac{i_{\infty} - i}{i}, \quad (3.22)$$

(though we have a peak instead of limit current, let us take $i_{\infty} = i_p$), we get a plot:

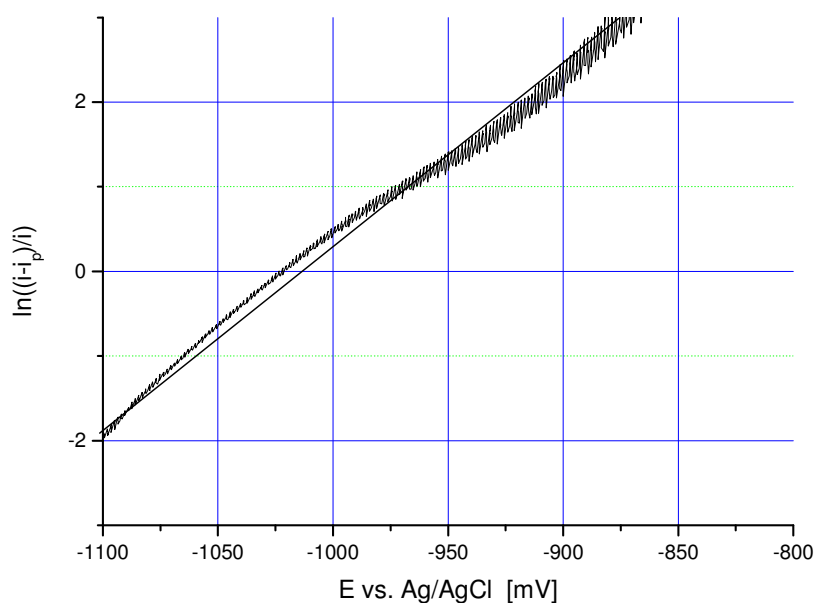


Fig. 3.36 Current potential curve in terms of Frumkin-Bagotsky equation.

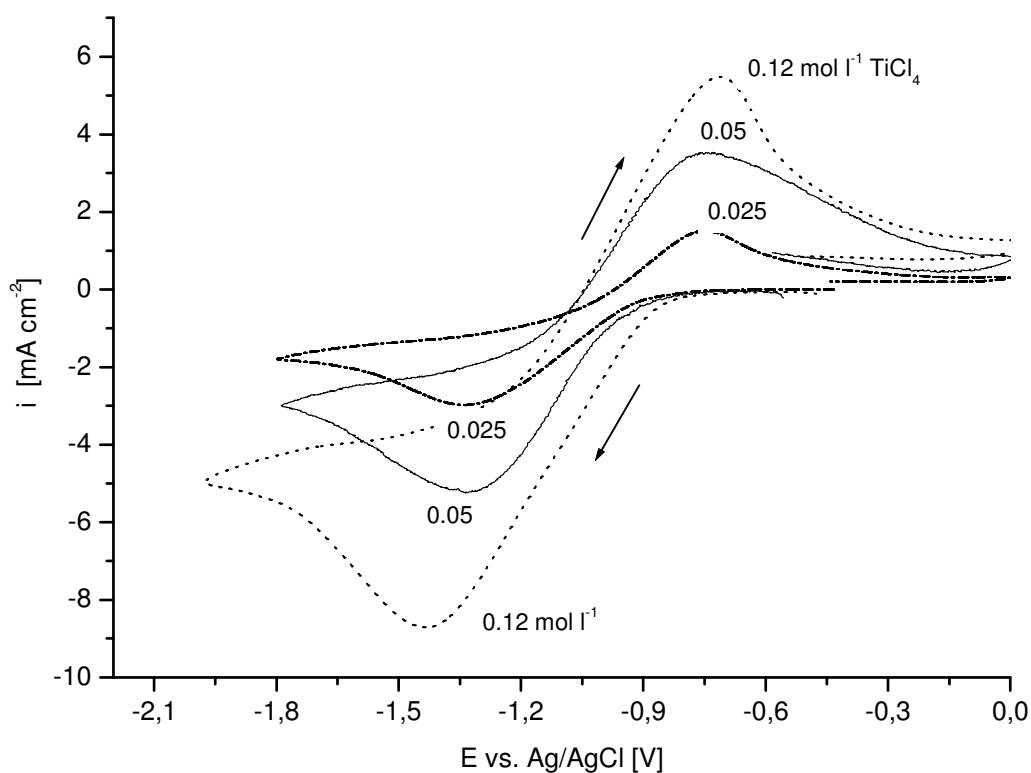
The average slope corresponds to $n\alpha = 0.71$.

The process corresponding to this wave is irreversible. It might be one-electron electrochemically irreversible process with transfer coefficient about 0.75. This is not common – the ~0.5 is expected in such a case. More likely, the irreversibility results from some accompanying chemical kinetics.

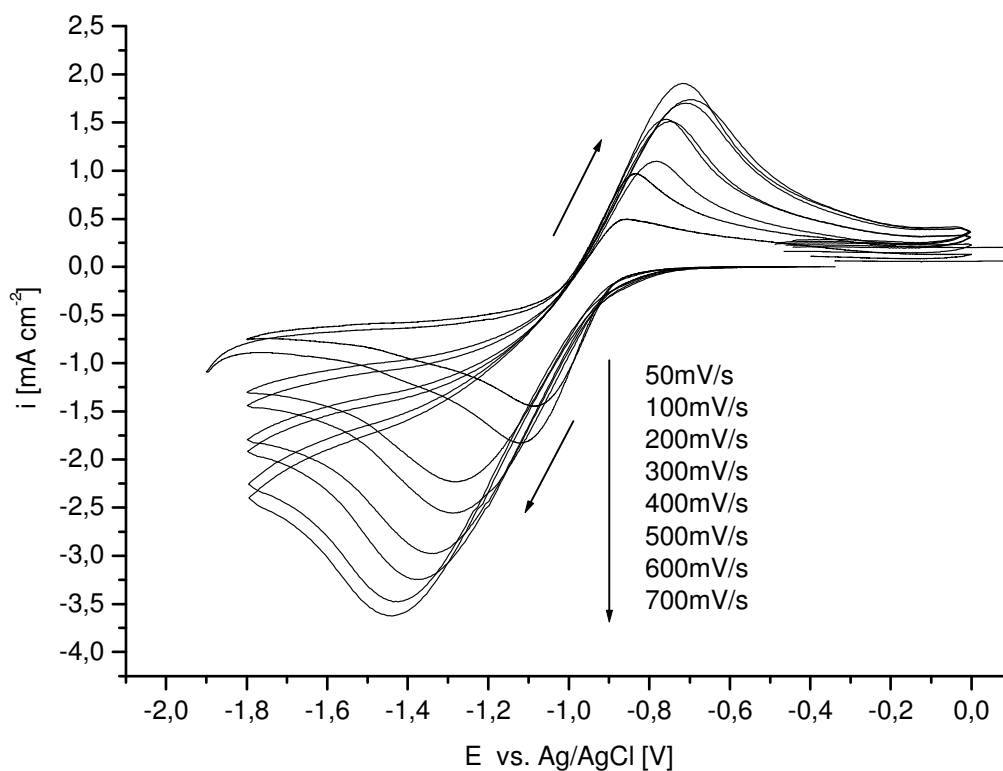
3.5.2 Electrochemistry of TiCl₄ in BMMImN₃

To investigate the electrochemical behaviour of Ti(IV) in the chosen IL, TiCl₄ was added in concentrations 0.025, 0.05 and 0.12 mol l⁻¹.

Only one broad wave appears in TiCl₄- BMMImN₃ solutions in the entire concentration range up to 0.12M TiCl₄ (Fig.3.37 a, b).



(a)



(b)

Fig.3.37 Cyclic voltammograms of TiCl₄ solutions in BMMImN₃: (a) with different TiCl₄ concentrations, sweep rate 0.4 V s⁻¹; (b) at different sweep rates; concentration of TiCl₄ 0.025 mol l⁻¹ (potential range 0V to -1.9V).

As seen from Fig.3.37, the wave is much wider than described for reversible diffusion-controlled process. The half-width

$$|E_p - E_{p/2}| \approx 120 - 250 \text{ mV}$$

is much larger compared to the theoretical value

$$|E_p - E_{p/2}| = 2.20 \frac{RT}{nF} = 64/n \text{ mV at } 65^\circ\text{C [2001Bar]},$$

where n is the number of electrons involved in the reaction, E_p is the peak potential and $E_{p/2}$ is the half peak potential.

This, and also shift of the peak position toward negative potentials with increasing of the sweep rate, indicate the irreversibility of the reduction process. The peak currents do not obey the Sevcik – Randles equation:

$$\frac{i_p}{\nu^{1/2}} = 0.4463 \cdot \left(\frac{F^3}{RT}\right)^{1/2} n^{3/2} A D_o^{1/2} C_o^* \quad (3.23)$$

where i_p is the peak current, ν is the sweep rate, n is the number of electrons involved in the reaction and A is the area of the electrode, D_o is the diffusion coefficient and C_o^* is the bulk concentration of the depolarizer.

The dependence of $\frac{i_p}{\nu^{1/2}}$ on the sweep rate, (Fig.3.38), is slightly non-linear, resembling the curves for irreversible process according to Matsuda-Ayabe theory [1955Mat].

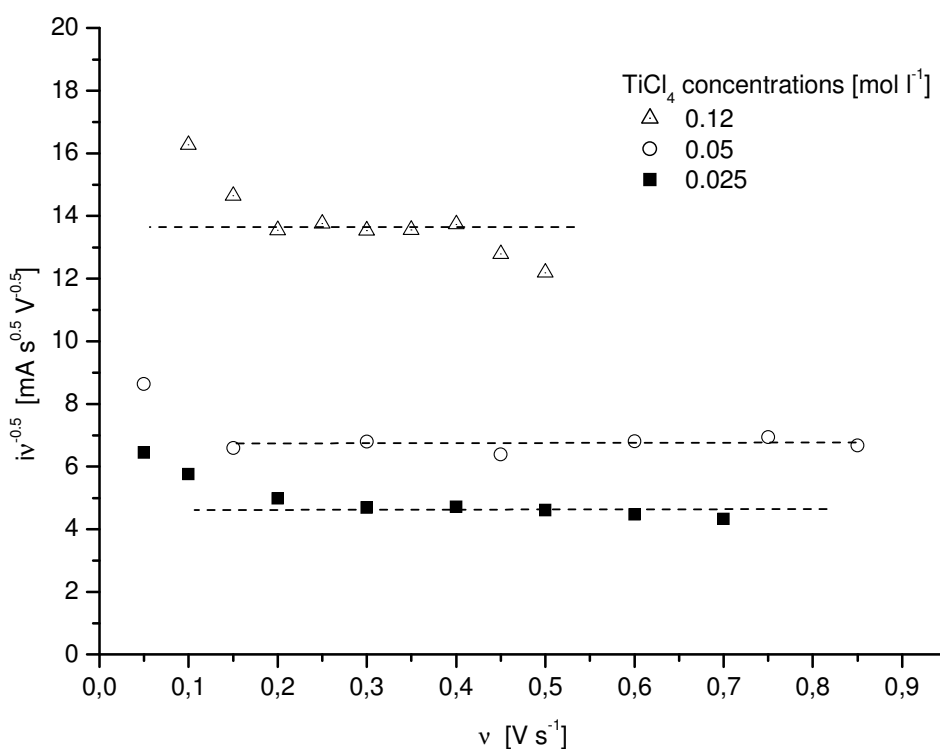


Fig.3.38 Peak current analysis for cyclic voltammetry studies of different TiCl₄ concentrations at 65°C in BMMImN₃.

Dependence of the average values of $\frac{i_p}{\nu^{1/2}}$ on concentration is a straight line (Fig.3.39), which does not fall into the origin, what is also a characteristic of irreversible (non-Nernstian) processes.

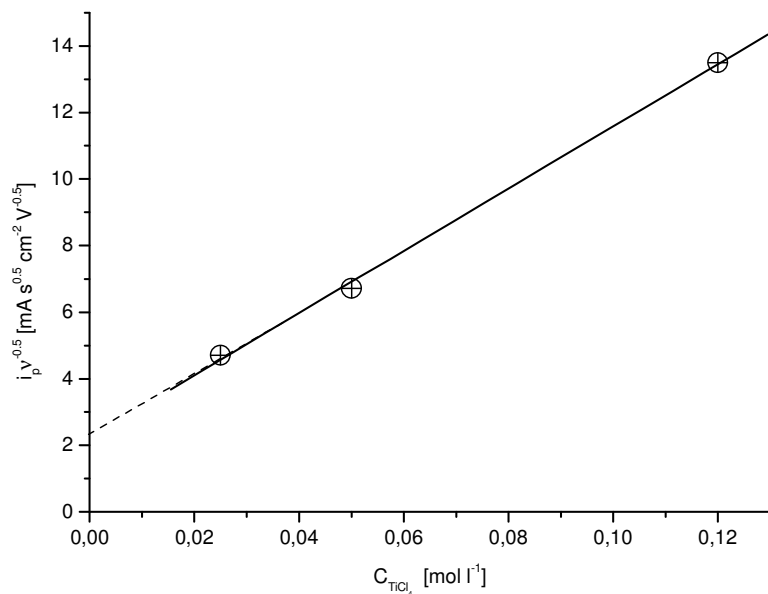


Fig.3.39 Concentration dependence of cyclic voltammetry peak currents.

Figure 3.40 shows an example of a stationary polarization curve for a melt of BMMImN₃ with 0.05 mol l⁻¹ concentration of TiCl₄. The limit current value, which is attained at -1V, is unsteady because of gas evolution starting at a potential of -1.05V which can be seen distinctly at the electrode. Thus, one can conclude that the product generated by the reduction reaction is not stable and gradually decomposes evolving volatile products, since the pure BMMImN₃ was found to be stable up to -1.8V.

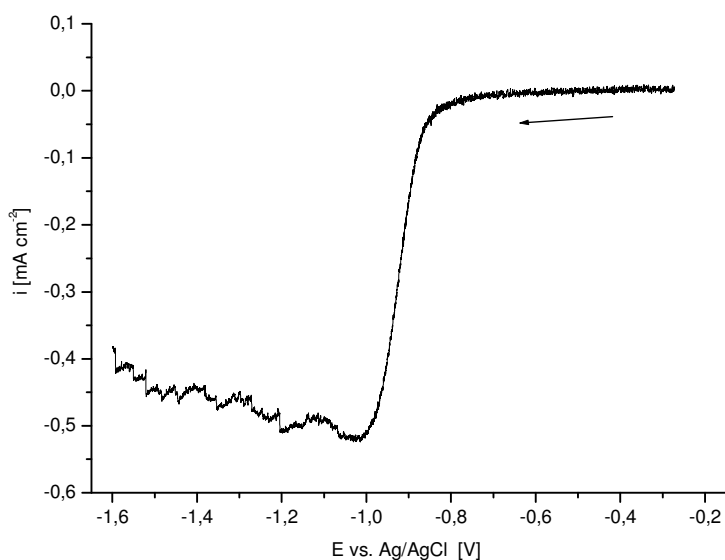


Fig.3.40 Current-potential curve at sweep rate 1 mV s⁻¹; concentration of 0.05 mol l⁻¹ TiCl₄ in BMMImN₃; temperature 65°C.

The large part of the curve in the potential range -865 to -920 mV (Fig.3.40) is a Tafel-like straight line in a $\ln(i)$ vs E plot (Fig.3.41).

The curve was recorded 3 times and the statistic distribution of the results is indicated.

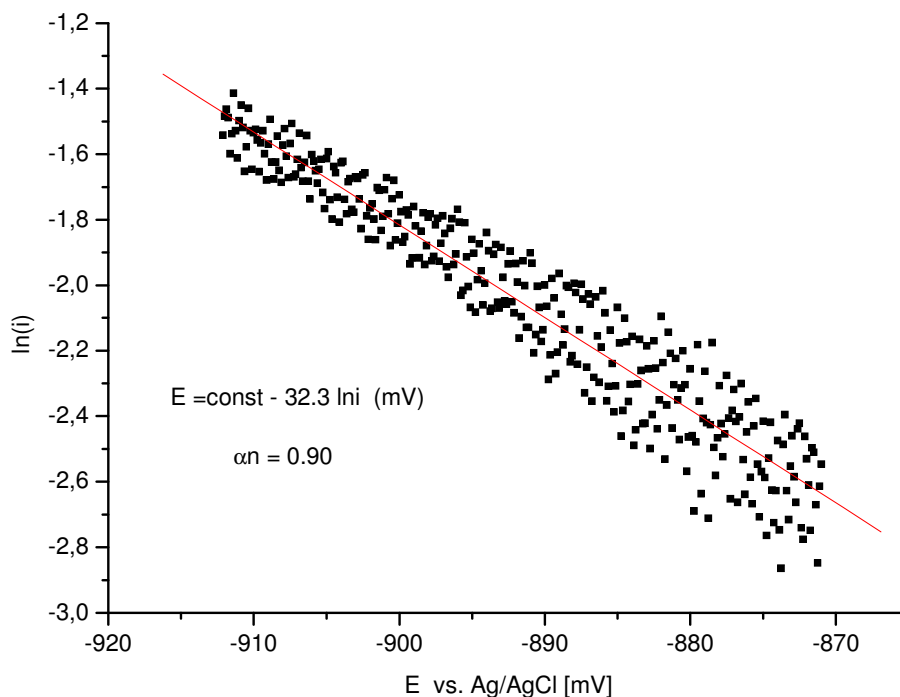


Fig.3.41 Part of stationary curve, Fig.3.40, fitted with Tafel equation.

Thus, as it follows from voltametric investigations, reduction of Ti(IV) in BMMImN₃ electrolyte is a one-step irreversible process. The product of this process is not stable and decomposes slowly in the conditions of stationary polarization.

More information on the reduction mechanism was obtained by chronopotentiometric method.

As CV, the potential-time chronopotentiometric curves also contain only one reduction wave (Fig.3.42).

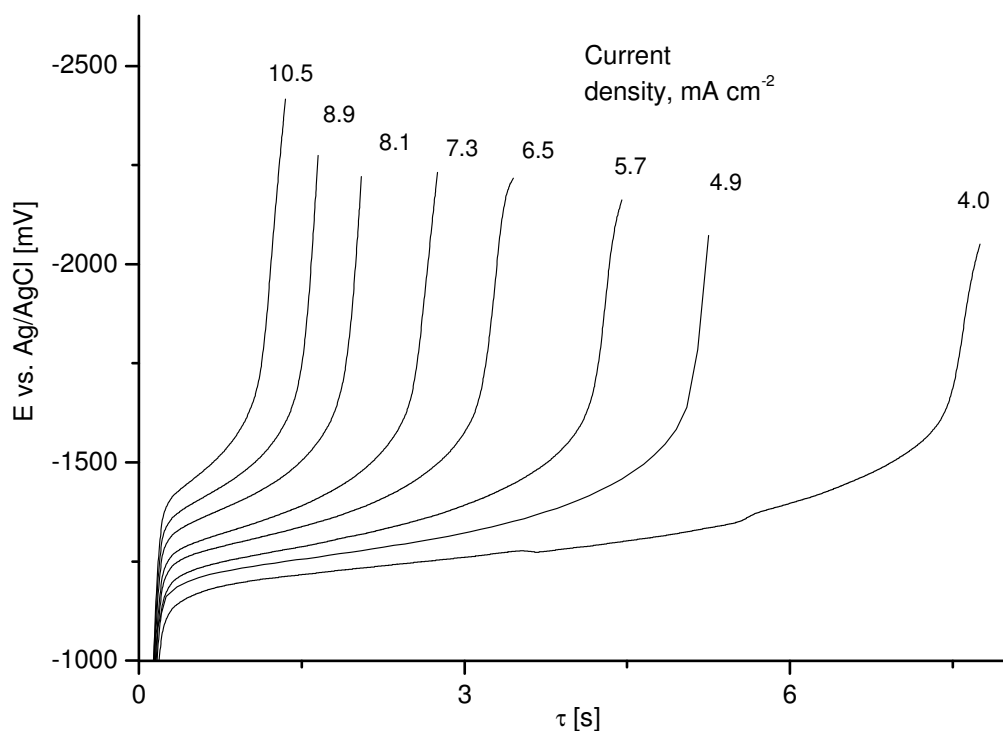


Fig.3.42 Potential response after applying constant current step (4.0 to 10.5) mA cm⁻²; BMMImN₃ with 0.12 mol l⁻¹ TiCl₄; temperature 65°C; Pt working electrode.

Shape of the curves is typically non-Nernstian. The plot E vs. $\ln(\sqrt{\tau} - \sqrt{t})$ is linear (Fig.3.43) in accordance with the theoretical equation for an irreversible process [2001Bar]:

$$E = \frac{RT}{\alpha F} \ln \left[\frac{2k_f^o}{(\pi D)^{1/2}} \right] + \frac{RT}{\alpha F} \ln[\tau^{1/2} - t^{1/2}] \quad (3.24)$$

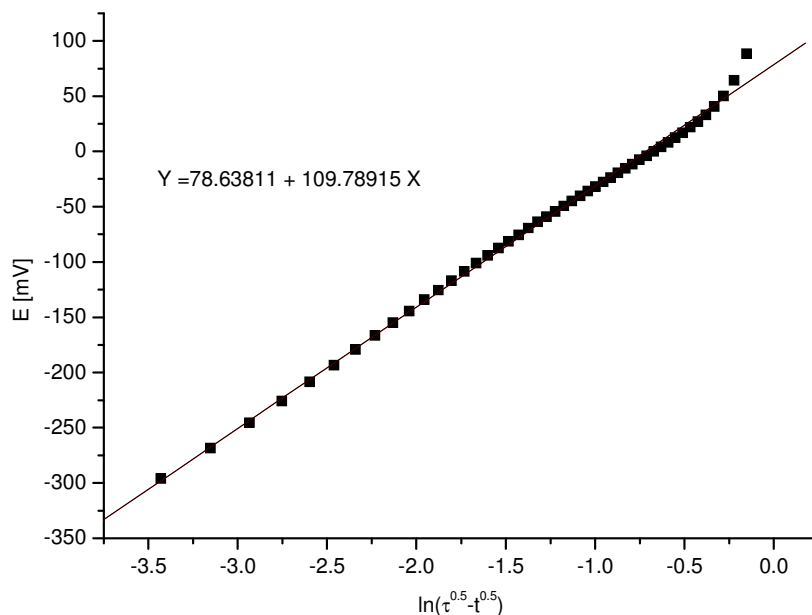


Fig.3.43 Semi-logarithmic plot of a potential-time curve; $C_{TiCl_4} = 0.12 \text{ mol l}^{-1}$; current step 4.9 mA cm^{-2} .

The analysis delivers a pre-logarithm coefficient $\frac{RT}{\alpha n F} \cong 115 \text{ mV}$, resulting in $\alpha n = 0.25$.

Obviously, it should correspond to one-electron process.

Transition time analysis for different Ti(IV) concentrations is given in Fig. 3.44. The $i\tau^{0.5}$ product is approximately constant and linearly depends on the concentration (Fig. 3.45), in accordance with Sand equation [2001Bar]:

$$i\sqrt{\tau} = \frac{1}{2} n F C \sqrt{\pi D} \quad (3.25)$$

where i is the applied current, τ is the transition time, n is a number of electrons involved in the reaction.

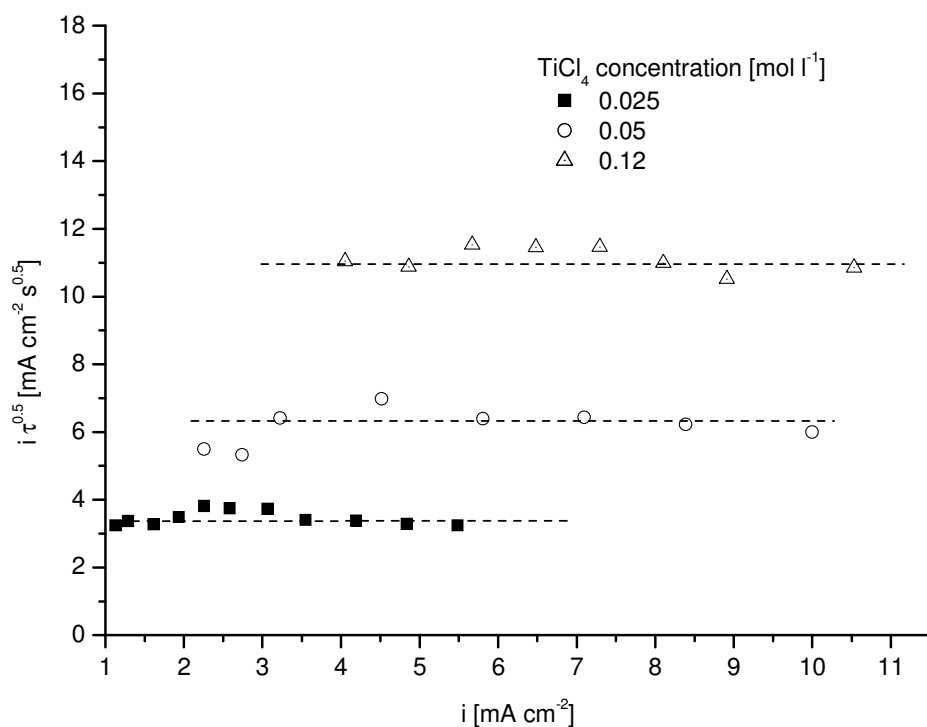


Fig.3.44 Analysis of the obtained transition times in terms of Sand equation (3.25); BMMImN₃ with different TiCl₄ concentrations; temperature 65°C; Pt working electrode.

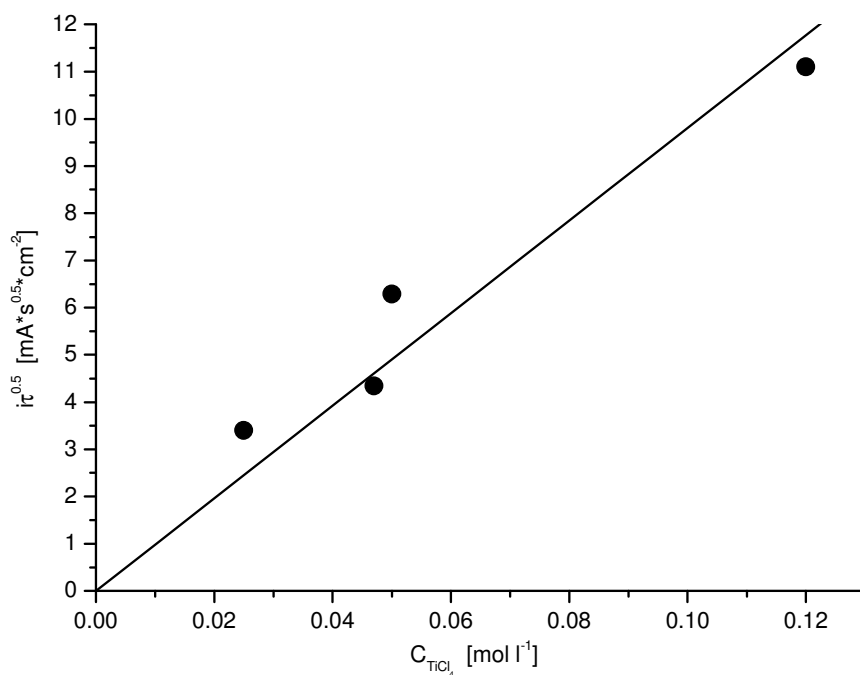


Fig.3.45 Dependence of $i\sqrt{\tau}$ on the concentration of TiCl₄.

Assuming $n=1$ in the equation (3.25), from the data of Fig.3.45 we obtain a value of the diffusion coefficient for the Ti⁴⁺ species in a coordinated complex of $(1.3\pm 0.6)\cdot 10^{-6}$ cm² s⁻¹, which is almost one order of magnitude higher than the diffusion coefficient in fluoroborate IL (see chapter 3.3).

Comparison of chronopotentiometry and CV data validates the conclusion that the reduction is a one-electron process. As follows from the theory, the ratios of $\frac{i_p V^{-1/2}}{i \tau^{1/2}}$ at the same conditions must be equal to:

$$\frac{i_p V^{-1/2}}{i \tau^{1/2}} = 0.284 \sqrt{\frac{nF}{RT}} = 1.67 \sqrt{n} \text{ at } 65^\circ\text{C} \quad (3.27)$$

for a diffusion-controlled reversible process and

$$\frac{i_p V^{-1/2}}{i \tau^{1/2}} = 0.317 \sqrt{\frac{\alpha n F}{RT}} = 1.86 \sqrt{\alpha n}, \text{ also at } 65^\circ\text{C}, \quad (3.28)$$

if the process is totally irreversible.

Using the data of Fig.3.39 and Fig.3.45, we have calculated the average ratio as 1.23 ± 0.09 , which should correspond to an irreversible process with $n=1$ and $\alpha=0.44$.

Comparing the reduction of Ti(IV) in TiCl₄- BMMImBF₄ and TiCl₄ - BMMImN₃ systems, one can see that the process in the azide electrolyte involves only one electron and is kinetically hindered. Inasmuch as physical properties of both ILs are almost equal, this fact could be attributed to different chemical state of Ti(IV) ions in these systems. To clarify the situation, in addition, IR spectra of TiCl₄ solutions were measured. Mixtures of BMMImN₃ with TiCl₄ in molar ratios 1:1 to 1:8 were prepared and investigated.

The FTIR spectrum of pure BMMImN₃ is shown in Fig.3.46 together with the spectrum of fluoroborate IL.

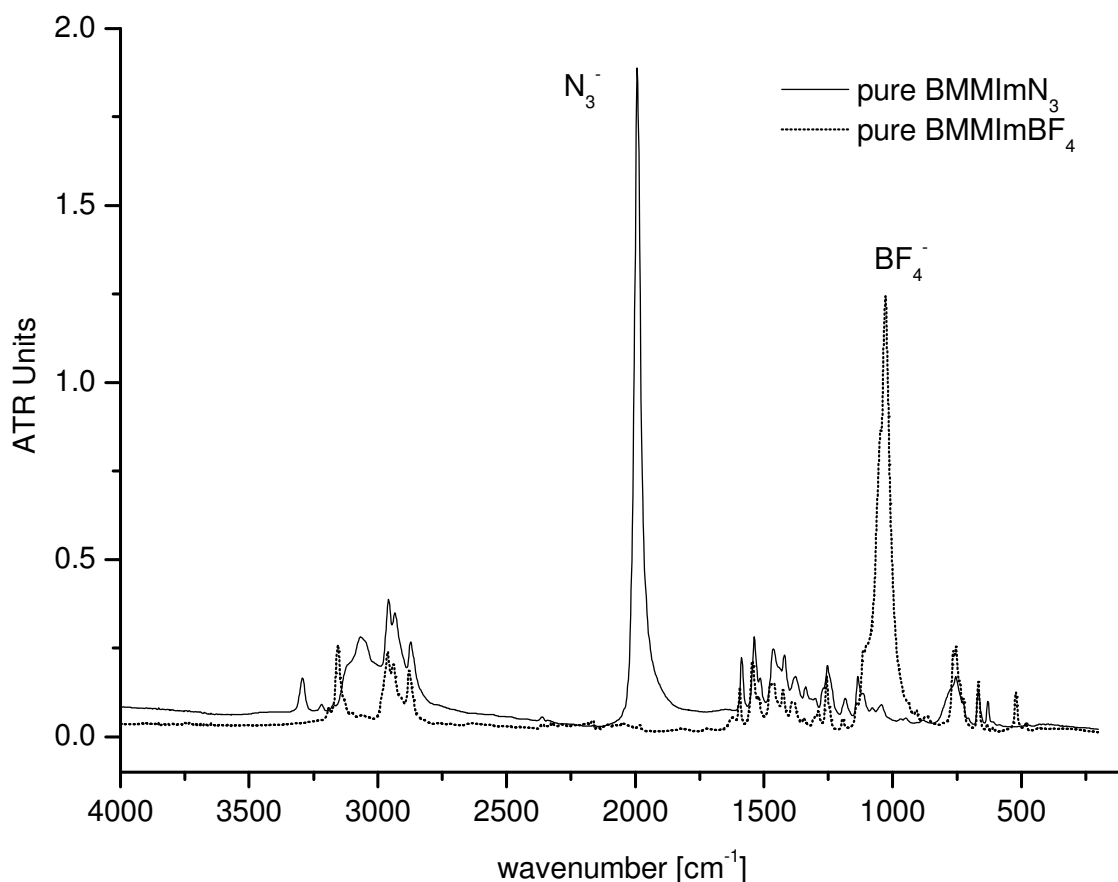


Fig.3.46 IR spectra of BMMImN₃ comparatively to the spectra of BMMImF₄

The strong vibrational band at 2000 cm⁻¹ can be attributed to the asymmetric stretching vibrations of “free” N₃⁻ anion in the IL. In polar and hydrogen bonding solvents, the band centre shifts to higher frequency compared to the gas phase value of 1986 cm⁻¹ [2005Dah]. Dissolution of TiCl₄ results in the additional vibrational bands at 2060 and 2110cm⁻¹ (Fig.3.47), which can be attributed to the vibrations of bonded azide anions [2004Haig, 2005Haig, 2003Gag, 1962Bry]. These bands were detected in solutions with different Ti⁺⁴/N₃⁻ molar ratios between 1:1 and 1:8. The spectra are shown in Fig.3.48.

Two kinds of bonded azide ions are present in the complex formed, with vibrational bands of N-N at 2110 and 2060 cm⁻¹. The vibrational band at 2060 cm⁻¹ is absent at the composition at a molar ratio of Ti⁺⁴/N₃⁻ of 1:1, appears at a higher content of azide and reaches a maximum intensity at molar ratio of Ti⁺⁴/N₃⁻ of 1:5 (Fig.3.49).

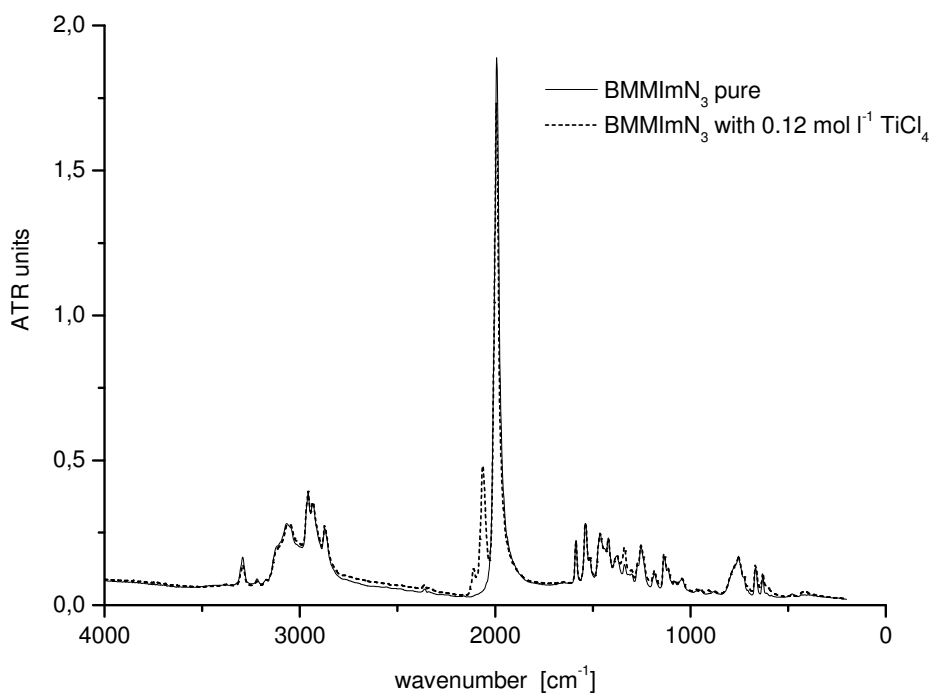


Fig.3.47 IR spectra of BMMImN₃ containing 0.12 mol l⁻¹ TiCl₄.

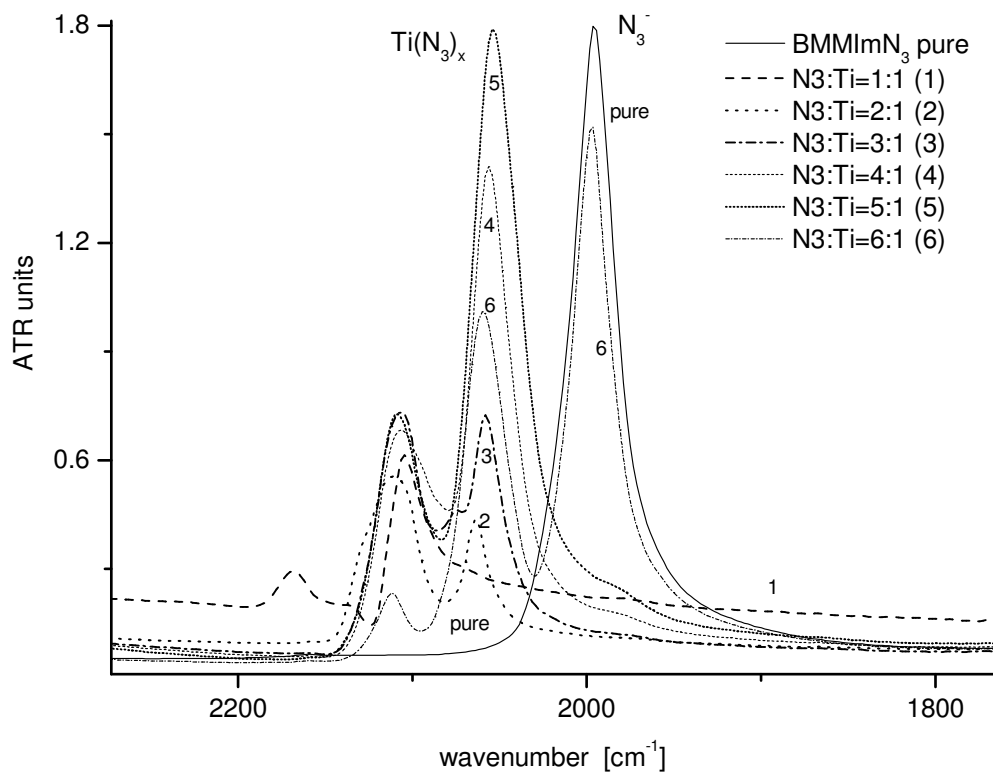


Fig.3.48 IR bands corresponding to N-N asymmetric vibrations in N₃⁻ at different Ti⁴⁺/N₃⁻ molar ratios.

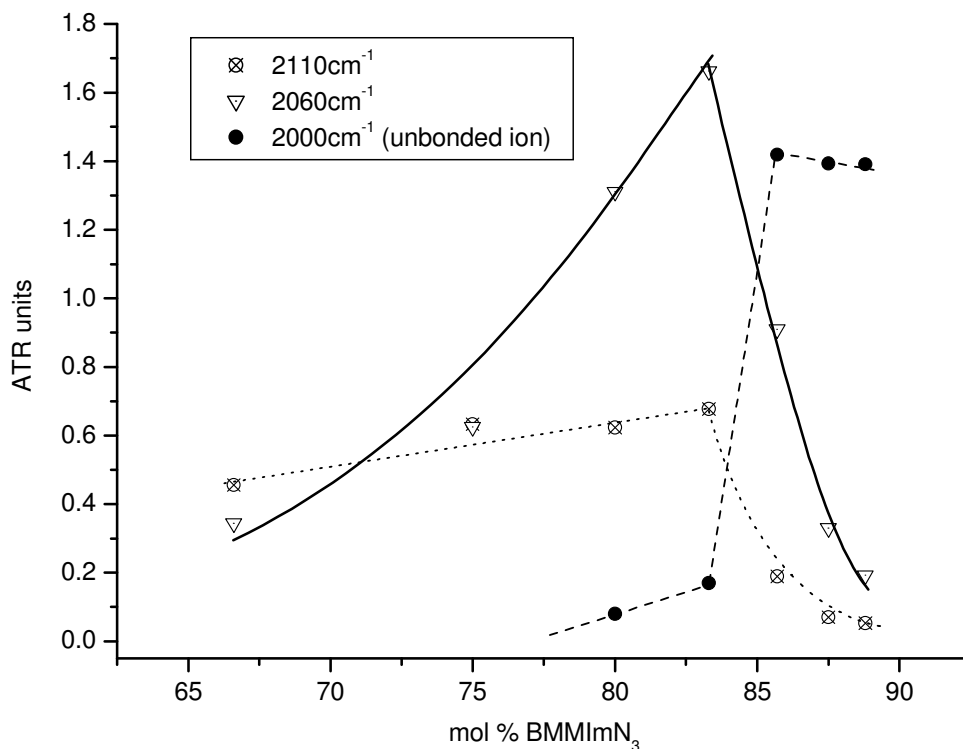


Fig.3.49 Intensity of N₃⁻ vibration bands at different compositions.

A single vibrational band corresponding to N-N symmetric stretching vibration of the bonded azide anion was found at 1340 cm⁻¹ (Fig.3.50). It is absent in the pure IL and also reaches a maximum at a molar ratio Ti⁺⁴/N₃⁻ = 1/5 (Fig.3.51) like the vibrational band at 2060 cm⁻¹.

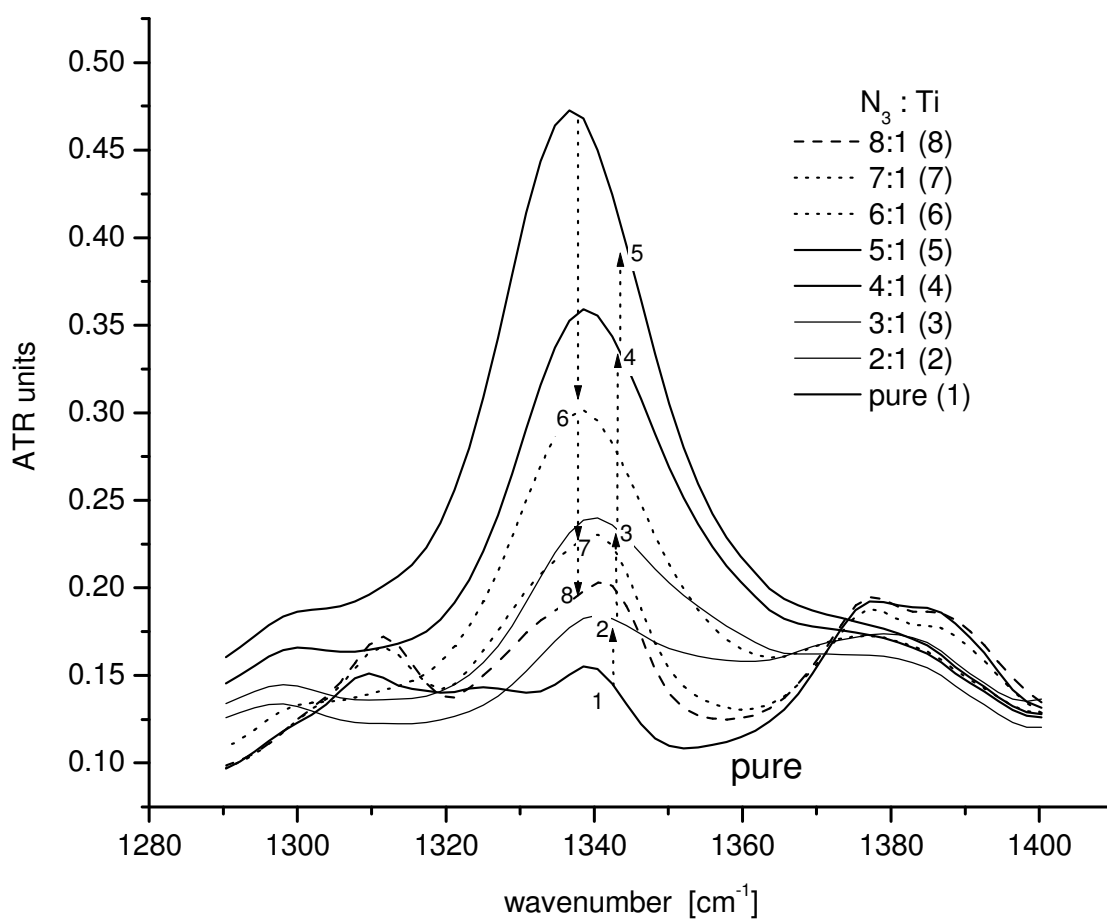


Fig.3.50 IR bands corresponding to N-N symmetric stretching vibrations of bonded N₃⁻ at different Ti⁺⁴/N₃⁻ molar ratios.

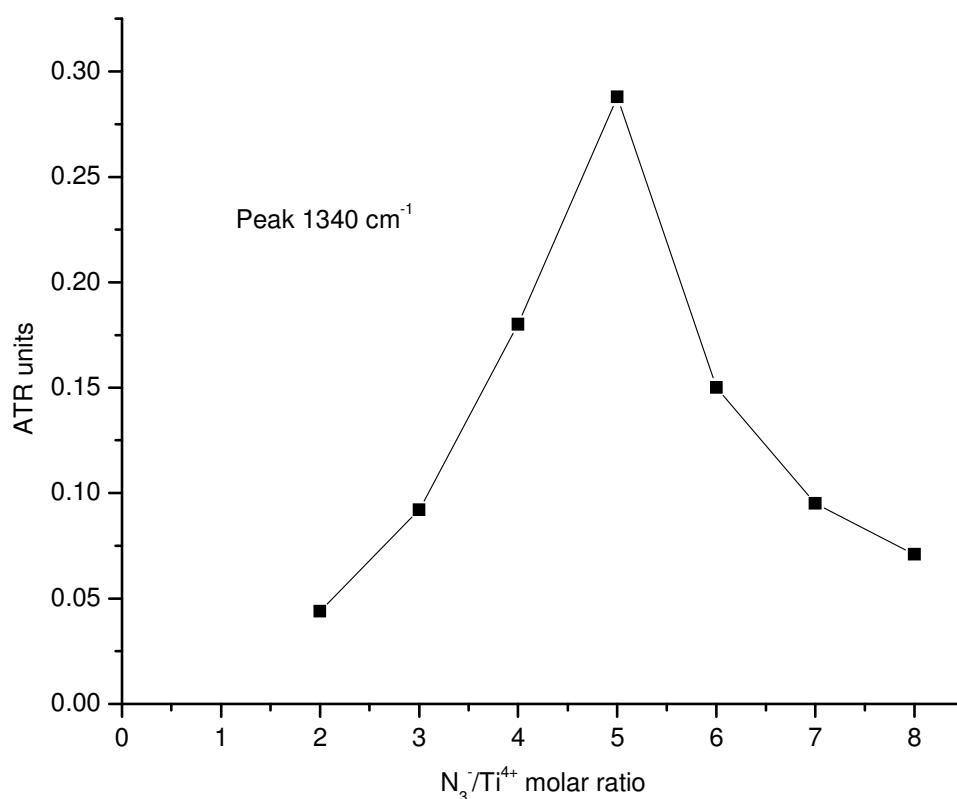


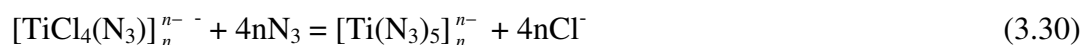
Fig.3.51 Intensity of N-N symmetric stretching vibrations in N₃⁻ at different Ti⁴⁺/N₃⁻ molar ratios.

In the large excess, TiCl₄ forms polynuclear complexes where TiCl₆²⁻ octahedrons are connected via edges by Cl bridge atoms. After adding one azide ion per Ti, the Ti-Cl-Ti bridges are replaced by Ti-N₃-Ti ones and the octahedrons become connected apically:



The bridged N₃⁻ group exhibits a typical vibrational feature at 2110 cm⁻¹.

The vibrational band at 2060 cm⁻¹ attributed to the non-bridge N₃⁻ group appears when the Ti to azide ratio is higher than 1 corresponding to the replacement of Cl⁻ by the N₃⁻ anions:



This vibrational band reaches a maximum in intensity at the molar ratio of BMMImN₃ : TiCl₄ of 5:1, indicative for the formation of a five coordinated complex.

At higher excess of azide ions, the vibrational band attributed to the bridged N₃⁻ group is weakened. The same behaviour was found for the vibrational band at 1340 cm⁻¹, attributed to the symmetric stretching vibration of the bonded N₃⁻.

This finding can be explained by a depolymerization of a polynuclear complex:



Additional work is running in the electrochemical and spectroscopic characterisation of the Ti complexes.

Due to the formation of strong azide complex, electroreduction of Ti(IV) in TiCl₄-BMMImN₃ solutions is kinetically retarded and confined to a single one-electron irreversible reaction:



The product of the reaction (3.32) slowly decomposes forming gaseous nitrogen. A detailed mechanism of this decomposition reaction, as well as all its products, is a subject of further investigations.

3.6 Electrodeposition experiments

The possibility of Ti electrodeposition was always attractive to the researchers, therefore electrochemistry of Ti was widely investigated in high temperature molten chlorides and fluorides [1992Tar, 1984Mak, 1999Shap]. The research on big scale Ti refinement in molten CaCl_2 melts was conducted actively by several groups of researchers in [1998Okab, 2001Tan, 2000Chen, 2002Ono, 2002Suz].

The discovery of ILs, completely ionic medium at temperatures much lower compared to the high temperature molten salts, initiated the research on Ti electrochemistry and electrodeposition possibility at low temperatures [1990Car, 2003Tsu, 2003Muk, 2005Muk, 2005Kat, 2006Abed(a,b), 2007And].

Three-substituted imidazolium cation-based ILs showed good electrochemical stability [1987Gif, 2005 Kat], relatively low viscosities and satisfactory conductivities (see chapter 3.1). For this reason, this system was chosen for the deposition studies.

3.6.1 TiCl_4 in BMMImN_3

The deposition was performed on Pt electrode (0.31 cm^2) from the solution of 0.12 mol/l TiCl_4 in BMMImN_3 at 65°C .

The sequence of pulses applied during the experiment is shown in Fig. 3.52. The experiment lasted 25h

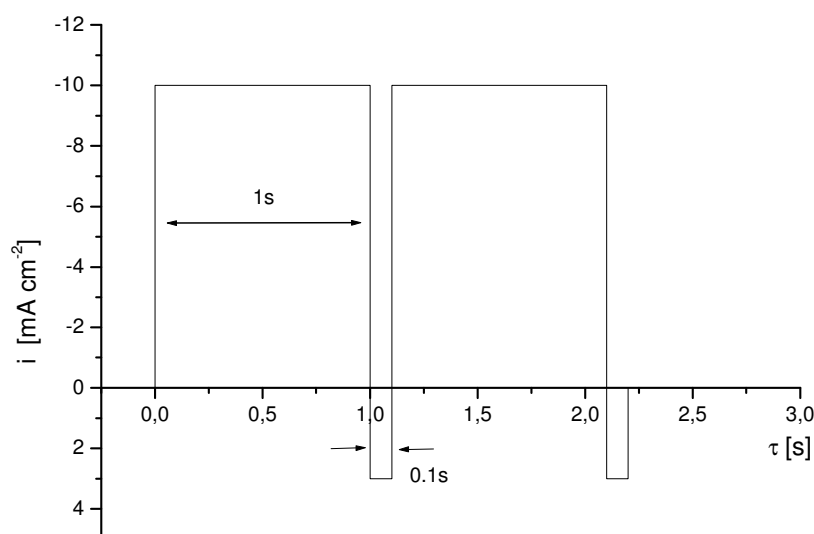


Fig. 3.52 Shape of the current pulse applied in the experiment.

The observed rate of the electrolyte decomposition was lower than in constant current experiments. The voltage on pulses didn't go under -2.5V (Pt vs GC)

After washing in methanol and drying, the sample has been analyzed by ESEM techniques.

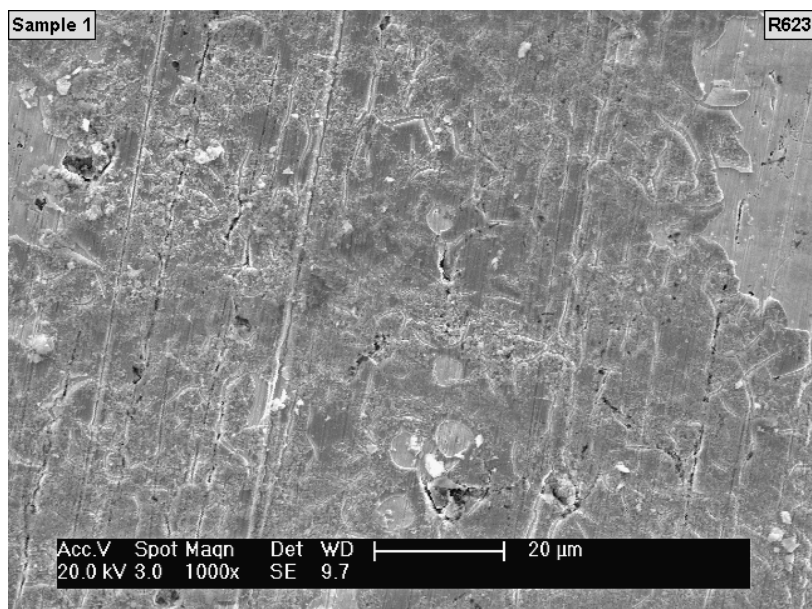


Fig. 3.53 ESEM picture of the deposit, 1000x magnification, secondary electrons, 20kV accelerating voltage.

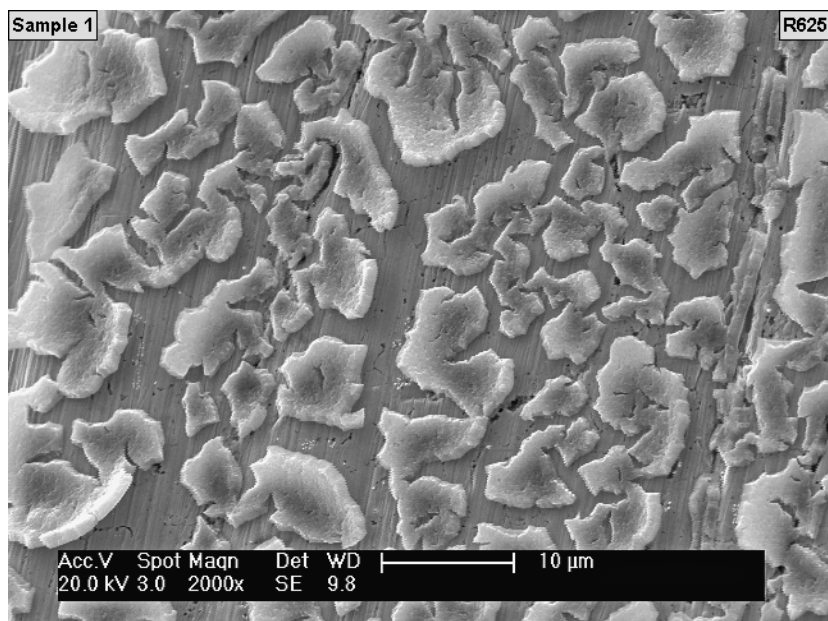


Fig.3.54 ESEM picture of the deposit, 2000x magnification, secondary electrons, 20kV accelerating voltage.

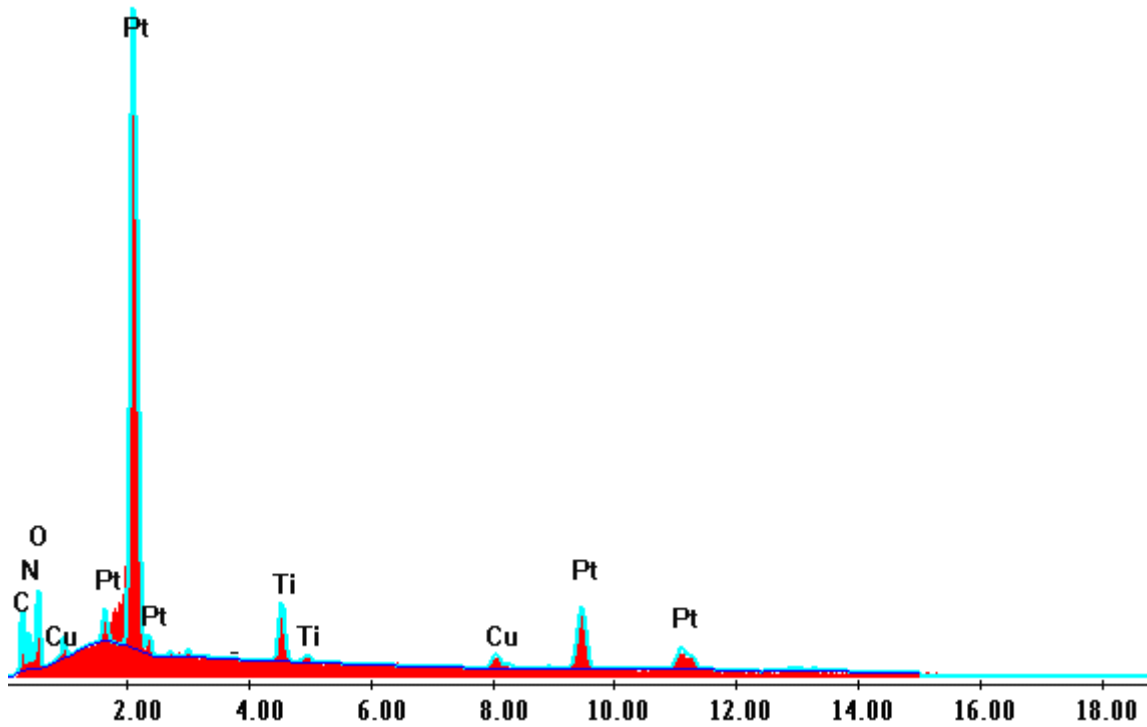


Fig. 3.55 EDX analysis of the deposit (picture in Fig. 3.56).

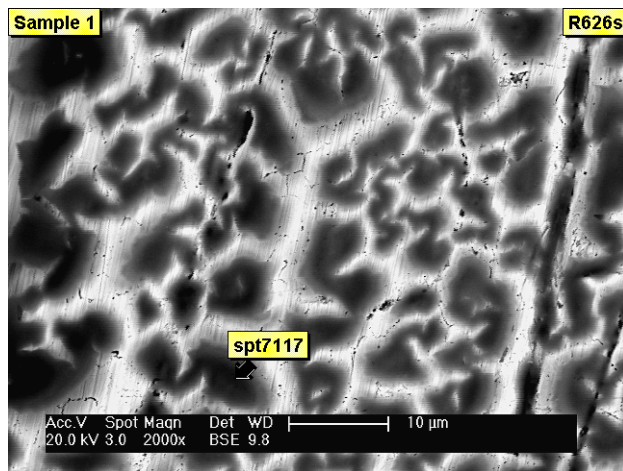


Fig. 3.56 Backscattered picture of the deposit, backscattered electrons, 20kV.

The dark areas on the Fig. 3.56 are the Ti deposit, the light ones – Pt substrate.

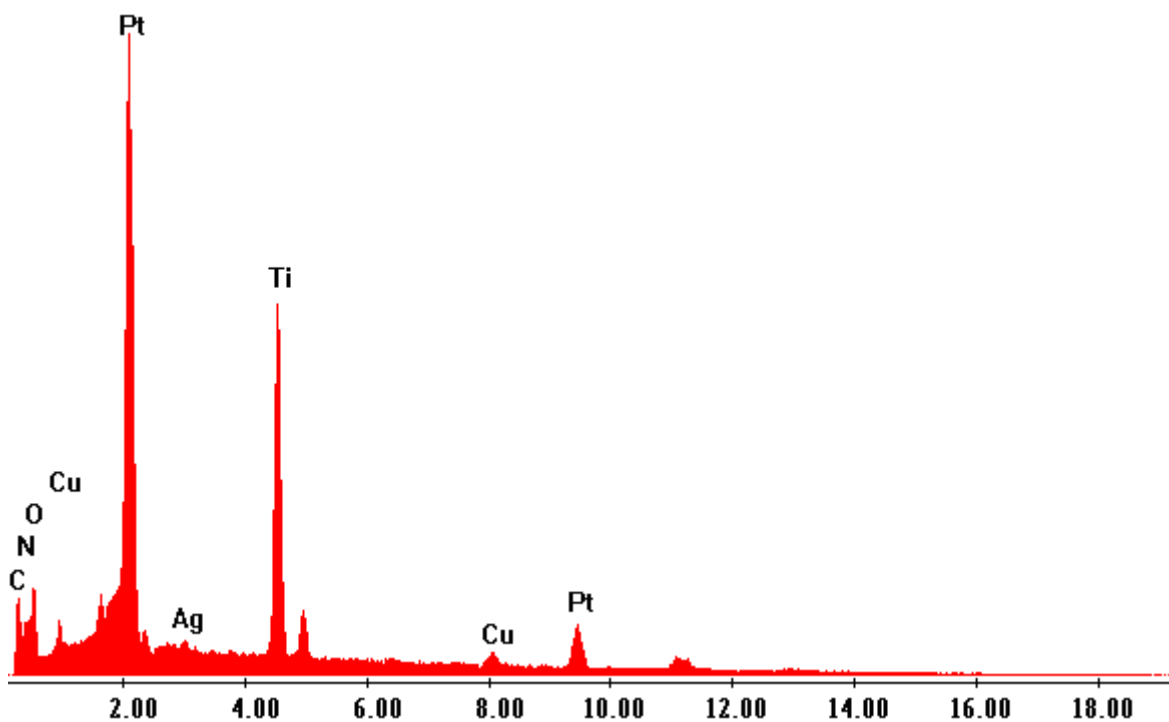


Fig. 3.57 EDX analysis of the spot 7117 (see Fig. 3.56).

After washing in methanol a very thin layer has been observed on some parts of the dipped Pt wire. But the adhesion is very poor and it can be easily rubbed off. There is not enough of the formed material on the surface to analyze it with XRD methods. The structure and properties of the deposit is still to be investigated.

3.6.2 TiCl₄ in BMMImBF₄ at elevated temperatures

In all experiments colourless IL BMMImBF₄ was used. When introducing Ti in the form of TiCl₄ (colourless liquid), the melt becomes yellow. The nature of the complexes formed is still poorly understood, but most probably it is a titanium-halogen-tetrafluoroborate complex.

Possible way of „weakening“ such complexes is to raise the temperature.

Other advantages of using higher temperatures for the deposition experiments are decrease of viscosity and an increase of the conductivity of the IL.

3.6.2.1 Medium concentration of TiCl₄ in BMMImBF₄ (0.05 mol l⁻¹)

Constant current deposition #1 (stepwise current)

The deposition was performed from a solution of TiCl₄ (0.047 mol/l) in BMMImBF₄ at 180°C. Stepwise current -2 mA/cm² - 3.5h; -4 mA/cm² - 2h.

Total amount of electricity: Q = 15 A s.

Assuming 100% current efficiency, a detectable amount of Ti (2 mg) can be deposited.

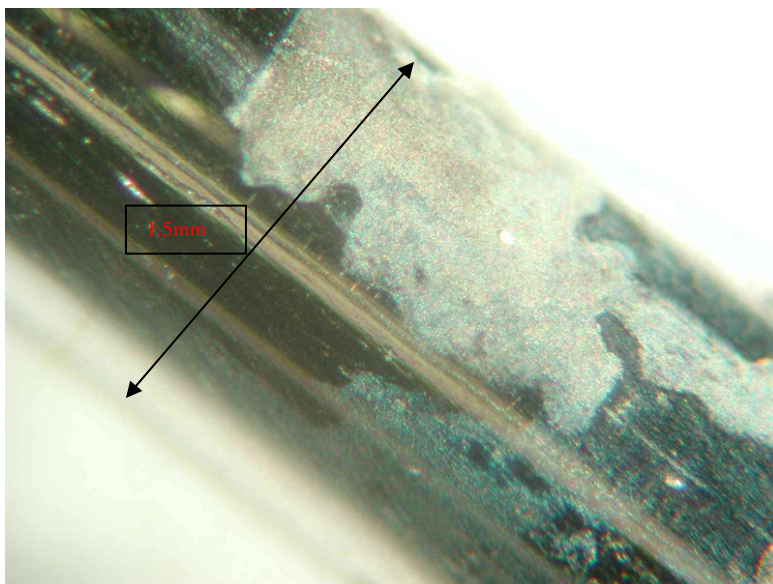


Fig. 3.58 Deposit on Pt wire (light microscope picture).

The deposit went immediately white after exposing to air. This indicates the formation of TiO₂.

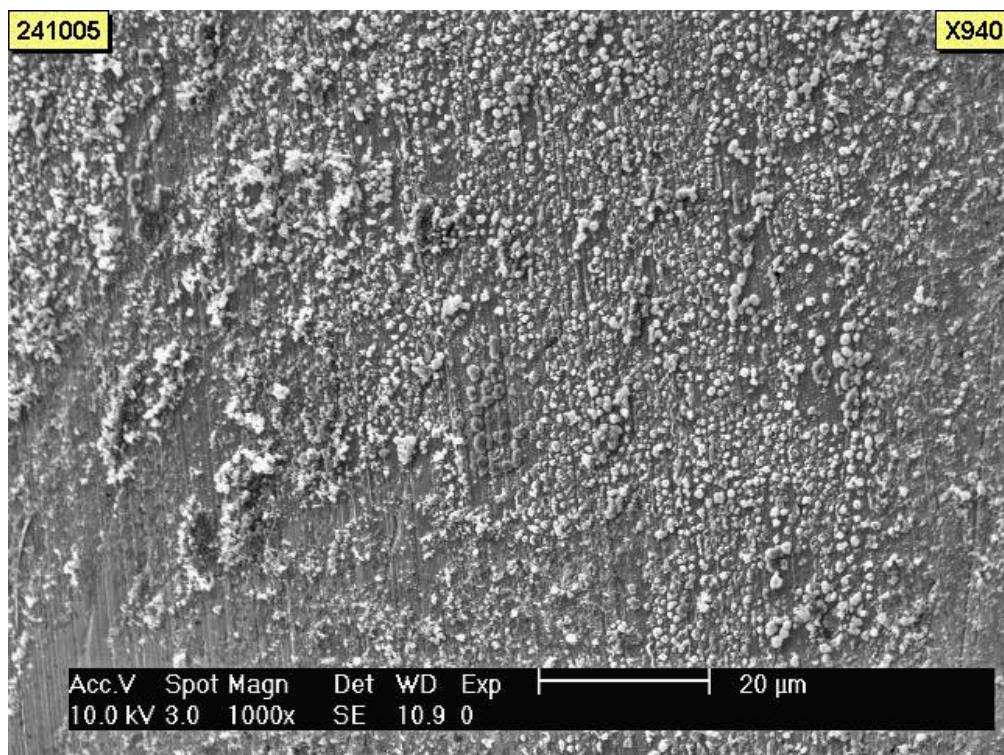


Fig. 3.59 ESEM picture of the deposit, magnification 1000x, secondary electrons, 10kV.

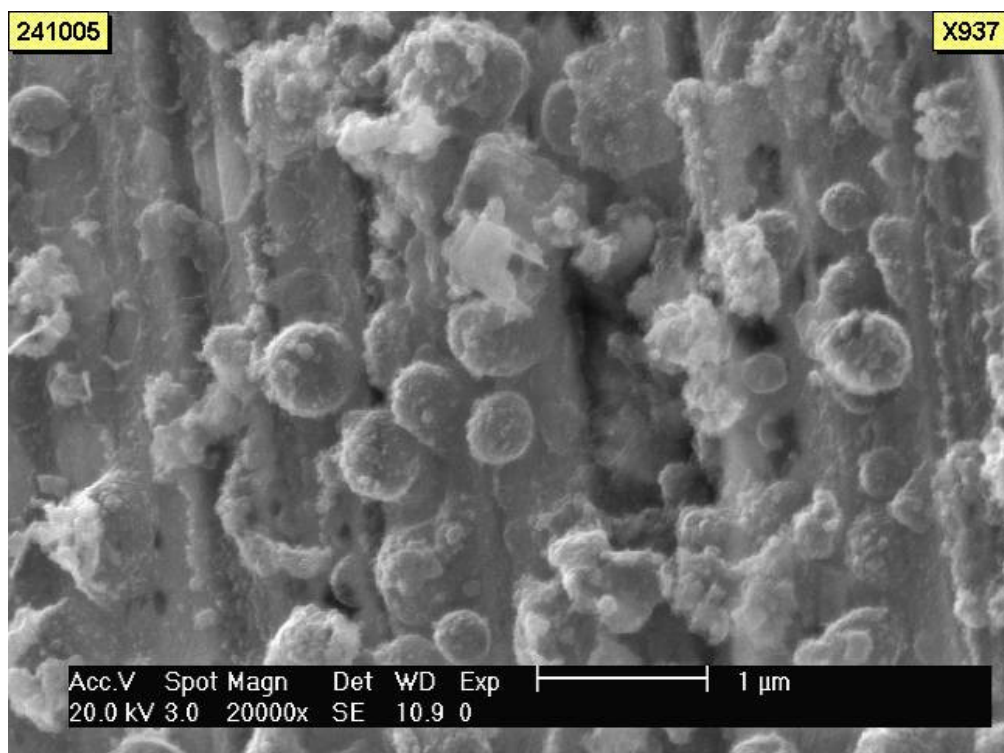


Fig. 3.60 ESEM picture of the deposit, magnification 20000x, secondary electrons, 20kV.

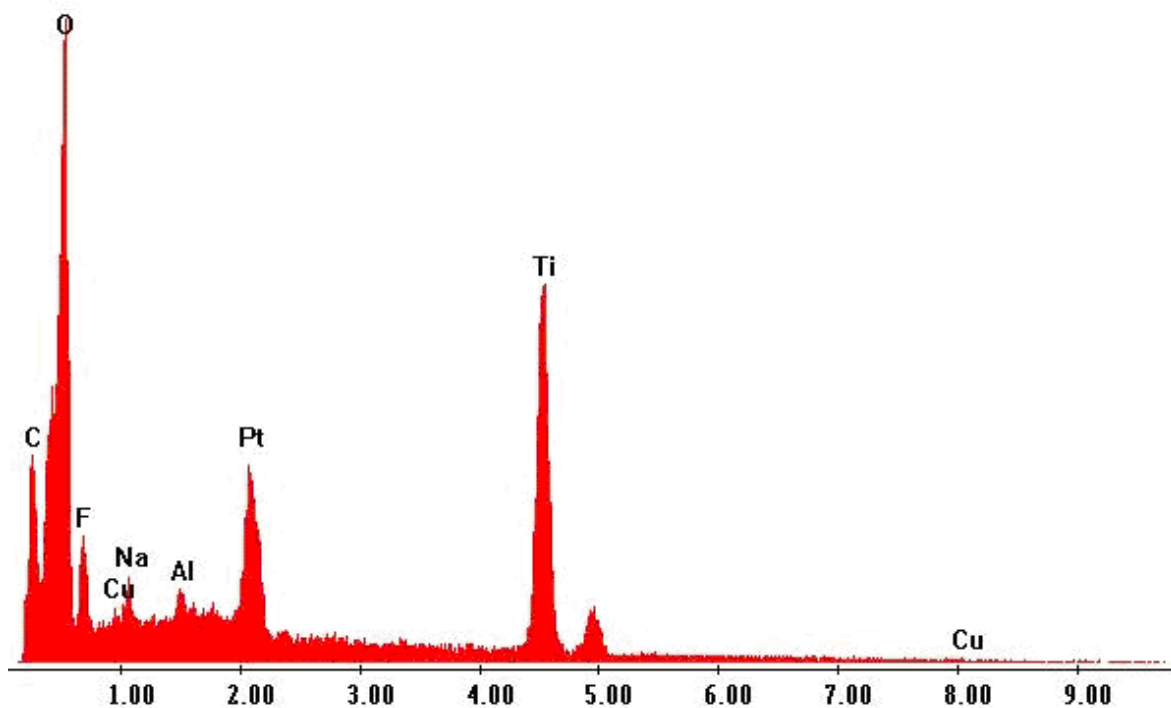


Fig. 3.61 EDAX analysis of the deposit (accelerating voltage 10kV).

The Pt electrode appeared to be contaminated with copper (see Fig. 3.61). The peak of Ti is very clear. The formation of TiO_2 results from handling the sample in air after the deposition.

Constant current deposition #2

The deposition was carried out from a solution of 0.05 mol/l TiCl_4 in BMMImBF_4 at 180°C . The constant current (-3.3 mA/cm^2) was applied for 18h.

Total amount of electricity $Q=64 \text{ A s}$.

To deposit all the Ti from the melt with 100% current efficiency, 110 A s is needed.

Potential response during the experiments is shown in Fig.3.62.



Fig. 3.62 Change of the potential between the cathode and anode during electrolysis.

The oscillations of the potential response (see Fig. 3.62) are due to the temperature variations (179 to 184°C). Probably the conductance of the film that is formed on the cathode during the deposition process, considerably depends on the temperature.



Fig. 3.63 Obtained deposit on a Pt wire (light microscope picture).

Two potential plateaus are clearly seen on the Fig.3.62. This points to the fact, that two electrochemical processes are taking place.

The first one is reduction of Ti(IV) to some lower oxidation state until the sufficient concentration is reached to shift the equilibrium to Ti(0) formation.

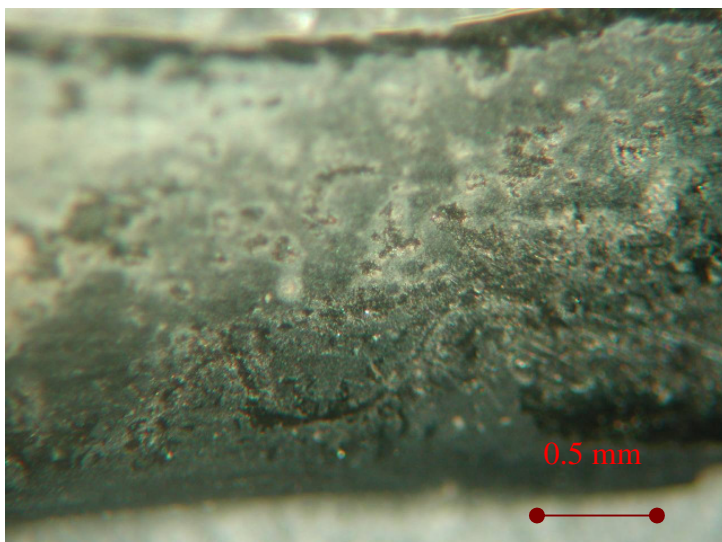


Fig. 3.64 Obtained deposit on Pt wire, after rubbing off the white powder (light microscope picture).

Decomposition of the IL was visible during the whole time of the electrolysis. After washing in MeOH, a powdery deposit was visible on the electrode (see Fig. 3.63). The deposit becomes white on air. After rubbing off the powder we can observe more dense deposit on the surface of the electrode (Fig. 3.64).

Constant current deposition #3 (stepwise current)

The current -1.5 mA cm^{-2} was applied for 2 hours at temperature 180°C .

Total amount of electricity that passé through the system - $Q=3.24 \text{ A s}$.

Potential between the electrodes of the cell:

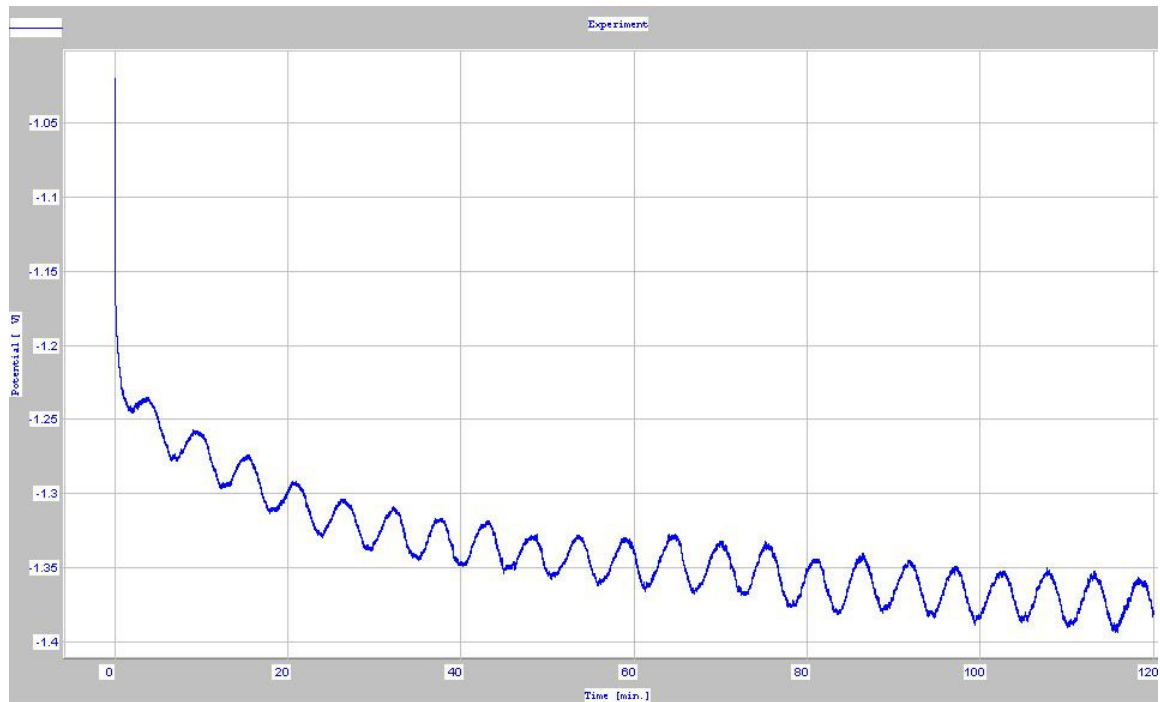


Fig. 3.65 Change of the potential between the cathode and anode during electrolysis ($i = -1.5 \text{ mA cm}^{-2}$).

A deposit was not visible on the electrode. The current was raised to -2.1 mA/cm^2 . Time of the experiment – 2h. Total amount of electricity $Q=4.54 \text{ A s}$.

Potential response

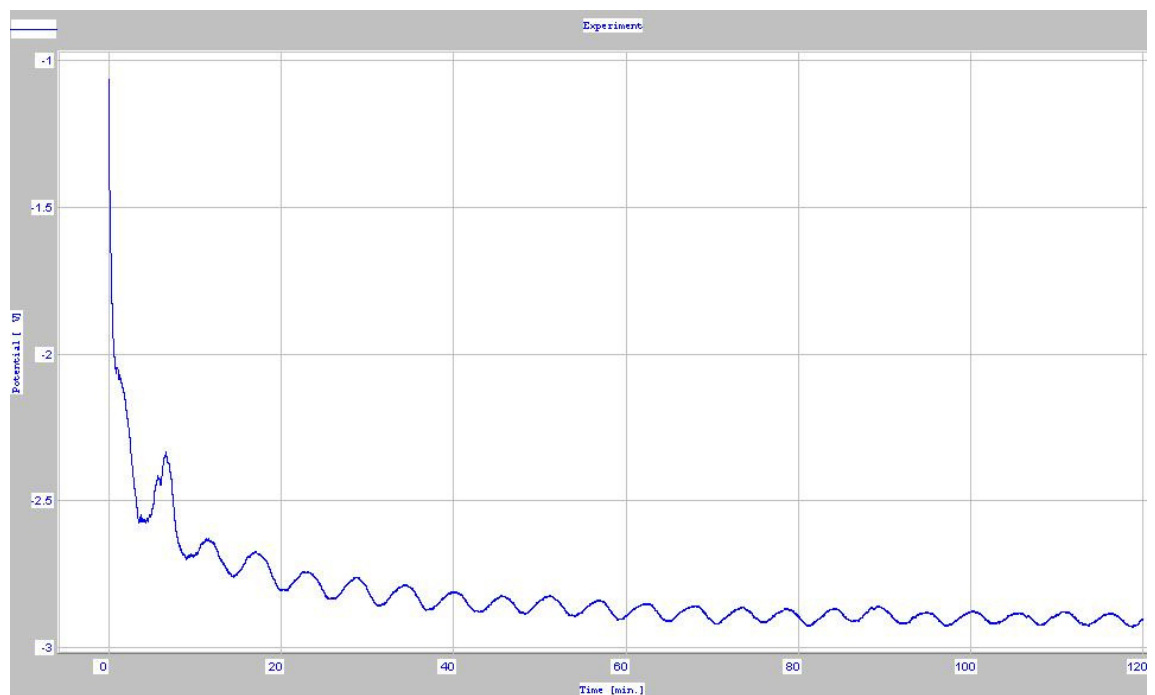


Fig. 3.66 Change of the potential between cathode and anode during electrolysis ($i = -2.1 \text{ mA cm}^{-2}$).

The picture of potential response (Fig. 3.65, 3.66) is similar to the constant current experiment with -3.3 mA cm^{-2} (see Fig. 3.62). But longer preconditioning of the electrolyte at lower current and smaller value of the final current improved the results. The IL decomposition rate was low and the deposit was more homogeneous (Fig. 3.67).

After exposing the electrode to air, the deposit turns white.

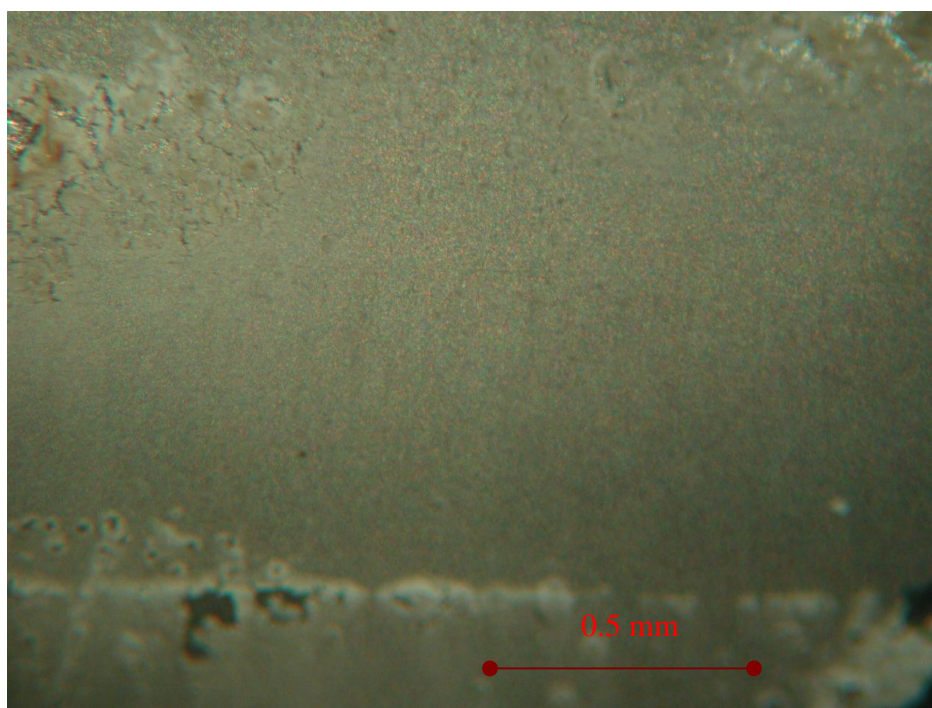


Fig. 3.67 Obtained deposit, light microscope picture.

ESEM analysis

The deposit is completely oxidised, which gives us much less possibilities for qualitative analysis. Assuming 100% current efficiency the amount of deposited Ti would be quite small and very finely dispersed. That means the deposit can be oxidised easily.

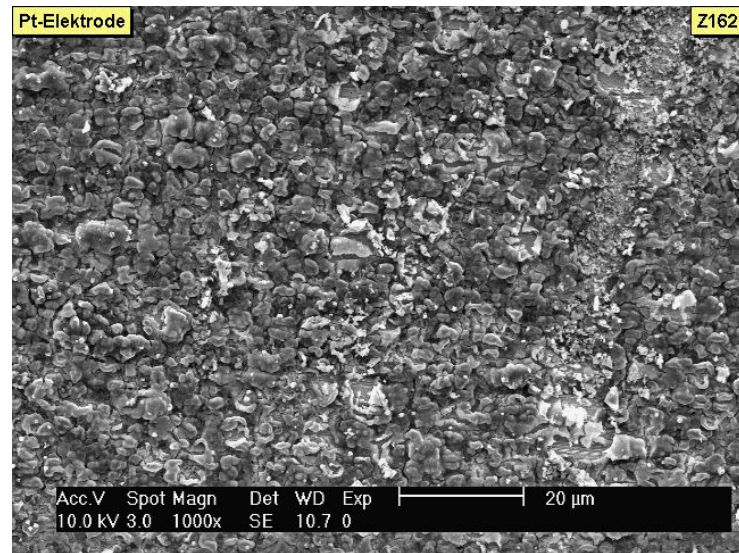


Fig.3.68 ESEM picture of the deposit (magnification 1000x, SE, 10 kV).

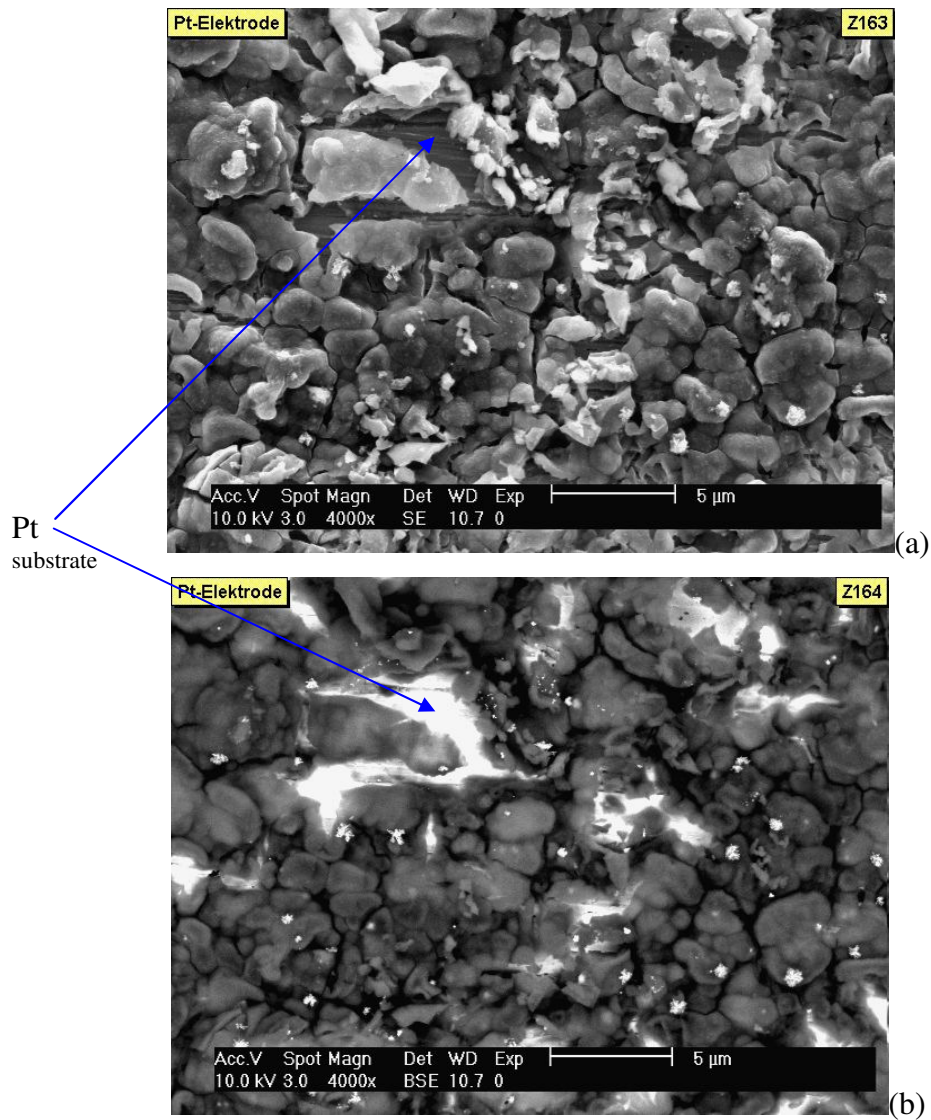


Fig. 3.69 ESEM picture of the deposit (magnification 4000x, 10 kV): a) secondary electrons, b) backscattered electrons.

Fig. 3.69 shows images of the deposit with magnification 4000x, recorded with different detectors. Light areas (Fig. 3.69 b) – Pt substrate without a deposit, all other particles – Ti deposit. The particle size is (2 to 5) μm .

EDX analysis

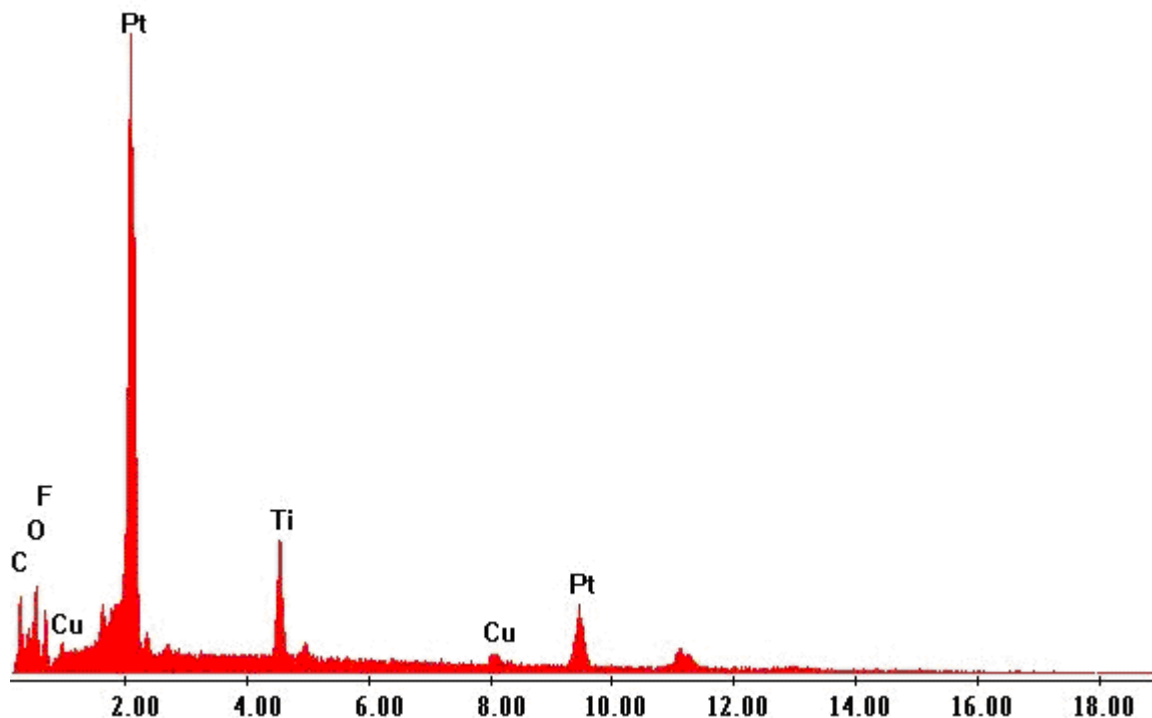


Fig. 3.70 EDX analysis of the deposit (acceleration voltage 20kV).

Table 3.8 Quantification of the deposit analysis at 10kV.

Element	Wt %	At %
C K	15.67	39.37
O K	15.44	29.12
F K	6.90	10.96
CuL	1.41	0.67
PtM	38.45	5.95
TiK	22.13	13.94
Total	100.00	100.00

Fig. 3.70 shows EDAX analysis of the received deposit at 20kV accelerating voltage of the electron beam. Ti peak is clearly seen.

Table 3.8 shows the quantification of the deposit composition with EDAX. We can see that the ratio between Ti and O is approximately 1:2. That points to the fact, that Ti on the surface is oxidised to TiO_2 .

Constant current deposition #4 (stepwise current)

Reproducibility experiment.

The conditions were maintained the same as in the previous experiment. Constant current - $1.5\text{mA}/\text{cm}^2$ was applied for 2 hours, followed with $-2.1\text{mA}/\text{cm}^2$ for the next 2 hours. Amount of electricity on the first step: $Q=2.6\text{ A s}$.

Second step: $Q=3.36\text{ A s}$.

Potential between cathode and anode change during the experiment.

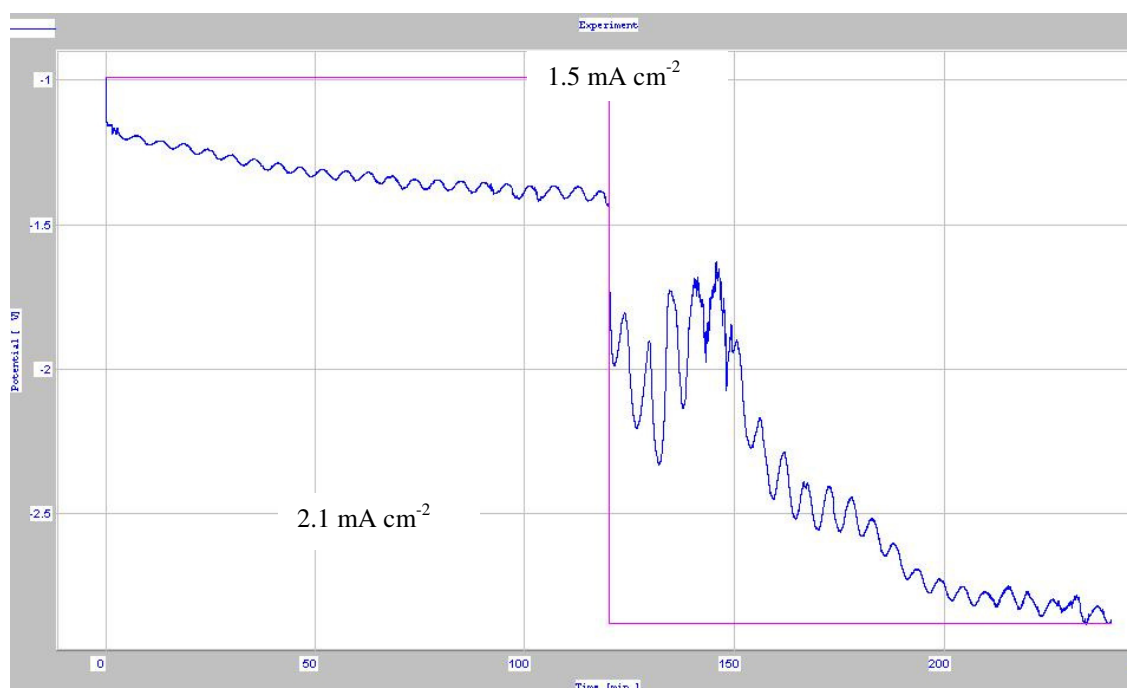
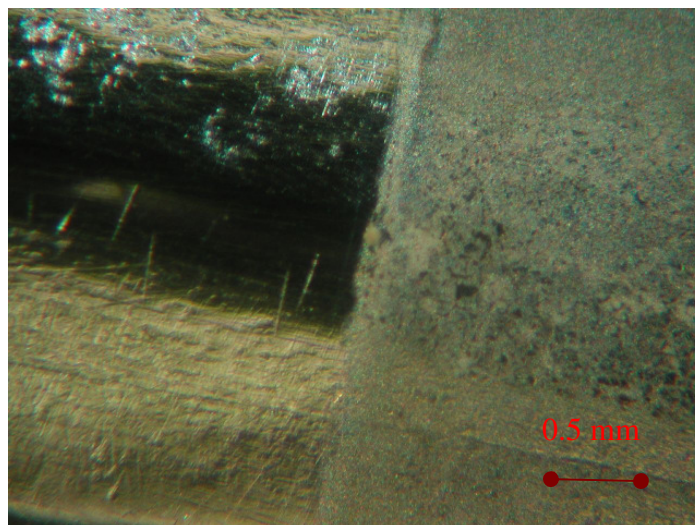


Fig. 3.71 Applied current and potential response during the experiment.

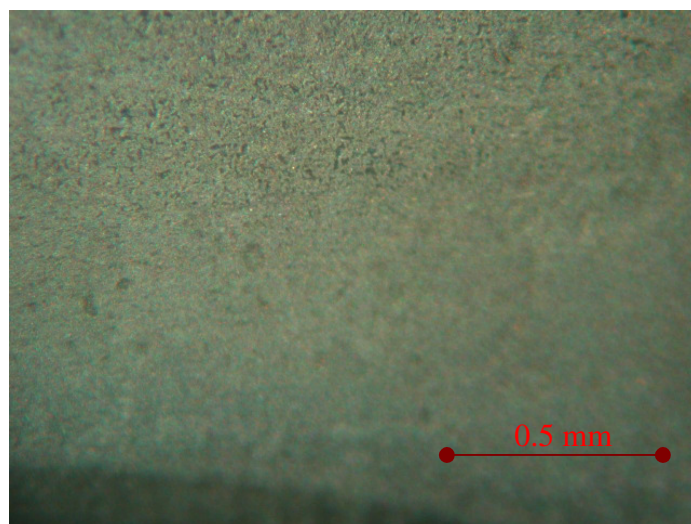
We were reproducing the last experiment with the difference that higher current followed preconditioning at lower current density with shorter interval. The area of Pt electrode was smaller in this experiment and naturally total amount of electricity passed through the system was smaller too (6.23 A s vs. 7.78 A s).

Upon raising the current, we observed an effect of rapid rise and fall of potential. We believe it is due to efforts of overcoming the difficulties of formation of the first crystals on the surface and after some have formed – lowering of the energy consumption for further

formation of the deposit (the potential becomes lower). After some time the potential rises again due to the increasing resistance of IL as well as of the deposit.



(a)



(b)

Fig. 3.72 Obtained deposit on the Pt substrate.

The deposit was turning white on exposing to air.

3.6.2.2 Saturated solution of TiCl_4 in BMMImBF_4

The electrolyte was oversaturated with TiCl_4 . Drops of undissolved tetrachloride are visible.

The total concentration of TiCl_4 was 0.35 mol l^{-1} .

As it was demonstrated in the previous experiments, the solubility of TiCl_4 in BMMImBF_4 is about 0.2 mol l^{-1} at 65°C . From these facts we can conclude that there was an excess of tetrachloride in the electrolyte as well as in the cell atmosphere.

A higher concentration allows us to work with higher current densities.

The current sequence was -15 mA cm^{-2} for 2h plus 2h of -30 mA cm^{-2} . But after switching to higher current, the potential between cathode and anode exceeded the cutoff voltage -4V . After a pause of 5 min, the experiment was re-established for another 2 h with a current density of 15 mA cm^{-2} .

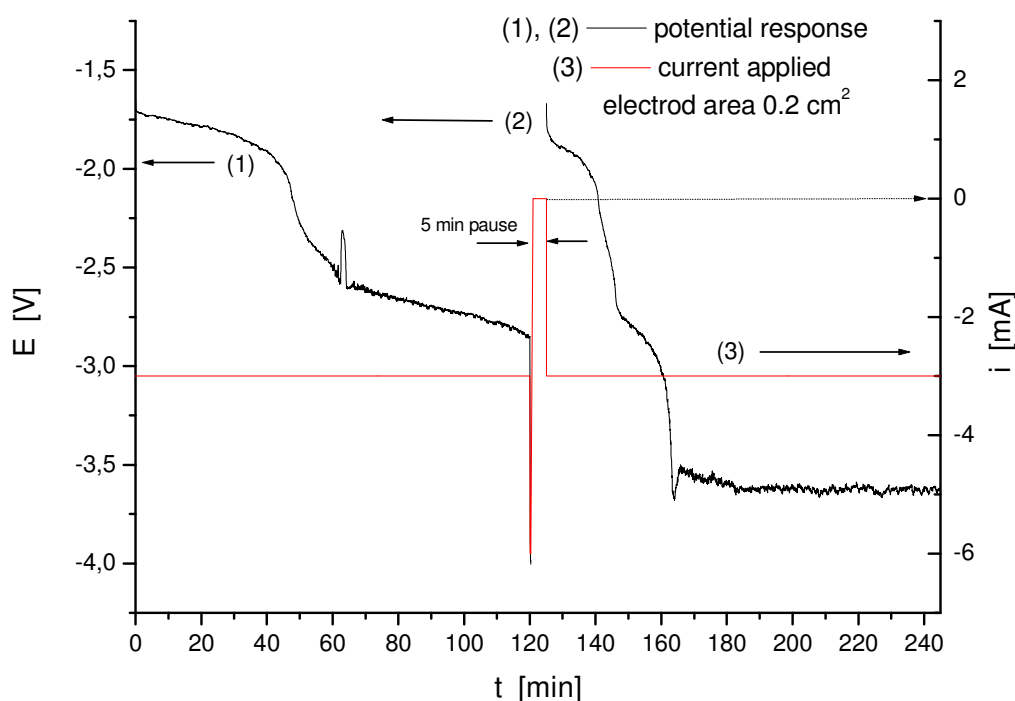
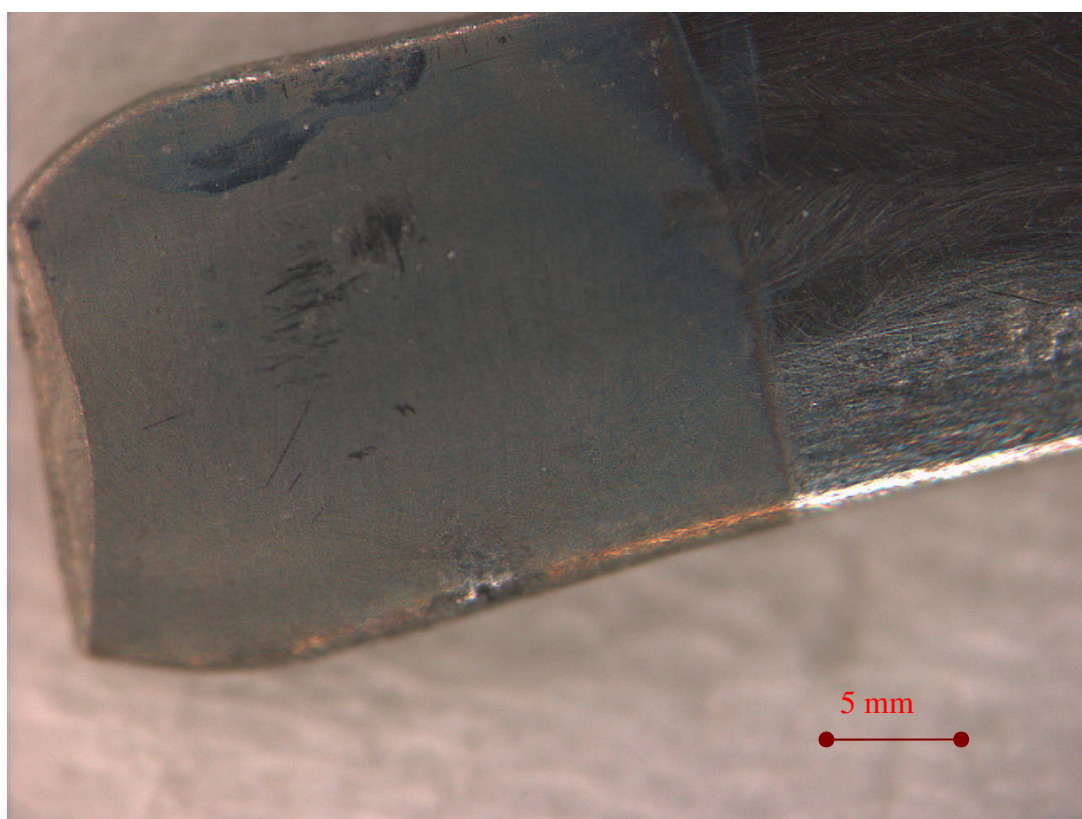


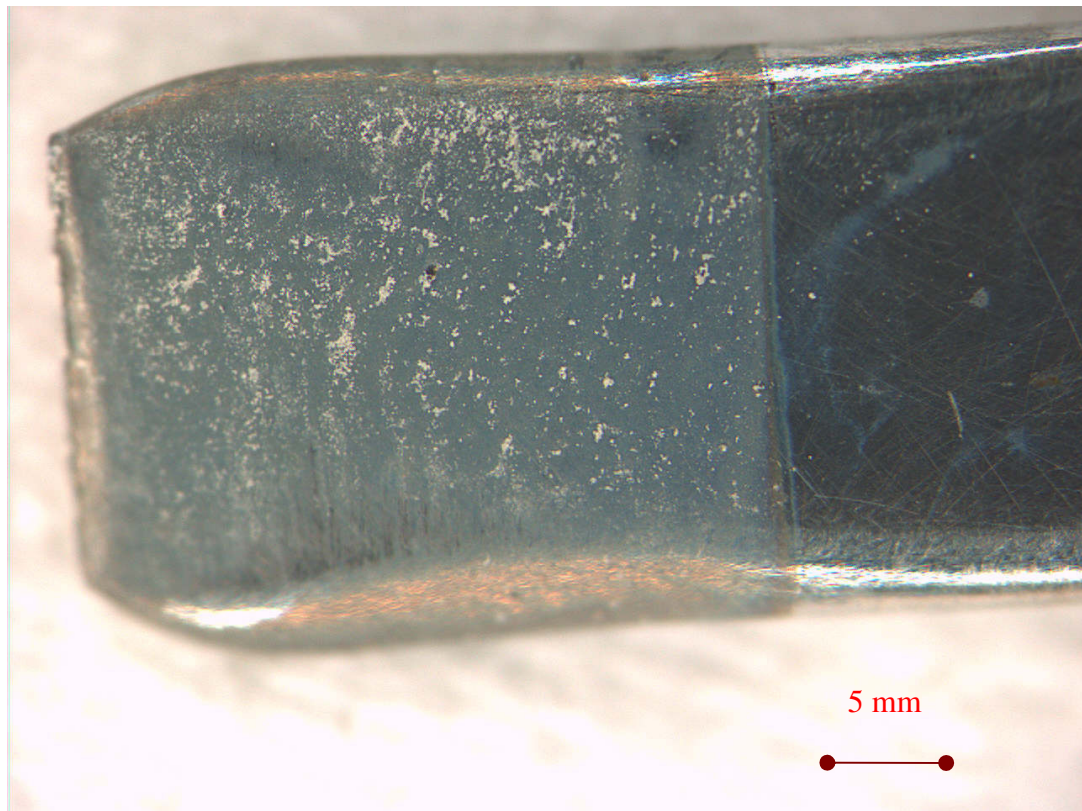
Fig. 3.73 Current applied and potential response during the experiment.

Change of voltage between cathode and anode (Fig.3.73 curves 1 and 2) during deposition experiment. Curve 3 – shape of the current applied.

The obtained deposit was examined on the optical microscope.



(a)



(b)

Fig. 3.74 Optical microscope pictures of the Pt electrode after the deposition experiment.

ESEM analysis of the deposit

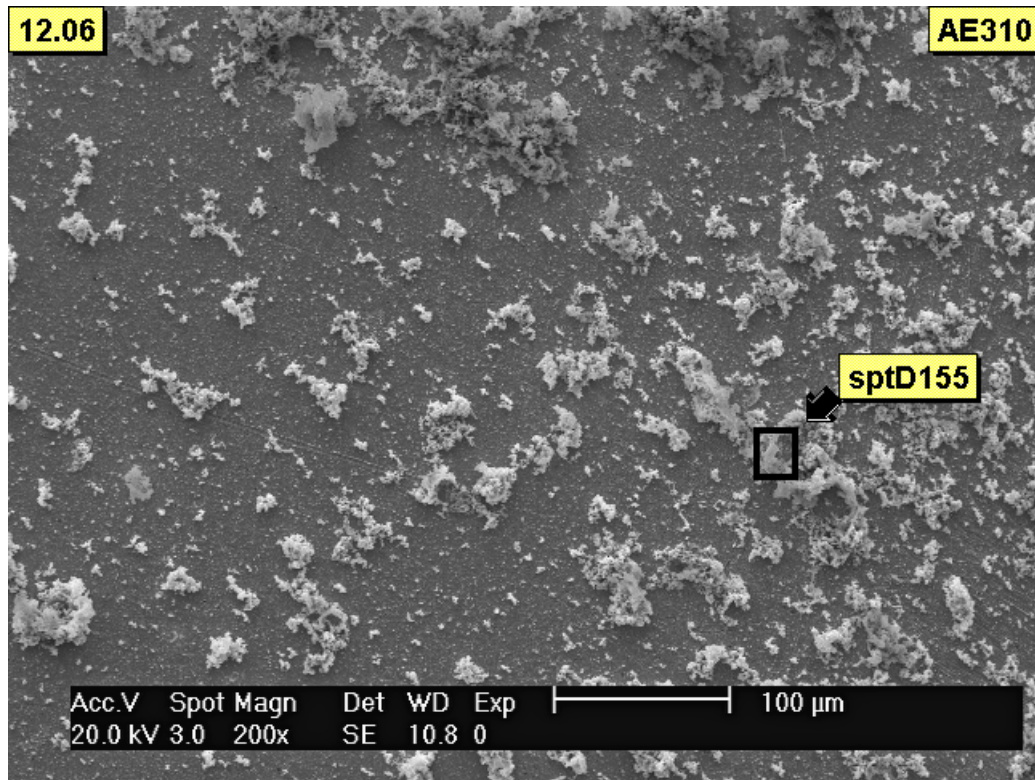


Fig. 3.75 ESEM picture of the obtained deposit (200x magnification, SE, 20 kV).

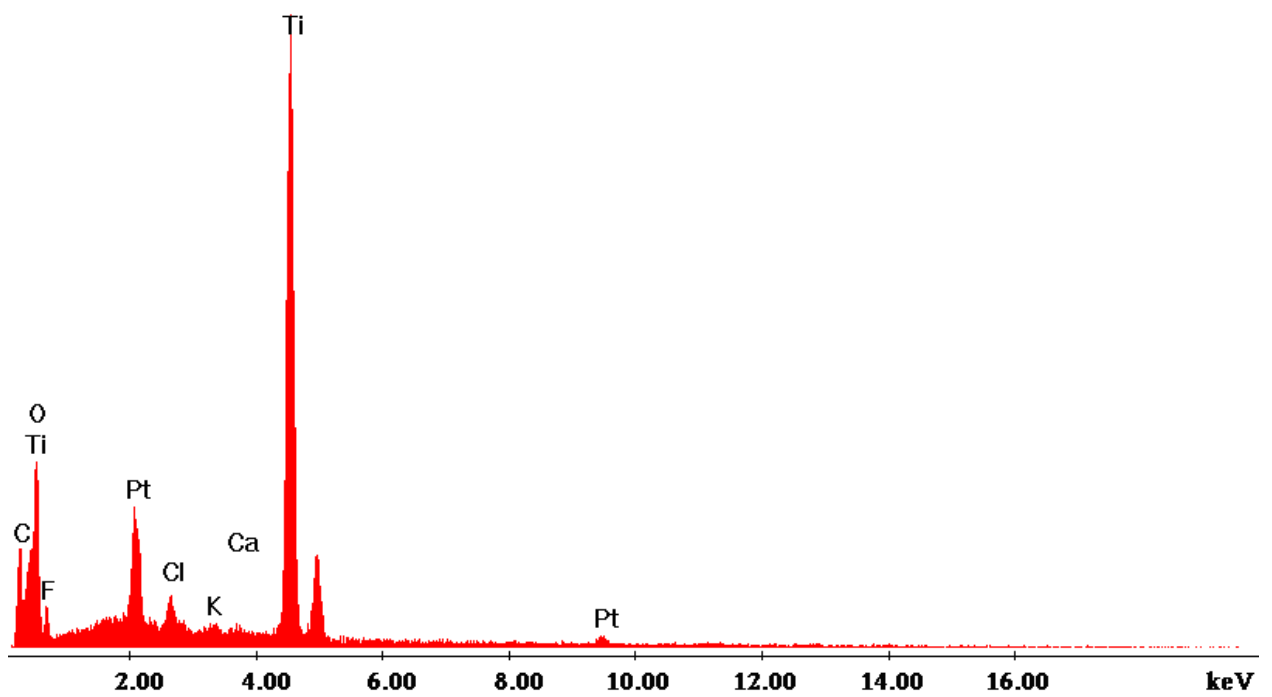


Fig. 3.76 EDX analysis of the deposit.

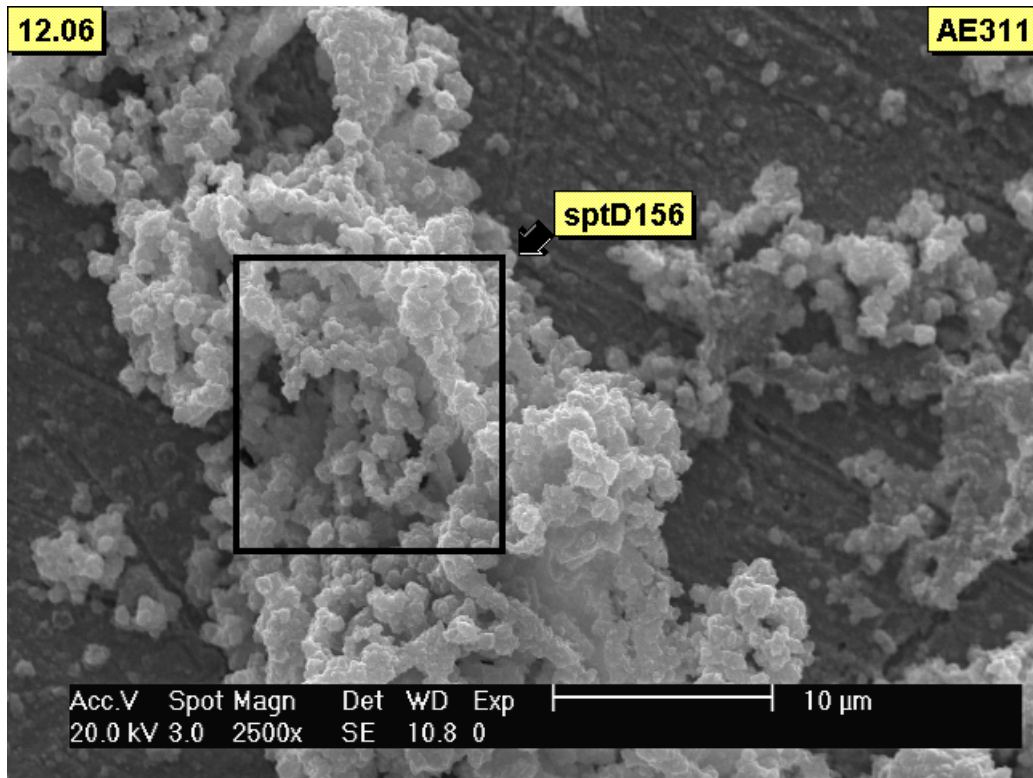


Fig. 3.77 ESEM picture of the deposit (2500x magnification, SE, 20 kV).

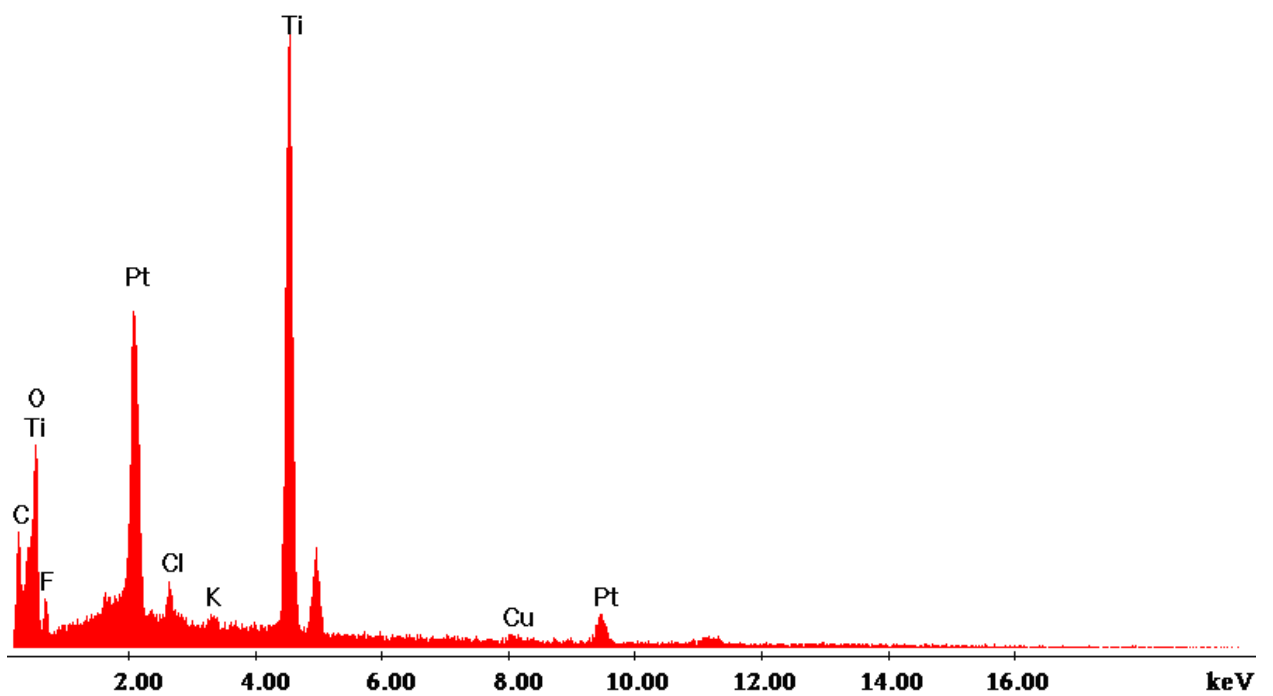


Fig. 3.78 EDX analysis of the spot 156 (see Fig.3.77).

3.6.2.3 Pulsed potential deposition at 180°C

The deposition was carried out in the solution 0.047 mol/l TiCl_4 in BMMImBF_4 at 180°C.

Pulses: -7V duration 0.1s

-0.06V duration 0.9s

Total amount of current that has flown through the system: $Q = 35 \text{ A s}$.

Sample 251005

To avoid anodic current after cathodic pulse we maintained a small cathodic potential (-0,06V) during the relaxation period.

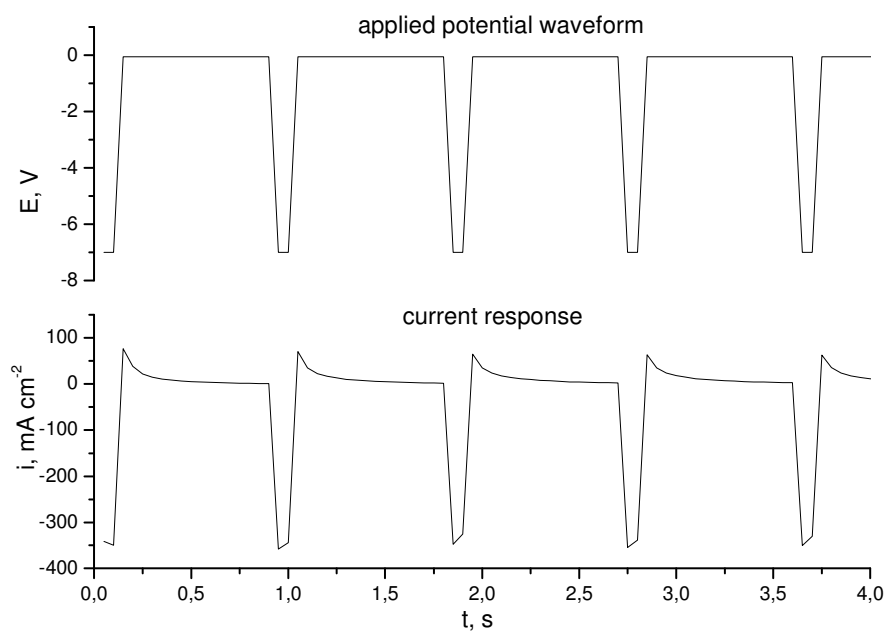


Fig. 3.79 Applied potential waveform and current response.

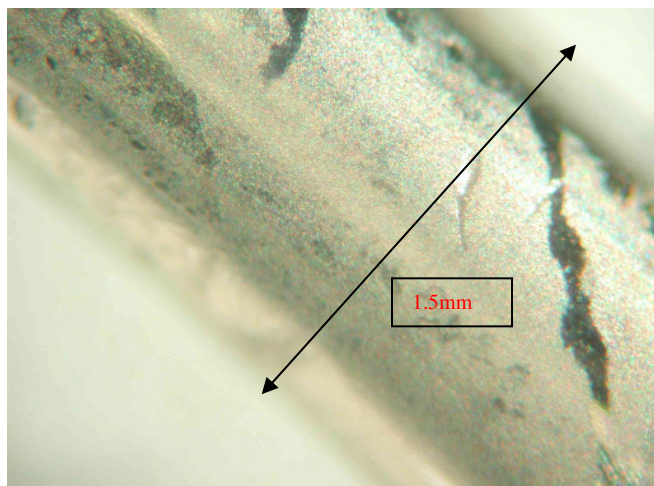


Fig. 3.80 Deposit on Pt wire (light microscope picture).

Potential pulses at 180°C improved the results. The deposit is more homogeneous and dense.

ESEM analysis

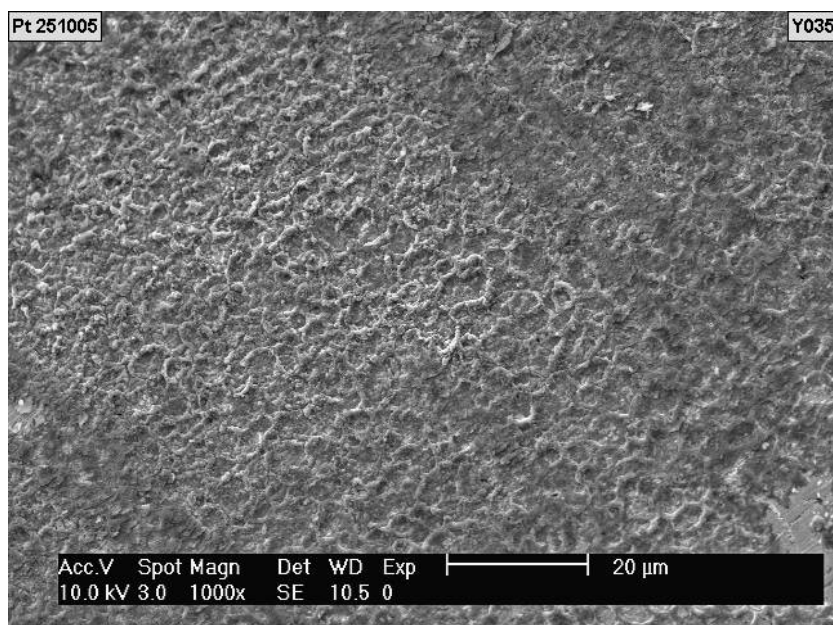


Fig. 3.81 ESEM picture of the deposit (magnification 1000x, SE, 10kV).

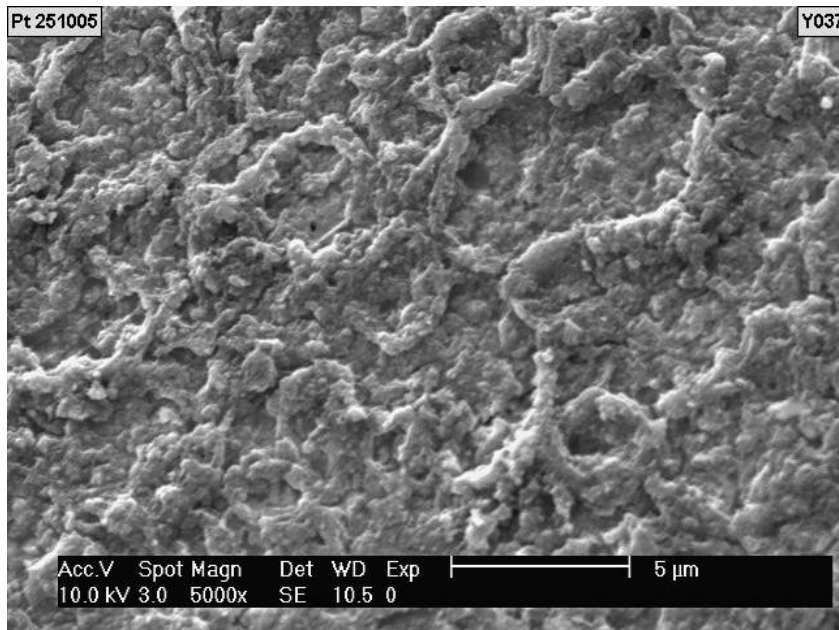


Fig. 3.82 ESEM picture of the deposit (magnification 5000x, SE, 10kV).

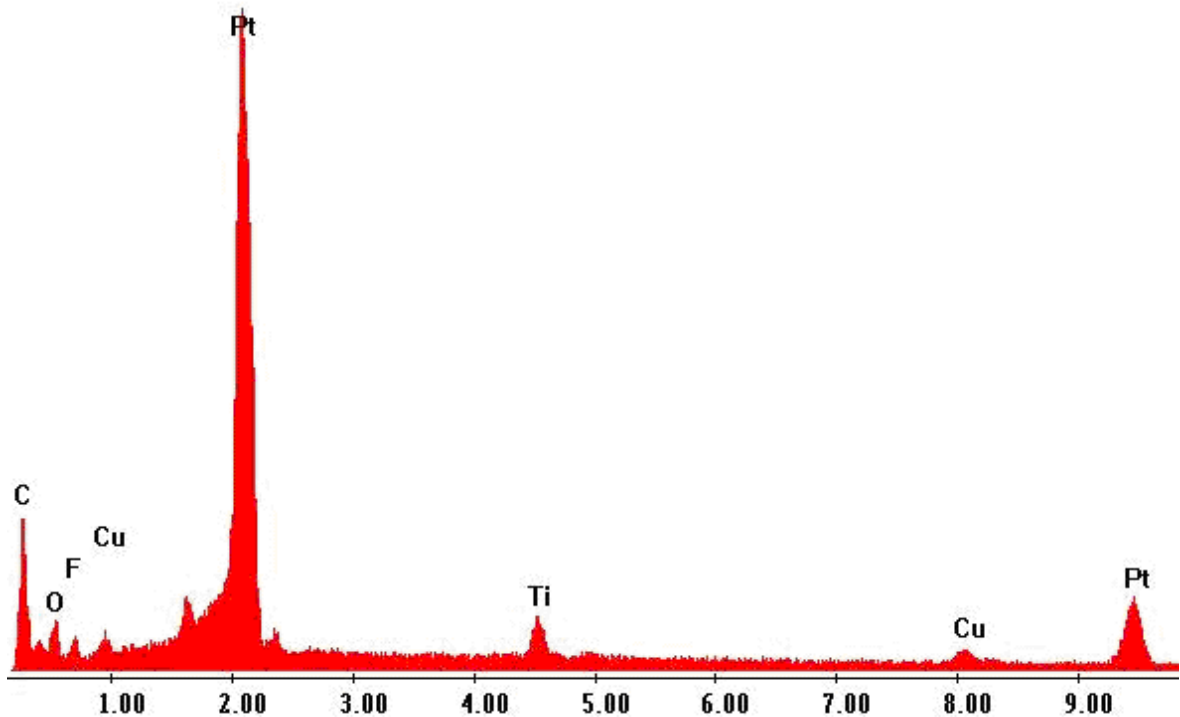


Fig. 3. 83 EDAX analysis of the deposit with 20kV.

EDAX analysis showed about the same results as after constant current deposition from this electrolyte.

A small quantity of Ti was deposited on the electrode, but it immediately oxidizes on air, which makes it difficult to analyze.

3.6.3 TiF_4 in BMMImBF_4 at elevated temperatures

The electrodeposition was carried out from the solution of titanium tetrafluoride (0.05 mol/l) in BMMImBF_4 at 180°C . A Pt chip (1.02 cm^2) was used as a working electrode. The deposit was visible on the electrode (Fig. 3.84).

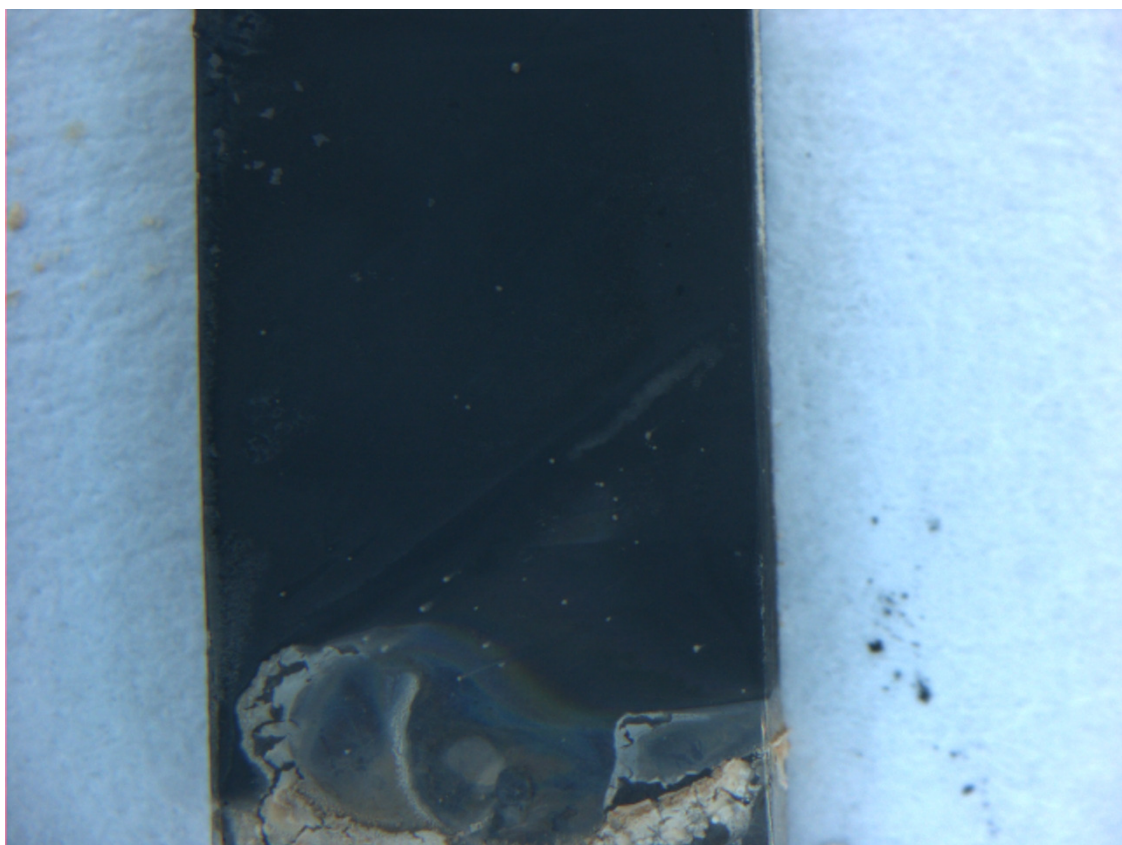


Fig. 3.84 Deposit on Pt wire (light microscope picture).

ESEM pictures and EDX analysis

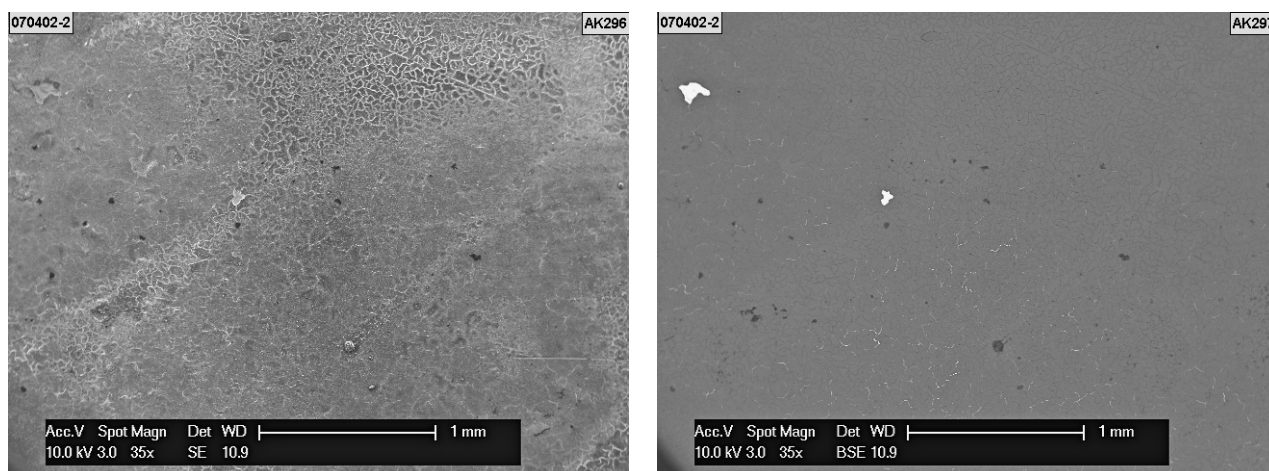


Fig. 3.85 ESEM picture of the deposit (magnification 35x, 10 kV), secondary electrons (left) and backscattered electrons (right).

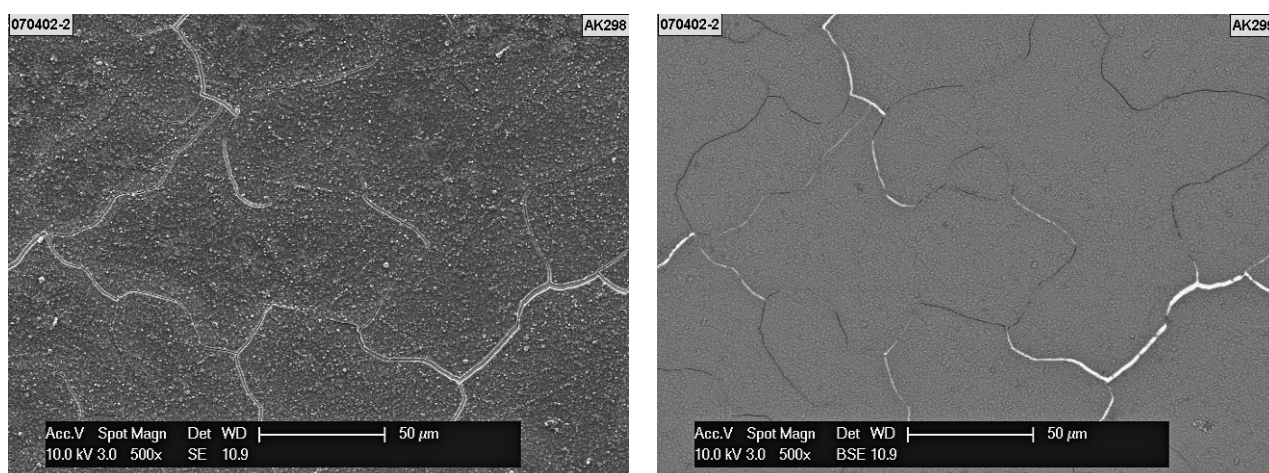


Fig. 3.86 ESEM picture of the deposit (magnification 500x, 10 kV), secondary electrons (left) and backscattered electrons (right).

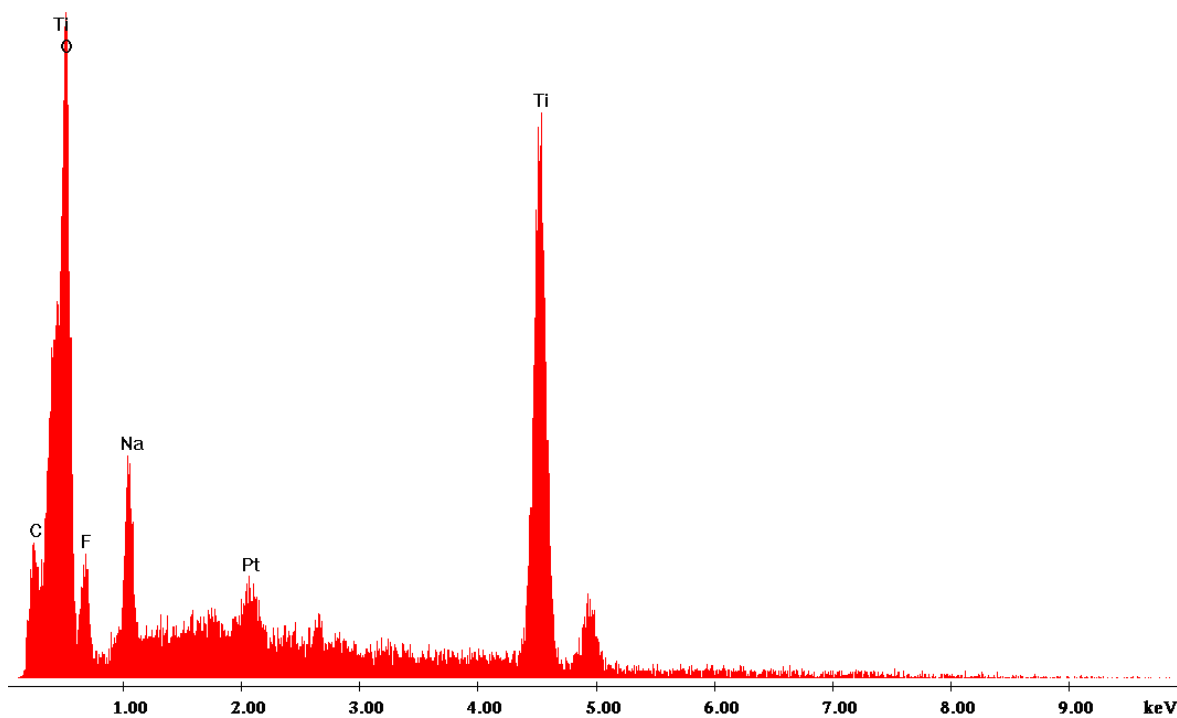


Fig. 3.87 EDAX analysis of the deposit (10kV accelerating voltage).

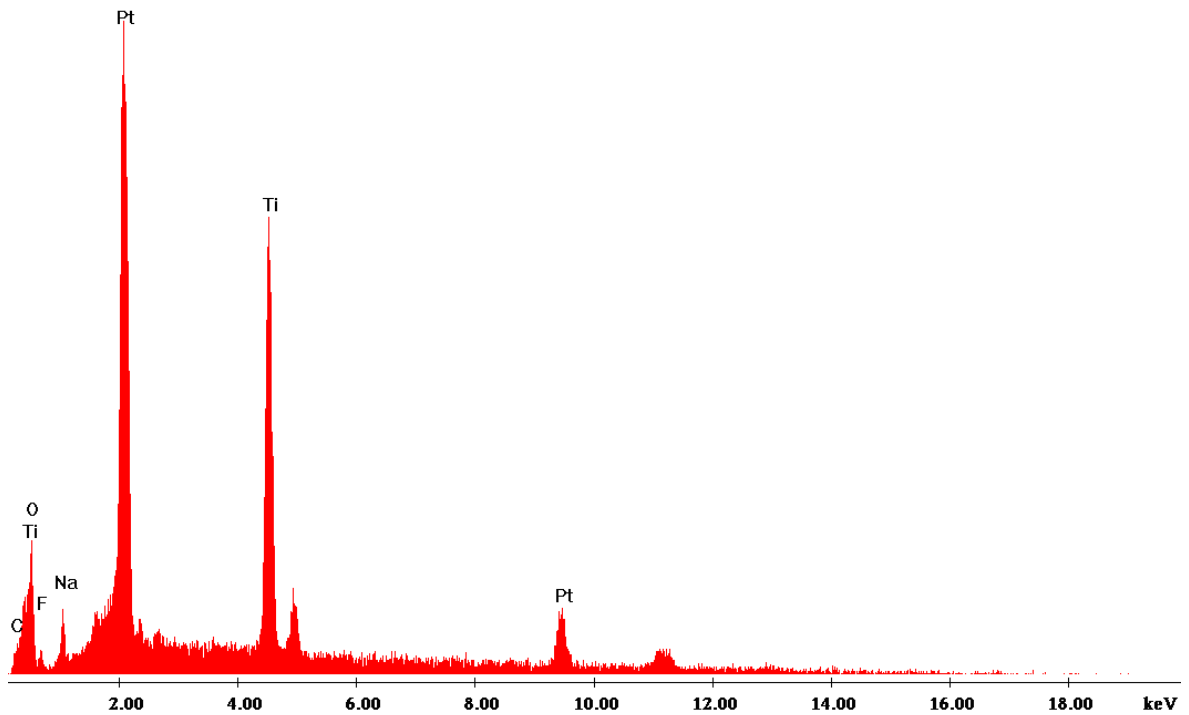


Fig. 3.88 EDAX analysis of the deposit (20 kV accelerating voltage).

On the surface of the deposit, the oxide film is formed. This has been proven by the Raman spectroscopy (Fig.3.89).

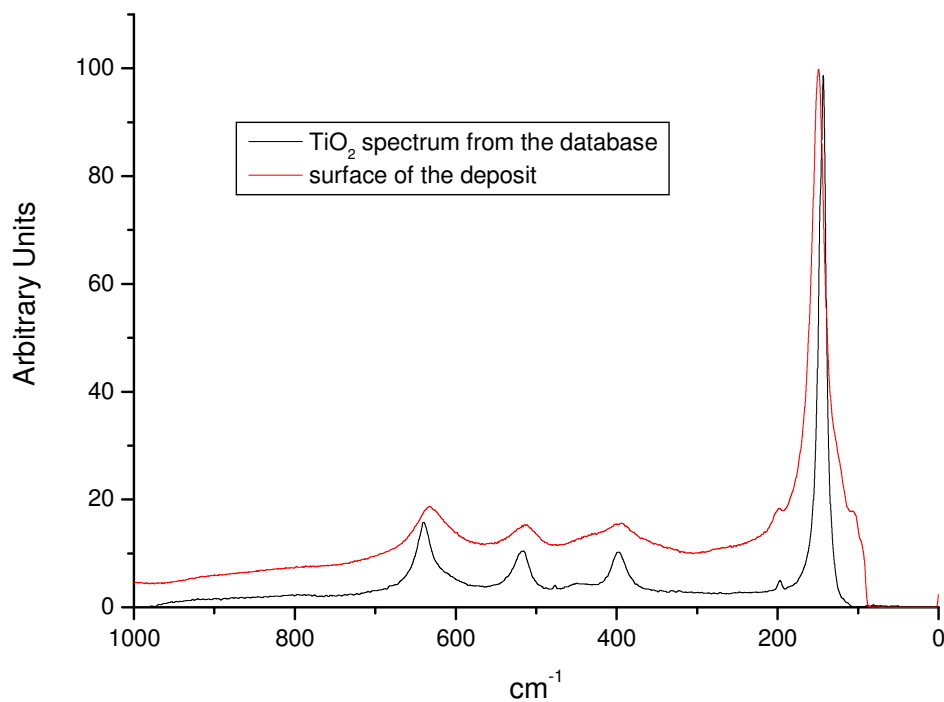
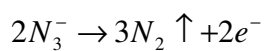


Fig. 3.89 Raman spectrum of the deposit surface.

Conclusions

Physical Chemistry of the ILs

Physical and electrochemical properties of two trisubstituted imidazolium salts as well as their mixtures with molar ratios 3:1; 1:1, and 1:3 have been studied. For BMMImBF₄ the cathodic stability is -1.9V and the anodic is +2.05V. If azide anions are added to the IL-mixture, the anodic decomposition potential decreases by 1.5V. The azide anion exerts therefore a great influence on the electrochemical stability and limits the anodic part of the electrochemical window. This is probably due to the anodic oxidation of the azide anion, following the reaction



In the case of mixing BMMImBF₄ with BMMImN₃, the conductivity values do not differ greatly by changing the composition of the mixture.

At room temperature, mixtures reveal a viscosity of approximately 250 to 450 mPa s. As expected, it decreases with increasing temperature. Higher viscosity values are observed in the mixtures with greater amount of IL containing an azide anion. This is due to the increased electrostatic interactions of the azide anions and the BMMIm cations.

Both, conductivity and viscosity dependencies on the temperature may be successfully approximated with a VTF - type equation. The differences in values of ideal glass transition temperatures, derived from VTF fit of conductivity and viscosity data, lies in the range of several degrees, which proves the right choice of the model used for interpretation. We note that VTF plots give a more linear correlation than Arrhenius - type plots.

Walden product which is thought to be constant over the range of temperatures was determined to be in the range of (70 to 80) cm² mPa s Ω⁻¹ mol⁻¹.

Density depends linearly on temperature and composition. The influence of the composition on the density is rather small. The influence of the anion structure on the conductivity is also very small, both anions seem to contribute equal amounts to the conductivity.

Mixing ILs has different effects on various physico-chemical properties. Observed linearity of the composition vs. density behavior contrasts to non-linear effects in viscosity and conductivity dependencies.

Electrochemistry of Ti(IV) in

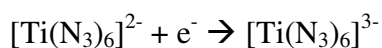
– BMImBF₄:

As follows from the obtained results, the overall electrochemical reduction mechanism can be represented in terms of general scheme: sequence of one-electron reduction steps with accompanying disproportionation reactions $2\text{Ti}(i) \rightleftharpoons \text{Ti}(i+1) + \text{Ti}(i-1)$, with possible formation of each species in the intermediate oxidation states. In diluted solutions, the Ti(II) intermediate is more stable, and also the disproportionation kinetics of Ti(I) can be detected. Total 4-electron reduction to Ti(0) is observed with the formation of Ti(III) and Ti(I) as the relatively stable intermediates. At concentration higher than 0.14 mol/l the limit of TiCl₄ solubility in the IL influences significantly the reduction mechanism, resulting in a very complicated reduction patterns. Theoretical explanation of the electrochemical processes in such heterogeneous system is still to be found.

– BMImN₃:

TiCl₄·2THF and TiCl₄·

Due to the formation of strong azide complex, electroreduction of Ti(IV) in TiCl₄-BMImN₃ solutions is kinetically retarded and confined to a single one-electron irreversible reaction:



The product of the reaction slowly decomposes forming gaseous nitrogen.

Ti anodic dissolution in BMImBF₄

Titanium was found to form a passive layer in the studied IL.

The anodized surface consists mostly of titanium fluoride. The oxide has formed as a result of the exposure to air after the experiment.

The anodic dissolution of Ti is overlapped with the electrolyte decomposition.

The released fluorine reacts with the active Ti anode surface with the fluoride formation.

Deposition experiments

In spite of the possible underpotential electrodeposition, reported in the literature, slight electrolyte decomposition can not be avoided when depositing titanium from the imidazolium based ILs. Thin deposits were received on a platinum substrate with the constant and pulsed current sequences.

The properties of the film formed on the electrode during the deposition process, is crucial for the deposit quality. Substitution of chloride ion for the smaller fluoride, improved the deposit quality, but production of a dense coherent layer is still a question of future investigations.

Literature index

- [1914Wal] P. Walden, *Bull. Acad. Imper. Sci. (St. Petersburg)*, (1914) 1800
- [1930Pok] E. Pokorney, German Patent 605551, (1930)
- [1940] W. Kroll, *Trans. Am. Electrochem. Soc.* **78**, (1940) 35
- [1948Hur] F. H. Hurley, U.S. Patent 4,446,331, (1948); T. P. Jr. Wier, F.H. Hurley, U.S. Patent 4,446,349, (1948); T. P. Jr. Wier, US Patent 4,446,350, (1948)
- [1955Mat] H. Matsuda, Y. Ayabe, *Z. Elektrochem.*, **59**, (1955) 494
- [1957Reid] W. E. Reid, Gr. G. M. Bish, A. Brenner, *J. Electrochem. Soc.*, **104**, (1957) 21
- [1959Fisch] O. Fischer, O. Dračka, *Collect. Czech. Chem. Commun.*, **24**, (1959) 3046
- [1959Mach] W. Machu, V. Kamel, *Werkstoffe und Korrosion*, **10**, (1959) 14
- [1962Bry] James I. Bryant, George C. Turrell, *Journal of Chemical Physics*, **37**, (1962) 1069
- [1963Kud] N. T. Kudryavtsev, R. G. Golovchanskaya, *Doklady Akademii Nauk SSSR*, **148**, (1963) 1339
- [1963Yok] J. T. Yoke, J. F. Wiess, G. Tollin, *Inorg. Chem.*, **2**, (1963) 1210
- [1964Fer] O. Ferenc, L. Prokaj, *Vespremi veryipari egyet. Közl.*, **8**, (1964) 163
- [1973San] E. Santos, F. Dymont, *Plating*, **60**, (1973) 821
- [1975Dob] D. Dobos, *Electrochemical Data: A Handbook for Electrochemists in Industry and Universities* (Elsevier, NY) 1975
- [1976Dan] V. Danek, I. Votava, K. Matiasovsky, *Chem. Zvesti*, **30**, (1976) 377
- [1976Atw] J. L. Atwood, J. D. Atwood, *Inorganic Compounds with Unusual Properties*, Advances in Chemistry Series No.150 (American Chemical Society: Washington, DC) (1975) 112
- [1977Lev] A.M. Levinskene, Proceedings of the 1st All-Union Symposium, Rostov-na-Donu (1977) 90 (in Russian)
- [1977Levin] A.I. Levin, N.A. Petrova, O.A. Manylov, V.M. Rudoj, A.V. Nechaev, Proceedings of the 1st All-Union Symposium, Rostov-na-Donu (1977) 88 (in Russian)
- [1978Gal] R. J. Gale, B. Gilbert, R. A. Osteryoung, *Inorg. Chem.*, **17**, (1978) 2728; G. C. Nardi, C. L. Hussey, L. A. King, U.S. Patent 4,122,245, (1978)
- [1979Tih] K.I. Tihonov, N.I. Agafonova, Electrodeposition of metals from organic solvents, Leningrad (1979) 60 (in Russian)

- [1980And] A. A. Andriyko, R. V. Chernov. *Ukrainian Chemical Journal*, **47**, (1980) 787 (in Russian)
- [1981Cha] E. Chassing, F. Basile, G. Lorthoir, *J. Appl. Electrochem.*, **11**, (1981) 187
- [1981Del] Yu. K. Delimarskiy, A. A. Andriiko, R. V. Chernov, *Ukrainian Chemical Journal*, **47**, (1981) 787 (in Russian)
- [1982Lis] A. Lisowska, S. Biallozor, *Electrochim. Acta*, **27**, (1982) 105
- [1982Wil] J. S. Wilkes, J. A. Levisky, R. A. Wilson, C. L. Hussey, *Inorg. Chem.*, **21**, (1982) 1263
- [1984Din] M. Dinu, *Metalurgia*, **36**, (1984) 261
- [1984Fann] A. A. Jr. Fannin, D. A. Floreani, L. A. King, J. S. Landers, B. J. Piersma, D. J. Stech, R. J. Vaughn, J. S. Wilkes, J. L. Williams, *J. Phys. Chem.*, **88**, (1984) 2614
- [1984Mak] M. Makyta, K. Matiasovsky, P. Fellner, *Electrochim. Acta*, **29**, (1984) 1653
- [1986Hus] C. L. Hussey, T. B. Scheffler, J. S. Wilkes, A. A. Jr. Fannin, *J. Electrochem. Soc.*, **133**, (1986) 1389
- [1986McM] G. E. McManis III, A. N. Fletcher, D. E. Bliss, U.S. Patent 4624755, (1986)
- [1987And] A. A. Andriiko, O. I. Boiko, *Ukrainian Chemical Journal*, **53**, (1987) 1165 (in Russian)
- [1987Gif] P.R. Gifford, J. B. Palmisano, *J. Electrochem. Soc.* 134(3) (1987) 610.
- [1989Mak] M. Makyta, K. Matiasovsky, V. I. Taranenko, *Electrochim. Acta*, **34 (6)**, (1989) 861
- [1990Car] R. T. Carlin, R. A. Osteryoung, J. S. Wilkes, and J. Rovang, *Inorg Chem.*, **29**, (1990) 3003
- [1990Tur] A. G. Tyurin, *Elektrokhimiya*, **26 (12)**, (1990) 1599
- [1992Tar] V. I. Taranenko, I. V. Zarutskii, V. I. Shapoval, M. Makyta, K. Matiasovsky, *Electrochim. Acta*, **37 (2)**, (1992) 263
- [1992Wil] J. S. Wilkes, M. J. Zavorotko, *J. Chem. Soc., Chem. Commun.*, (1992) 965
- [1992Xu] X. H. Xu, C. L. Hussey, *J. Electrochem. Soc.*, **139**, (1992) 1295
- [1993Har] G. M. Haarberg, W. Rolland, J. Thonstad, *J. Appl. Electrochem.*, **23**, (1993) 217
- [1993Abb] A. P. Abbot, A. Bettley, D. J. Schiffrin, *J. Electroanal. Chem.*, **347**, (1993) 153
- [1993Mak] M. Makyta, T. Utigard, *Light Metals*, (1993) 1137
- [1994Ful] J. Fuller and R. T. Carlin, *J. Chem. Crystal*, **24**, (1994) 489

- [1994Kis] L. Kisova, S. Sotkova, I. Komendova, *Collect. Czech. Chem. Commun.*, **59**, (1994) 1280
- [1994Staf] G. R. Stafford, *J. Electrochem. Soc.*, **141** (4), (1994) 945
- [1996Bon] P. Bonhote, A.-P. Dias, N. Papageorgiou, K. Kalyanasundaram, M. Grätzel, *Inorg. Chem.*, **35**, (1996) 1168
- [1996Mit] J. A. Mitchel, W. R. Pinter, C. L. Hussey, G. R. Stafford, in *10th International Symposium on Molten Salts* (eds R. T. Carlin, S. Deki, M. Matsanaga, D. S. Newman, J. R. Selman, G. R. Stafford, D. A. Shores) *Proc. Electrochem. Soc.*, **36**, (1996) 96
- [1996Shap] V. I. Shapoval, G. Kaptay, S. V. Devyatkin, in: *Electrochemical Technology: Innovation and New Developments* (Ed.: N. Masuko, T. Osaka, Y. Ito) 1996 (Gordon and Breach Science Publishers S.A.), p.361
- [1997Dan] V. Danek, M. Chrenkova, A. Silny, *Coordination Chemistry Reviews*, **167**, (1997) 1
- [1997Dev] S. V. Devyatkin, G. Kaptay, V. I. Shapoval, I. V. Zarutskii, V. P. Lugovoi, S. A. Kuznetsov, NATO Advanced Research Workshop - *Refractory Metals in Molten Salts*, Apatity, Russia, Kluwer Academic Publishers, (1997) 73
- [1997Ue] M. Ue, M. Takeda, M. Takehara, S. Mori, *J. Electrochem. Soc.*, **144**, (1997) 2684
- [1998Ful] J. Fuller, C. A. Breda, R. T. Carlin, *J. Electroanal. Chem.*, **459**, (1998) 29
- [1998Okab] T. Okabe, D. Sadoway, *Journal of Materials Research*, **13**(12), (1998) 3372.
- [1999Boi] O. Boiko, K. Serrano, P. Chamelot, P. Taxil, in: *Advances in Molten Salts. From Structural Aspects to Waste Processing* (Eds. M. Gaune-Escard), Begell House, Inc., New York, (1999) 581
- [1999Hol] J. D. Holbrey, K. R. Seddon, *J. Chem. Soc., Dalton Trans.*, (1999) 2133
- [1999Mak] M. Makyta, K. Matiasovsky, P. Fellner, *Electrochim. Acta*, **29**, (1984), 1653
- [1999McEwen] A. B. McEwen, H. L. Ngo, K. LeCompte, J. L. Goldman, *J. Electrochem. Soc.*, **146**, (1999) 1687
- [1999Shap] V. I. Shapoval, I. V. Zarutskii, V. V. Malyshev, N. N. Uskova, *Russian Chemical Reviews*, **68** (11), (1999) 925
- [1999Tar] V. I. Taranenko, I. V. Zarutskii, V. I. Shapoval, M. Makyta, K. Matiasovsky, *Electrochim. Acta*, **37** (2), (1992) 263
- [2000Eve] H. Every, A. G. Bishop, M. Forsyth, D. R. MacFarlane, *Electrochim. Acta*, **45**, (2000) 1279

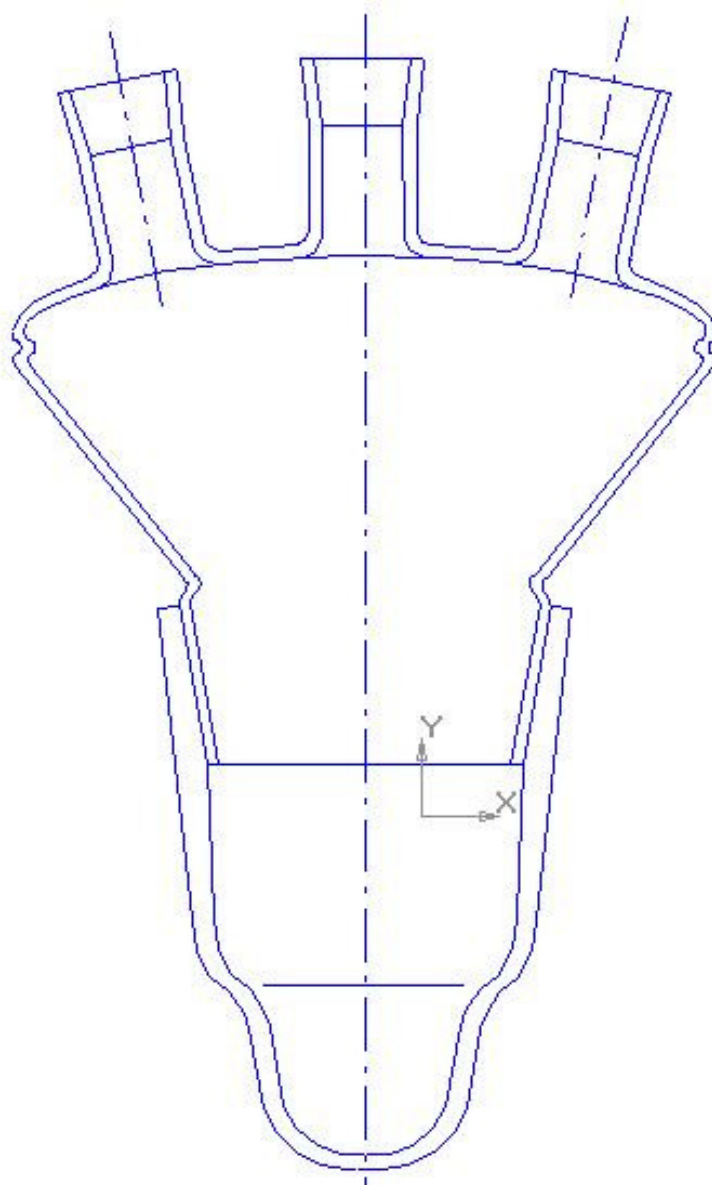
- [2000Chen] G. Zh. Chen, D. J. Fray, T. W. Farthing, *Nature* (London), 407(6802), (2000) 361.
- [2000Ham] J. T. Hamill, C. Hardacre, M. Nieuwenhuyzen, K. R. Seddon, S. A. Thompson, and B. Ellis, *Chem. Commun.*, (2000) 1929
- [2000Har] R. Harigava, Y. Ito, *J. Fluorine Chem.*, **105**, (2000) 221
- [2000Kit] T. Kitazume, G. Tanaka, *J. Fluor. Chem.*, **106**, (2000) 211
- [2000Lee] C. K. Lee, H. W. Huang, and I. J. B. Lin, *Chem. Commun.*, (2000) 1911
- [2000Ngo] H. L. Ngo, K. LeCompte, K. Hargens, A. B. McEwen, *Thermochim. Acta.*, **97**, (2000) 357
- [2000Nod] A. Noda, M. Watanabe, *Electrochim. Acta*, **45**, (2000) 1265
- [2000Sed] K. R. Seddon, A. Stark, and M.-J. Tores, *Pure Appl. Chem.*, **72**, (2000) 2275
- [2001Bar] A. J. Bard and L. R. Faulkner, *Electrochemical Methods: fundamentals and application* (John Wiley & Sons, New York) 2001
- [2001Huang] Huang Jing-Fang, Chen Po-Yu, Sun I-Wen, S. P. Wang, *Inorganica Chimica Acta*, **320**, (2001) 7
- [2001Kat] Y. Katayama, S. Dan, T. Miura, and T. Kishi, *J Electrochem. Soc.*, **148**, (2001) C102
- [2001Nod] A. Noda, K. Hayamizu, M. Watanabe, *J. Phys. Chem. B*, **105**, (2001) 4603
- [2001Sed] K. R. Seddon, A. J. Carmichael, M. J. Earle, International Patent Appl. Wo 800104146, (2001)
- [2001Lan] N.L. Lancaster, T. Welton, G.B. Young, *J. Chem. Soc., Perkin Trans. 2* 2001, 2267
- [2001Tan] J. Tanaka, T. Okabe, N. Sakai, T. Fujitani; K. Takahashi, N. Michishita, Yo. Umetsu, K. Nikami, *Nippon Kinzoku Gakkaishi*, 65(8) (2001)
- [2002Ohn] H. Ohno, M. Yoshizawa, *Solid State Ionics*, **154-155**, (2002) 303
- [2002Okab] T. H. Okabe, Proceedings of the Molten Salts Conference (EUCHEM 2002), Oxford (2002), PL2
- [2002Gol] J. Golding, S. Forsyth, D. R. MacFarlane, M. Forsyth, G. B. Deacon, *Green Chem.*, **4**, (2002) 223
- [2002McL] A. J. McLean, M. J. Muldoon, C. M. Gordon, I. R. Dunkin, *Chem. Comm.*, (2002) 1880
- [2002Ono] K. Ono, R.O. Suzuki, *Materia*, **41(1)**, (2002) 28.
- [2002Suz] R.O. Suzuki, K. Ono, *Proceedings - Electrochemical Society*, 2002-19(Molten Salts XIII, Philadelphia), (2002) 810

- [2002Ue] M. Ue, M. Takeda, *J. Korean Electrochem Soc.*, **5**, (2002) 192
- [2003Gag] L. Gagliardi, P. Pyykkoe, *Inorganic Chemistry*, **42 (9)**, (2003) 3074
- [2003Gor] Ch. M. Gordon in: *Ionic liquids in synthesis* (Eds. P. Wasserscheid and T. Welton) 2003 (Wiley-VCH, Weinheim), p.7
- [2003Muk] I. Mukhopadhyay and W. Freyland, *Langmuir*, **19**, (2003) 1951
- [2003Nis] T. Nishida, Y. Tashiro, M. Yamamoto, *Journal of Fluorine Chemistry*, **120**, (2003) 135
- [2003Tsu] T. Tsuda, C. L. Hussey, G. R. Stafford, J. E. Bonevich, *J. Electrochem. Soc.*, **150 (4)**, (2003) C234
- [2003Xia] Li Xiao, K. E. Johnson, *J. Electrochem. Soc.*, **150 (6)**, (2003) E307
- [2004Eve] H. Every, A. G. Bishop, D. R. MacFarlane, G. Orädd, M. Forsyth, *Phys. Chem. Chem. Phys.*, **6**, (2004) 1758
- [2004Haig] R. Haiges, J. A. Boatz, S. Schneider, T. Schroer, M. Yousufuddin, K. O. Christe, *Angewandte Chemie*, **43 (24)**, (2004) 3148
- [2004Hol] J. D. Holbrey, R. D. Rogers, in: *Ionic liquids in synthesis* (Eds. P. Wasserscheid and T. Welton) 2004 (Wiley-VCH, Weinheim), p.41-55
- [2004For] S. A. Forsyth, J. M. Pringle, D. R. MacFarlane, *Aust. J. Chem.*, **57**, (2004) 113
- [2004Trul] P. Trulove and R. A. Mantz, in: *Ionic liquids in synthesis* (Eds. P. Wasserscheid and T. Welton) 2004 (Wiley-VCH, Weinheim), p.56-68 and 103-125
- [2004Was] P. Wasserscheid and T. Welton, *Ionic liquids in synthesis*, 2004 (Wiley-VCH, Weinheim)
- [2005And] Y. Andriyko, U. Fastner, G. E. Nauer, *Proceedings of the 7th International Symposium on Molten Salts Chemistry and Technology*, (Eds. P. Taxil, C. Bessada, M. Cassir, M. Gaune-Escard), Toulouse, (2005) 1071
- [2005Dah] K. Dahl, G. M. Sando, D. M. Fox, T. E. Sutto and J. C. Owrutsky, *J. Chem. Phys.*, **123**, (2005) 084504
- [2005Grim] B. K. M. Chan, N.-H. Chang, M. R. Grimmet, *Aust. J. Chem.*, **30**, (2005) 1977
- [2005Haig] R. Haiges, J. A. Boatz, S. Schneider, T. Schroer, M. Yousufuddin, K. O. Christe, *Angewandte Chemie*, **44 (12)**, (2005) 1860
- [2005Kat] Y. Katayama in: *Electrochemical aspects of Ionic Liquids* (Eds. H. Ohno) 2005 (John Wiley & Sons, New Jersey,), p.111

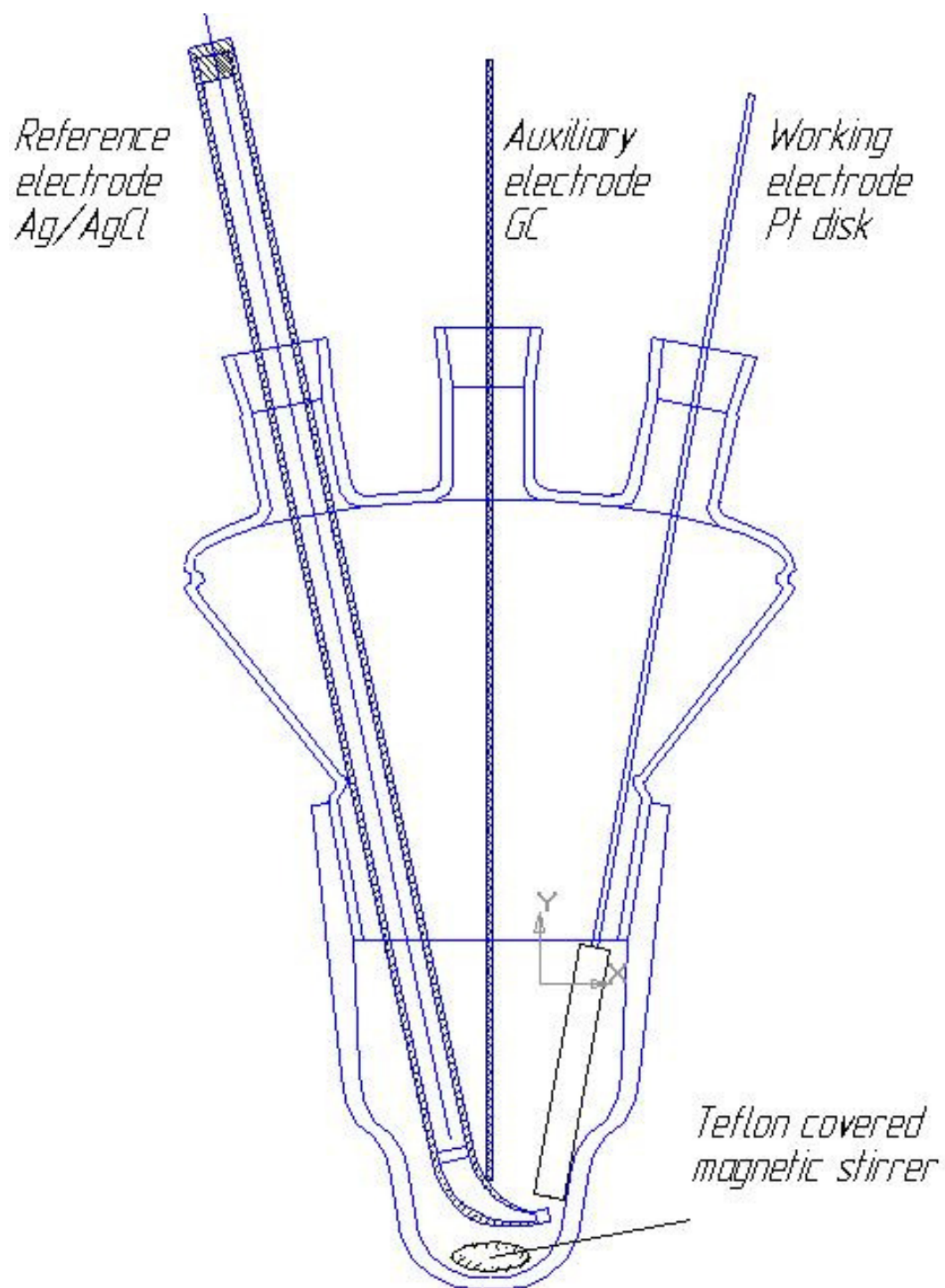
- [2005Mat] H. Matsumoto in: *Electrochemical aspects of Ionic Liquids* (Eds. H. Ohno) 2005 (John Wiley & Sons, New Jersey), p.35
- [2005Muk] I. Mukhopadhyay, C. L. Aravinda, D. Borissov and W. Freyland, *Electrochim. Acta*, **50**, (2005) 1275
- [2005Ue] M. Ue in: *Electrochemical aspects of Ionic Liquids* (Eds. H. Ohno) 2005 (John Wiley & Sons, New Jersey), p.205
- [2006Abed] a) SZ El Abedin, F. Endres, *ChemPhysChem*, **7**, (2006) 58
b) S. Zein El Abedin, E. M. Moustafa, R. Hempelmann, H. Natter, F. Endres, *ChemPhysChem* 7 (2006) 1535.
- [2006Ho] Ho, Kam-Piu; Wong, Kwok-Yin; Chan, Tak Hang, *Tetrahedron*, **62 (28)** (2006) 6650
- [2007And] Y. Andriyko, U. Fastner, H. Kronberger, G. E. Nauer, *Z. Naturforsch.*, **62a** (2007) 529

Appendixes

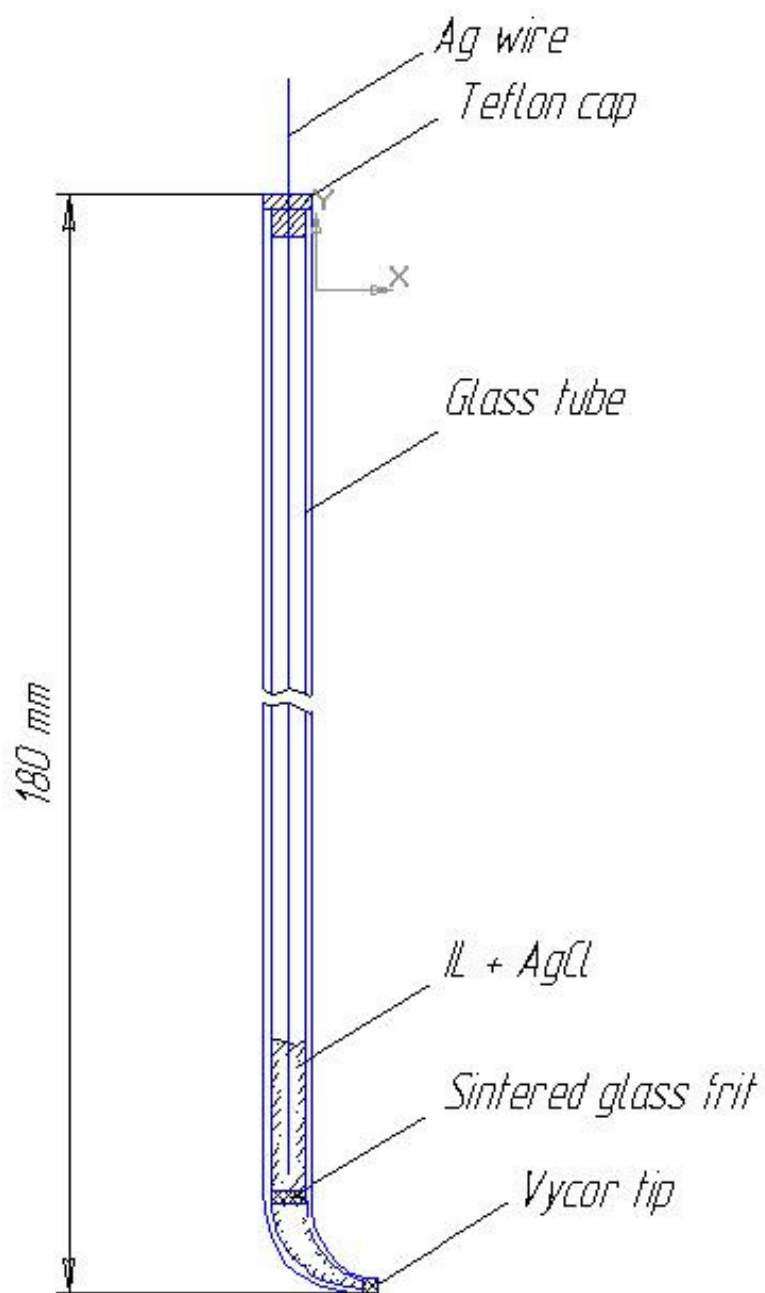
Construction of the standard three electrode cell used in the experiments



Cell with electrodes



Reference electrode



Yuriy Andriyko



Address: Viktor-Kaplan-Strasse 11, apt. 307, Wr. Neustadt, Austria
tel. +43 (0) 2622-222-66 ext. - 47
mobile: +43 (0) 699-11420354
e-mail: yuriy.andriyko@gmail.com

EDUCATION:

Sept.1998 - July 2002 National Technical University of Ukraine "KPI"
Bachelor in Chemical Technology and Engineering, Diploma
KB#21292085
June 2004 MS degree in electrochemistry
Thesis: "Electrochemical properties of the thermal decomposition
products of lithium permanganate", Supervisor - Prof. D.A.Tkalenko

WORK EXPERIENCE:

Sept.2004 –present **Junior researcher, PhD Student**
ECHEM Center of Competence in Applied Electrochemistry, Wr.
Neustadt, Austria
Sept.2002– June 2004 **Technician**
Joint Department for Electrochemical Systems (JDES), Kyiv,
Ukraine
Sept.2000–June 2002 **Technician**
Research lab "TechAN", Kyiv, Ukraine
Sept.2000–June 2001 **Junior Researcher**
Kyiv National University of Technology and Design (KNUTD),
Kyiv, Ukraine

PARTICIPATION in Internship Programs, Seminars, Conferences:

Sept. 2006 Conference on Molten salts and Ionic Liquids chemistry and technology, Tunisia.
Sept. 19-22, 2005 Österreichische Chemietage, Montanuniversität Leoben
June 19-22, 2005 1st International Congress on Ionic Liquids (COIL), Salzburg, Austria
April 2004 Conference of Young Scientists and Students,
in Kyiv National University of Technology and Design (KNUTD)
May 2002 Conference of Young Scientists and Students,
in Kyiv National University of Technology and Design (KNUTD)
April 2002 report on The 4th NATO "Science for Peace" project Meeting in Kyiv.
Held in Kyiv National University of Technology and Design (KNUTD)
Feb.– March 2002 workshop on Project Management in Engineering and Construction Industry
(NTUU "KPI" Dr. Griesser, Switzerland).
June – Sept. 2001 International Camp Counselor Program (ICCP). Worked as a counselor in the
United States.
May 2001 Conference of Young Scientists and Students,
held in Kyiv National University of Technology and Design (KNUTD)

LANGUAGES: Ukrainian – native, Russian – fluent, English – fluent, German - good
PERSONAL DATA:

Born: May 22, 1981
Nationality: Ukrainian
Marital status: married
Hobbies: basketball, football, guitar